

Master's Thesis

## Master's degree in Energy Engineering

Techno-economic analysis of Hybrid CSP/DAC system

**Autor:** Sukhrob Shakirov  
**Director:** Cristobal Voz Sanchez  
**Ponent:** Silvia Trevisan



Escola Tècnica Superior  
d'Enginyeria Industrial de Barcelona



## Abstract

In the wake of climate change, the carbon dioxide in the atmosphere continuously intensifies. People are confronted with the sad reality that the implementation of renewable energy technologies may not be enough to fight climate change. As known, every technology that during manufacture contributes to GHG, hence, carbon-negative technologies started to get a special interest from side researchers.

Direct air capture is a carbon-negative technology that catches carbon dioxide from the atmosphere by chemically interacting with air. DAC operates by utilizing thermal energy.

In conventional DAC systems, thermal energy usually comes from fossil fuels. Hence, the hybridization of DAC and renewable energy technologies such as CSP can be a crucial factor in the economics of DAC.

The current thesis explores the different ways of integrating CSP and DAC systems to investigate what factors impact and improves the economics of DAC when it is integrated with CSP.

Since the topic of integration of CSP and DAC is a novelty, firstly the technical evaluation of the technologies is being conducted in order to validate the technical feasibility of the integration, does the current state of the art of CSP technologies makes it possible to integrate the systems or further R&D is required.

After the validation of the technical aspects of the integration, several layouts of the Hybrid DAC/CSP system are proposed to determine which factors mostly affect the economics of this DAC, and whether is it economically feasible to power it with Solar thermal energy

Using different engineering tools different DAC/CSP layouts were modeled.

The models have shown that the cost of avoided carbon, which includes the carbon emission generated by the system, to be twice cheaper than conventional DAC systems, 300-400 \$/t-CO<sub>2</sub> for Hybrid CSP/DAC, and 600-800 \$/t-CO<sub>2</sub> for conventional DAC system developed by [National Academies of Sciences (U.S.)] and powered by fossil fuels.



## Table of contents

<b>ABSTRACT .....</b>	<b>I</b>
<b>TABLE OF CONTENTS .....</b>	<b>III</b>
<b>LIST OF ABBREVIATIONS / GLOSSARY .....</b>	<b>V</b>
<b>1. INTRODUCTION.....</b>	<b>1</b>
1.1       OBJECTIVES AND SCOPE.....	2
<b>2     BACKGROUND INFORMATION .....</b>	<b>3</b>
2.1       SOLID SORBENT DAC.....	3
2.2       AQUEOUS DAC.....	4
2.3       DAC FOR HYBRIDIZATION .....	5
<b>3     METHODOLOGY AND KPI.....</b>	<b>6</b>
3.1       KPIs .....	9
3.2       REPORT STRUCTURE .....	10
<b>4     LITERATURE REVIEW.....</b>	<b>11</b>
4.1       DAC .....	11
4.1.1 <i>Plant layout and equipment description</i> .....	13
4.1.2 <i>Economics of DAC</i> .....	16
4.2       CSP .....	17
4.2.1 <i>CRS receivers</i> .....	20
4.2.2 <i>Technical challenges with receiver and integration with DAC</i> .....	25
4.2.3 <i>Solar field and efficiency</i> .....	27
4.2.4 <i>Modular solar plants</i> .....	28
4.2.4.1 <i>Aora-solar</i> .....	28
4.2.4.2 <i>247Solar</i> .....	29
4.2.5 <i>Heat exchanger</i> .....	31
4.2.6 <i>Thermal Energy Storage System (TES)</i> .....	33
<b>5     LAYOUTS.....</b>	<b>35</b>
5.1       SOLE CSP (LAYOUT A) .....	36
5.2       CSP/DAC + TES (LAYOUT B) .....	37
5.3       CSP/DAC + PB (LAYOUT C) .....	39
5.4       OPERATION STRATEGY.....	39
<b>6     MODEL DESCRIPTION .....</b>	<b>40</b>
6.1       INTEGRATION .....	40
6.1.1 <i>Heat delivery analysis</i> .....	40
6.1.2 <i>Temperature analysis</i> .....	43
6.1.3 <i>Pre-heaters</i> .....	45
6.1.4 <i>Layouts A,B (without PB)</i> .....	47
6.1.5 <i>Layout C (with PB)</i> .....	49
6.1.6 <i>Power Island</i> .....	52
6.2       MODEL PREPARATION .....	53
6.2.1 <i>Modelling assumptions</i> .....	53
6.2.2 <i>Cost</i> .....	53
6.3       MODULAR CSP .....	56
6.3.1 <i>Location</i> .....	56
6.3.2 <i>Receiver</i> .....	56
6.3.3 <i>Heliostat field</i> .....	59
6.3.4 <i>Compressor</i> .....	60

6.3.5 Tower .....	60
<b>7 RESULTS.....</b>	<b>63</b>
7.1 LAYOUT A.....	63
7.2 LAYOUT B.....	67
7.3 LAYOUT C.....	72
7.4 DISCUSSION.....	75
<b>8 CONCLUSION .....</b>	<b>76</b>
<b>9 REFERENCES .....</b>	<b>78</b>
<b>10 APPENDIX.....</b>	<b>84</b>
10.1 MAIN HEX CODE.....	84
10.2 PB CODE.....	87

## List of abbreviations / Glossary

HTHE – High-temperature heat exchanger

LTHE – Low-temperature heat exchanger

HEX – Heat exchanger

CSP – Concentrated solar power

TES – Thermal energy storage

DAC – Direct air capture

CRS – Central receiver system

GT – Gas turbine



## 1. Introduction

Recent research clearly indicates that 1.5–2 °C global temperature moderation pathways include fast and deep implementation of low-carbon technologies in all energy sectors globally. However, past and present greenhouse gas (GHG) emissions are not compatible with directly achieving the target. Moreover, Renewable technologies are not entirely carbon neutral since all the production and supply chains contribute to GHG emission. Hence, the implementation of carbon-negative technologies may be mandatory to achieve Climate change goals.

Most of the integrated assessment models (IAM) made by IPCC, which is the tool used to draw the typical prediction of climate change, intensely rely on bioenergy carbon capture and storage (BECCS) ignoring Direct air capture (DAC) technologies. Even though, the feasibility of BECCS for large scale is under question due to the fact that BECCS require a huge land area, may pose a particular risk on water management, low energy output per area, as well as an impact on the environment in form of biodiversity. Whereas, DAC technologies based on electricity may be a quite appealing alternative since it takes less space, is very efficient, and importantly it is scalable. As DAC technology is electrical and thermal energy based type negative carbon technology, the integration of Renewable energy technologies, or in fact, solar energy technologies are possible. In this paper, it will be conducted the technical and economical assessment of such an integration.

The capture of CO<sub>2</sub> from ambient air was commercialized in the 1950s as a pre-treatment for cryogenic air separation. In the 1960s, capture of CO<sub>2</sub> from air was considered as a feedstock for production of hydrocarbon fuels using mobile nuclear power plants.<sup>1</sup> In the 1990s, Klaus Lackner explored the large-scale capture of CO<sub>2</sub> as a tool for managing climate risk,<sup>2</sup> now commonly referred to as direct air capture (DAC)

## 1.1 Objectives and scope

This project aims to study the Hybridization of DAC and CSP systems. Since inherently these two systems technically are very distinct.

In this work, the first part is the elaboration of the technical feasibility of such integration, defining its problems, and finding technical solutions considering the state-of-the-art of CSP technology.

Since the topic is new, there is no existing DAC/CSP plant. Therefore, the process of integration is not straightforward, and the thesis is forced to be innovative. However, every innovative step has to be technically validated so that a specific CSP part is possible to manufacture and commercialize.

Hence, the problems of integration are solved by referencing the existing research works done in that specific field or referencing existing projects, companies and plants.

The second part of the thesis is to analyze the economic feasibility of the system. As for that, different layouts of DAC/CSP systems are proposed and their impact on economics

The scope of the thesis will be solely on analyzing the integration of two systems. No manipulation will be done on the chemical part of DAC technology, but rather the investigation of the integration. The hybridization or integration will be done using commercialized technologies in reference to existing plants, research papers, and projects. Therefore, any technology that is in a non-commercial state, in other words, which is only in an experimental laboratory, is neglected for integration.

## 2 Background information

Generally, the concentration of CO<sub>2</sub> in the air is quite low, around 400 ppm [27]. The concept that makes it possible to remove such low concentrated gas from the air, is that large volumes of air have to be in contact with a surface that reacts with carbon dioxide in the air. There exist two types of DAC: DAC using strong base sorbents (liquid solvent DAC), and DAC using solid sorbents, also they are named as High-temperature DAC and Low-temperature DAC accordingly.

The working principles are completely distinct for each DAC type. In this part of the report will be given a small description of each of the DAC technologies.

### 2.1 Solid sorbent DAC

This DAC can be described in two stages: adsorption and desorption.

In this system, to capture the CO<sub>2</sub> from the blown air are used solid-state chemical compounds called amines.

The large volume of air passing the structured layers of solid sorbents is being adsorbed by them. So, this stage mainly consumes electrical energy because of fans that drive air and high pressure drop that has to be overcome.

The second stage is desorption, after solid sorbents are soaked with CO<sub>2</sub>, the contractor is closed, and now regeneration process begins, the CO<sub>2</sub> gas is being desorbed. The desorption of CO<sub>2</sub> proceeds using somewhat low-temperature heat steam around 100 Celsius, moreover, a vacuum pump to get rid of air in the chamber.

Compared to the liquid solvent DAC system, the bond of CO<sub>2</sub> and sorbent [27] is weaker, therefore, less energy required to separate CO<sub>2</sub> from a sorbent.

Such a low-temperature requirement makes this type of DAC highly applicable to the integration with PV, Wind technologies

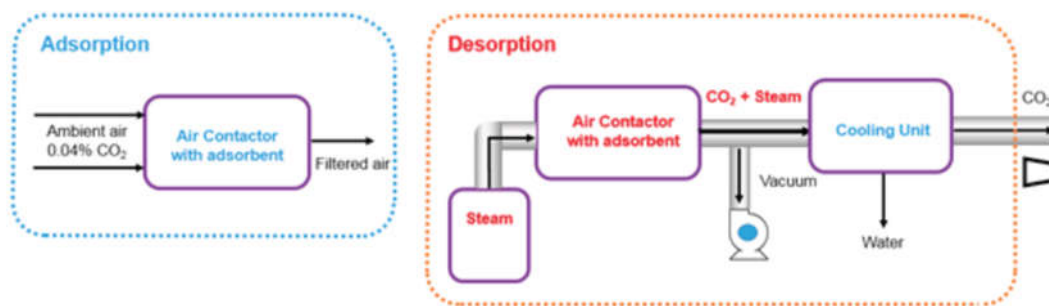


Figure 1. Solid sorbent DAC system

## 2.2 Aqueous DAC

It is considered to be more mature method of capturing carbon dioxide. Generally, since the CO<sub>2</sub> is ultra-diluted in air, a solution of a strong base is used here, such as potassium hydroxide (KOH), or Sodium hydroxide (NaOH) [Fig.2], where CO<sub>2</sub> dissolves into the solution.

So, mainly, the aqueous DAC can be represented by 4 stages: air contractor, Causticising, Calcination, and Slaker.

The chemical reactions are shown in [Fig.2]. Mainly, it is important to pay attention to the Calciner. In the calciner, the regeneration of CO<sub>2</sub> originates. In contrast to solid DAC, the temperature required for calcination reaction to take place is especially high (about 800-900 C)

Such an high-temperature requirement, naturally suggests that the most appropriate renewable energy technology that can fulfill the requirements of liquid solvent DAC is CSP technology [2].

For now, to talk about the disadvantages and advantages of both the systems is quite illogical since solid DAC systems are very immature, due to that reason and also this field just have started developing. The elaborations about the specifics of the systems may lack sources that could one rely on. Fortunately, currently, there are three big companies working in this piece, who will probably cast light on the topic of DAC.

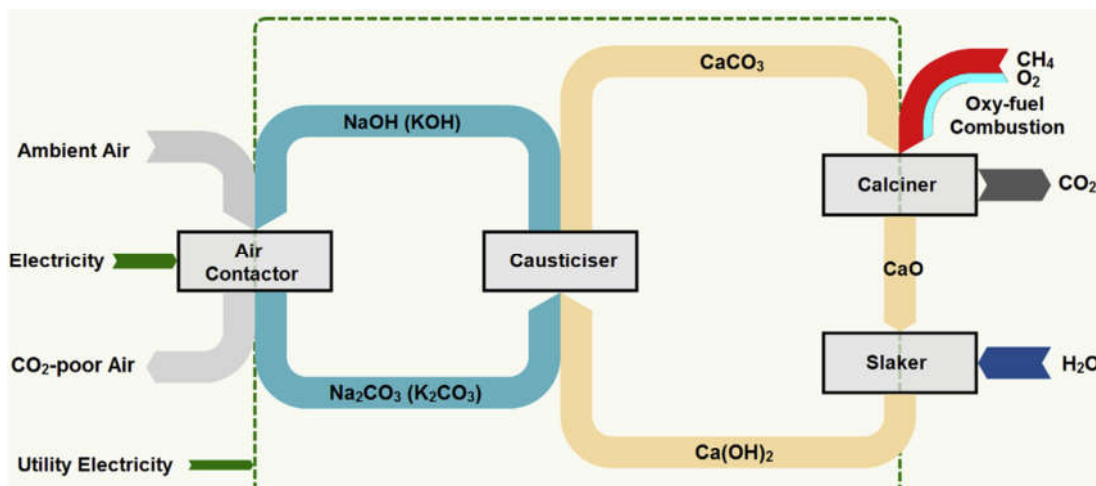


Figure 2. Liquid solvent DAC system

Currently, there are three big companies who launched pilot DAC plants, Climeworks, Carbon engineering and Global thermostat. The [Fig. 3] illustrates the existing companies in this piece.

Climeworks is Swiss company founded in Zurich 2009, in 2017 was the first who launched a pilot plant that is capable to capture 1 MT of CO<sub>2</sub> a yer [28].

Global thermostat, formed in 2010 by Eisenberger in New York, USA, is a very ambiguous company that claims very ambitious plants to deliver CO<sub>2</sub> at cost range 11-38 eur/ton [29].

However, considering, that the plans yet are not going very smoothly. Currently, the company seems like in paralyzed stage [30].

Carbon Engineering, established in 2009 by Keith in Squamish, Canada, is the single company that works with high-temperature DAC systems. By October 2015, introduced a plant that is able to capture 1 t CO<sub>2</sub>/ day. Yet, based on the results gotten from the pilot plant published very disclosed and detailed report as well as a techno-economical assessment of the liquid DAC system [2]. The company is partially founded by Bill Gates.

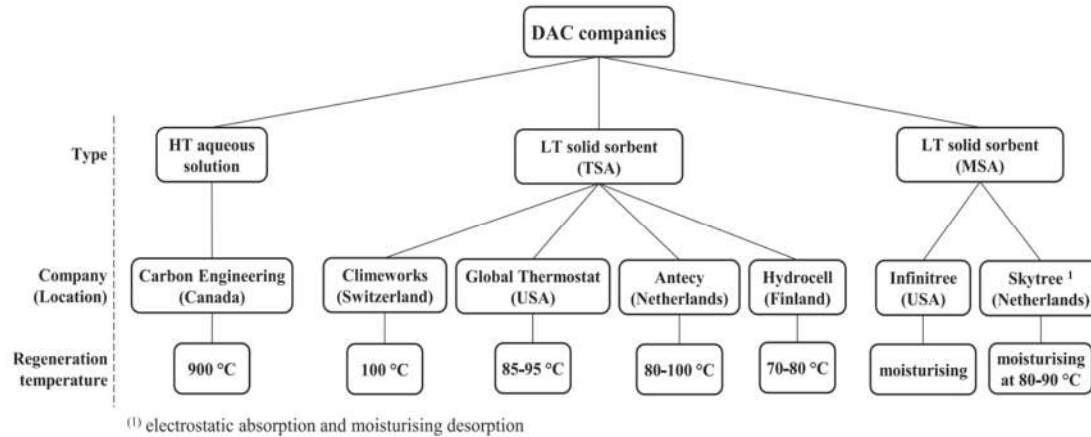


Figure 3. Active companies in the field of DAC

### 2.3 DAC for hybridization

Considering the current state of DAC technologies, and the availability of resources, the maturity of liquid solvent DAC proposes much more freedom to conduct the techno-economical assessment of its hybrid system with CSP technology, in contrast to solid sorbent DAC. Unfortunately, the lack of life-cycle analysis of solid sorbent DAC systems proposes nothing more than analysis around a big analytical gap. Consequently, a techno-economic assessment of solid sorbent DAC with solar technologies doesn't deliver a validated assessment at the present time.

Hence, this thesis will mainly focus on the hybridization of CSP and liquid solvent DAC system. From now on, the liquid solvent DAC system will be referenced as just DAC.

### 3 Methodology and KPI

In order to conduct a techno-economical assessment of the hybrid DAC/CSP system, various tools were used to build the model for the system: Python, Excel, SolarPilot, SAM, and Coolprop plugin for Python and Excel.

The methodology can be divided into three parts: DAC layout modification, modular CSP modeling, and modeling the layouts.

Specifically, why modular CSP plant is considered, not single tower CSP, will be explained in the upcoming chapter.

At first, the appropriate layout of a DAC system is built for CSP, in our case, the layout of DAC system from [2] was modified to fit the specifics of a CSP system. [Fig.4] illustrates in detail the procedure of the integration of two systems.

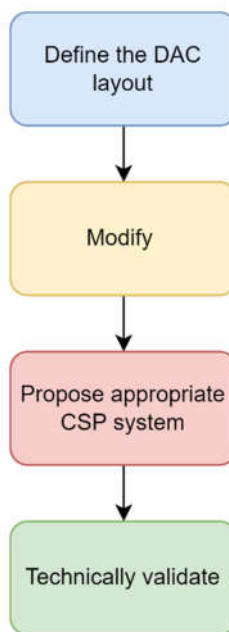


Figure 4. Technical validation

Next, after defining the power input and temperature difference for the CSP system, the CSP system is modeled.

Taking into consideration that the modular CSP plants are being used to fulfill the heating demand, the approach for scaling the CSP system will vary from single tower CSP.

In the case of modular CSP, the number of modular plants is increased to scale it up, whereas in single tower CSP its solar field, and tower including its receiver.

Hence, the modular CSP plant first has to be optimized, then the optimized modular CSP will be used in the final layouts [Fig.5].

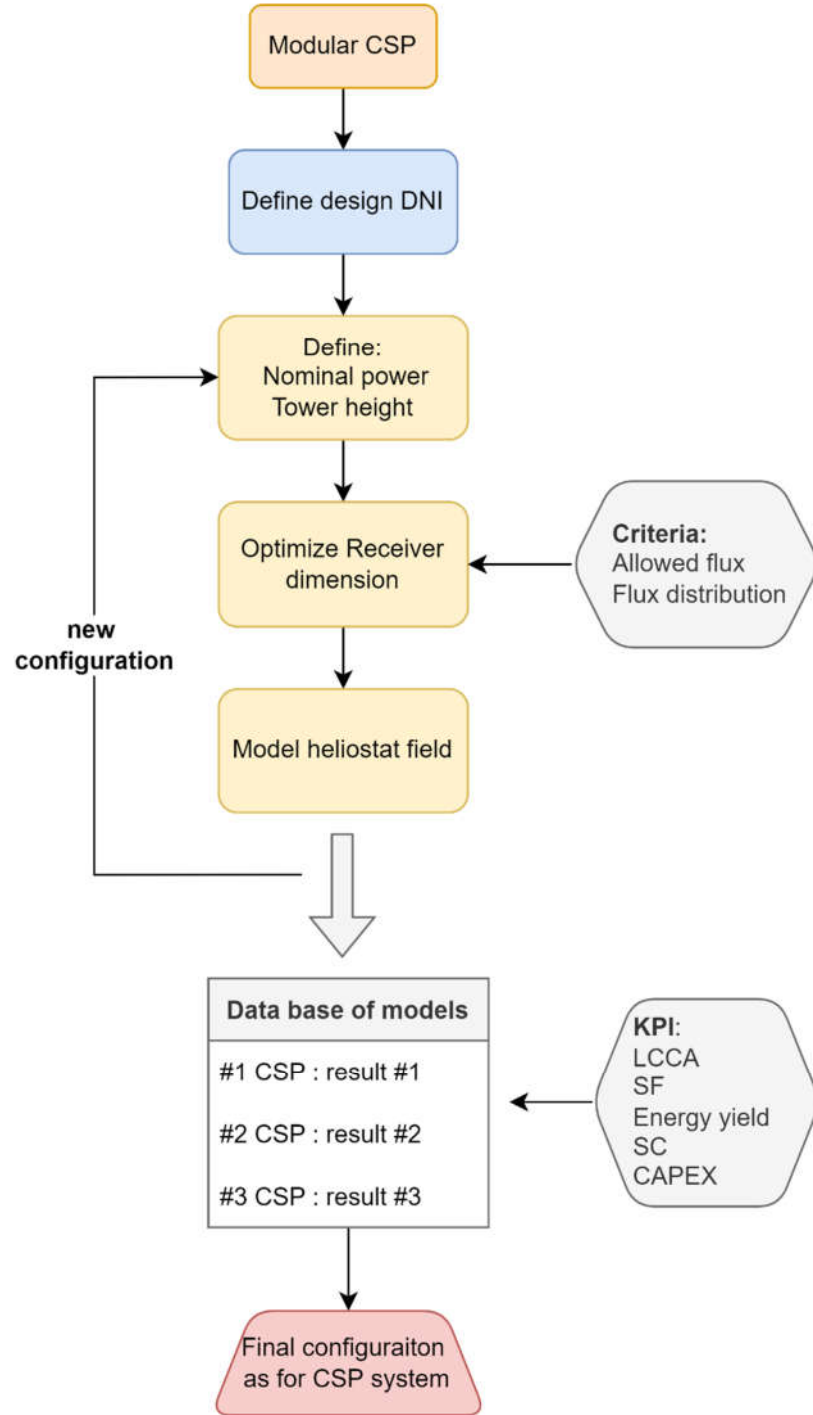


Figure 5. Modular CSP modelling

Afterward, using the optimum modular CSP plant, different layouts were built and optimized using corresponding KPIs [Fig.6]

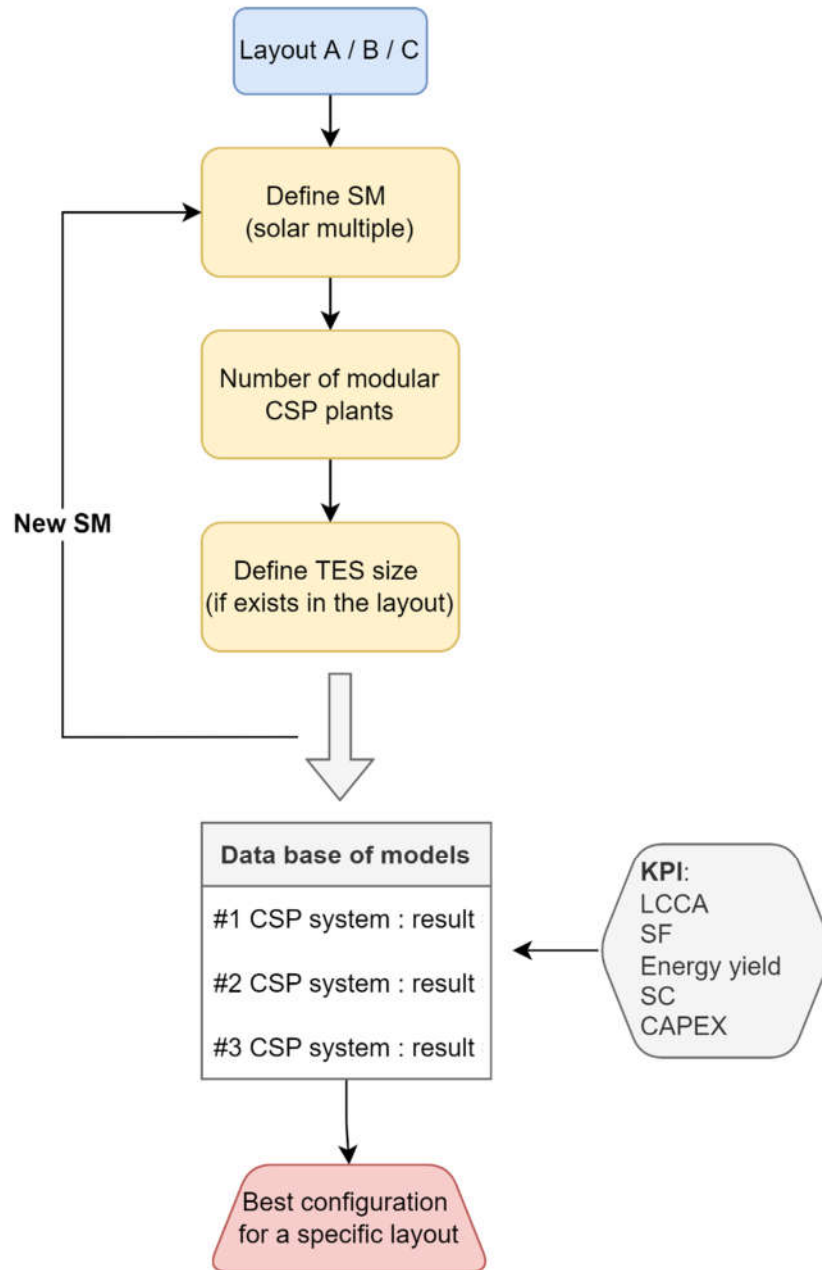


Figure 6. Layout modelling

### 3.1 KPIs

#### Technical:

**Solar fraction [%]** - In this thesis, it describes the ratio between annual solar energy by CSP and annual heat demand of DAC, including a power block, when it exists.

$$SF = \frac{\text{Thermal energy provided by CSP [kWh]}}{\text{DAC thermal energy demand [kWh]}}; \quad (3.1)$$

**Solar consumption [%]** - describes the ratio of annual solar energy used by the total solar energy produced.

$$SC = \frac{\text{Solar energy used [kWh]}}{\text{Solar energy produced [kWh]}}; \quad (3.2)$$

**Energy yield [kWh/kW]** - the ratio of annual energy produced by the system by its nominal power.

$$\text{Energy yield} = \frac{\text{Solar energy produced [kWh]}}{\text{Nominal system power capacity [kW]}}; \quad (3.3)$$

#### Economical:

The Levelized cost of carbon abatement is an economical KPI which is commonly used in the field of Carbon negative technologies.

Similarly, to LCOE (Levelized cost of electricity), LCC / LCCA shows the cost of captured or avoided carbon, considering all the expenses that come during lifespan.

$$LCCA = \frac{\text{Net CSP exp.} + \text{Net DAC exp.} + \text{Energy exp.}}{CO_2_{\text{captured}} - CO_2_{\text{emitted}}}; \quad (3.4)$$

$$LCCA = \frac{\left( \text{CAPEX} + \text{CAPEX}_{dac} + \sum_x^1 \frac{\text{OPEX}}{(1+wacc)^t} + \frac{\text{energy * price}}{(1+degradation_{csp})^t} + \frac{\text{OPEX}_{dac}}{(1+wacc_{dac})^t} \right)}{CO_2_{\text{captured}} - CO_2_{\text{emitted}}}; \quad (3.4)$$

$$LCC = \frac{\left( \text{CAPEX} + \text{CAPEX}_{dac} + \sum_x^1 \frac{\text{OPEX}}{(1+wacc)^t} + \frac{\text{energy * price}}{(1+degradation_{csp})^t} + \frac{\text{OPEX}_{dac}}{(1+wacc_{dac})^t} \right)}{CO_2_{\text{captured}}}; \quad (3.5)$$

- **Net CSP exp. (NCE)** – sum of expenditures created during the lifetime of a CSP system including its operational costs
- **Net DAC exp. (NDE)** – sum of expenditures created during the lifetime of a DAC system including its operational costs

- *Energy exp. (EE)* – sum of expenditures created due to the purchase of energy from external sources
- $x$  – life of the project
- $i$  – discount rate

The DAC plant itself has inherent emission that is generated due to the usage of non-renewable energy sources such as natural gas, coal, or electricity generated by these sources.

Therefore, in some cases, the LCCA can become negative which signifies the invalidity of the project. Whereas LCC is always positive since it doesn't account for the emitted carbon

Hence, indeed, the LCCA is the KPI that truly shows the performance of the plant.

This thesis will mainly focus on improving this KPI.

### 3.2 Report structure

The current report is split up into the following chapters:

1. The first chapter represents the introduction to the topic of DAC and the objectives of the thesis and its scope
2. The second chapter introduces the explanatory background information of DAC technology
3. The third chapter covers the methodology of the thesis
4. The fourth chapter investigates the state of the art of CSP systems and DAC layout that is used for the integration. Moreover, in this chapter is discussed the obstacles of the CSP system, and what/which type of CSP technology is suitable for use for the integration. This chapter functions as the foundation for technical validation
5. The fifth chapter introduces the finished versions of layouts of DAC/CSP system
6. The sixth chapter discusses the procedure of integration. Moreover, finalizes the configurations of the CSP plant in reference to existing research papers, plants, and companies, which is technical validation.
7. The seventh chapter presents modeling results and summarizes the results

## 4 Literature review

This chapter will discuss the DAC topic in detail, including its layout, and economics. Also, the topic of CSP is covered, which includes the current state of art of CSP technology, thermal storage, and heat exchangers

### 4.1 DAC

As was discussed in the previous chapter. DAC systems are categorized into two types, liquid solvent, and solid sorbent. Liquid solvent DAC being prioritized, the focus will be on companies that operate with liquid DAC systems.

Considering that, even though aqueous DAC is more mature than solid DAC, not many companies work with this system [Fig.3]

Generally, two types of strong base solutions are used in air contractor [Fig.2] [1][27]: potassium hydroxide or sodium hydroxide.

Currently, carbon engineering is a leading company in the field of aqueous DAC systems. Therefore, it was chosen to use [2], as a basement for DAC plant layout. Moreover, not every company discloses the economics of their plant, while in publication [2] they open-mindedly revealed lots of needed to conduct hybridization and economical assessment.

The working principle of Carbon Engineering DAC is quite similar to the one presented in the former chapter. Potassium hydroxide serves as a bases solution in their plant

It also consists of four general stages, Air contractor, pellet reactor (causticizer), Calcination reaction chamber (Calciner), and Slaker [Fig.7].

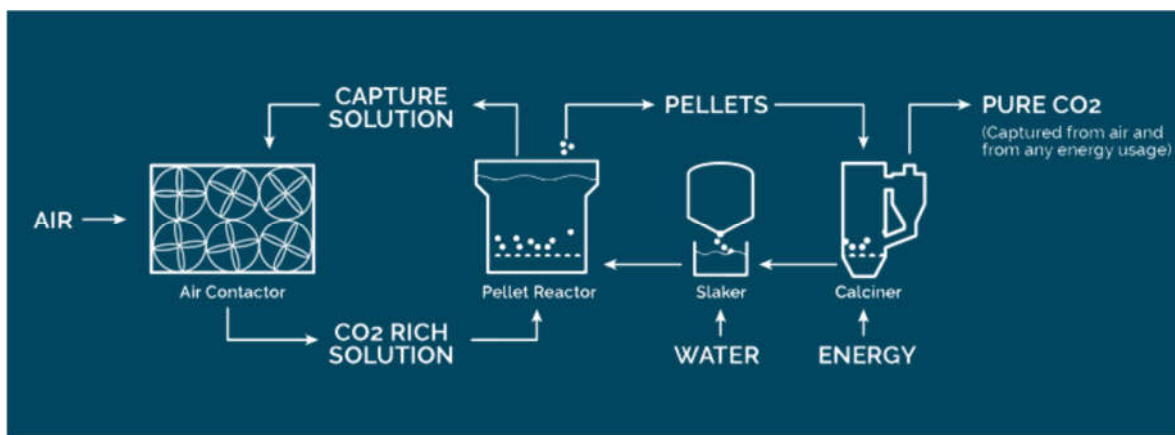


Figure 7. Carbon engineering DAC description [3]

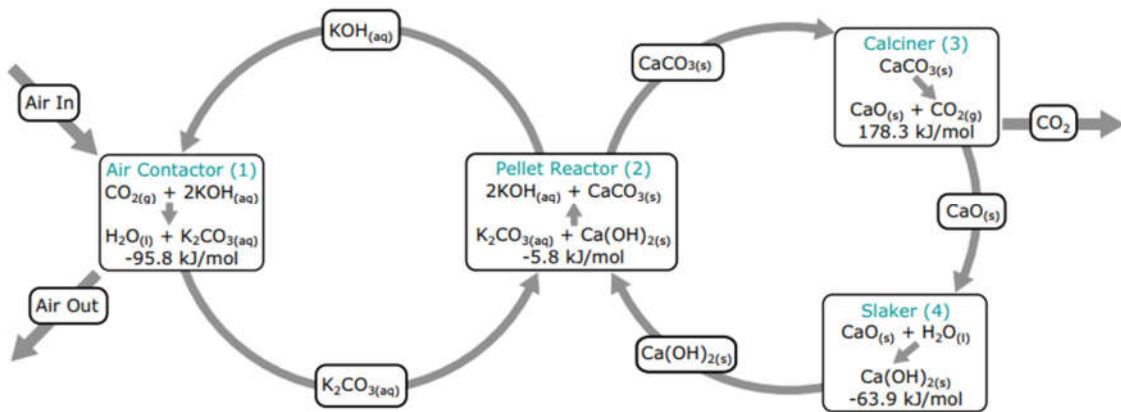
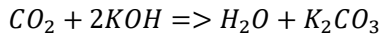


Fig. 8 Process Chemistry and Thermodynamics [2]

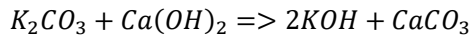
Generally, the chemistry background of the Carbon engineering DAC can be summarized as follows [Fig. 8].

#### 1<sup>st</sup> – Air contactor



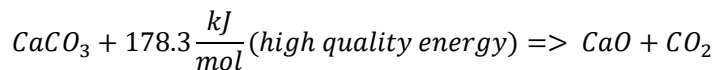
During this process, the air is brought into contact with an aqueous solution of KOH which helps to capture carbon dioxide by exothermically reacting with  $\text{CO}_2$ , and releasing some energy

#### 2<sup>nd</sup> – Pellet reactor



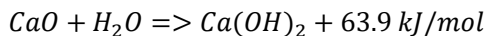
The reaction where former produced  $\text{K}_2\text{CO}_3$  is being causticized by Calcium hydroxide regenerating KOH and releasing  $\text{CaCO}_3$  solid pellets.

#### 3<sup>rd</sup> – Calciner



It is an endothermic reaction that requires high quality energy of temperature 900 C, where at last,  $\text{CO}_2$  is being regenerated in very pure form [2], over 90%  $\text{CO}_2$  gas.

#### 4<sup>th</sup> – Slaker



It is an exothermic reaction, where  $\text{Ca(OH)}_2$  is being regenerated using the by-products from Calciner. The released heat is captured and is used for the drying purpose of pellets, which is the case for this model.

#### 4.1.1 Plant layout and equipment description

To begin with, when it comes to technical and economic analyses of DAC plants, there exist that is a standard used to develop and analyze the DAC plants, DAC systems are built for 1 Mt CO<sub>2</sub>/year [2][4].

In the same manner, in publication [2], the DAC is sized for 1 Mt/year. In [Fig.3] can be observed, the layout for the plant developed by Carbon engineering. It shows all the required equipment and material and the energy balance of the plant. According to the [2], the plant at full capacity can capture 0.98 Mt-CO<sub>2</sub>/year from an atmosphere of high purity. However, the manual calculation shows that according with [Fig.3] the actual captured amount of far more than 0.98 Mt, but it is almost 150% more, which can be explained by the plant specifics. In the paper, Carbon Engineering uses fossil fuels to deliver the heat, therefore that emissions are directed into DAC, which in turn increases the amount of carbon dioxide. However, the actual avoided carbon dioxide is the capacity of 1 Mt.

The integration of DAC and CSP is mainly will be with the part of Calciner where heat is delivered [Fig.9]. However, the next, it will be given a quick overview of the main equipment of the DAC

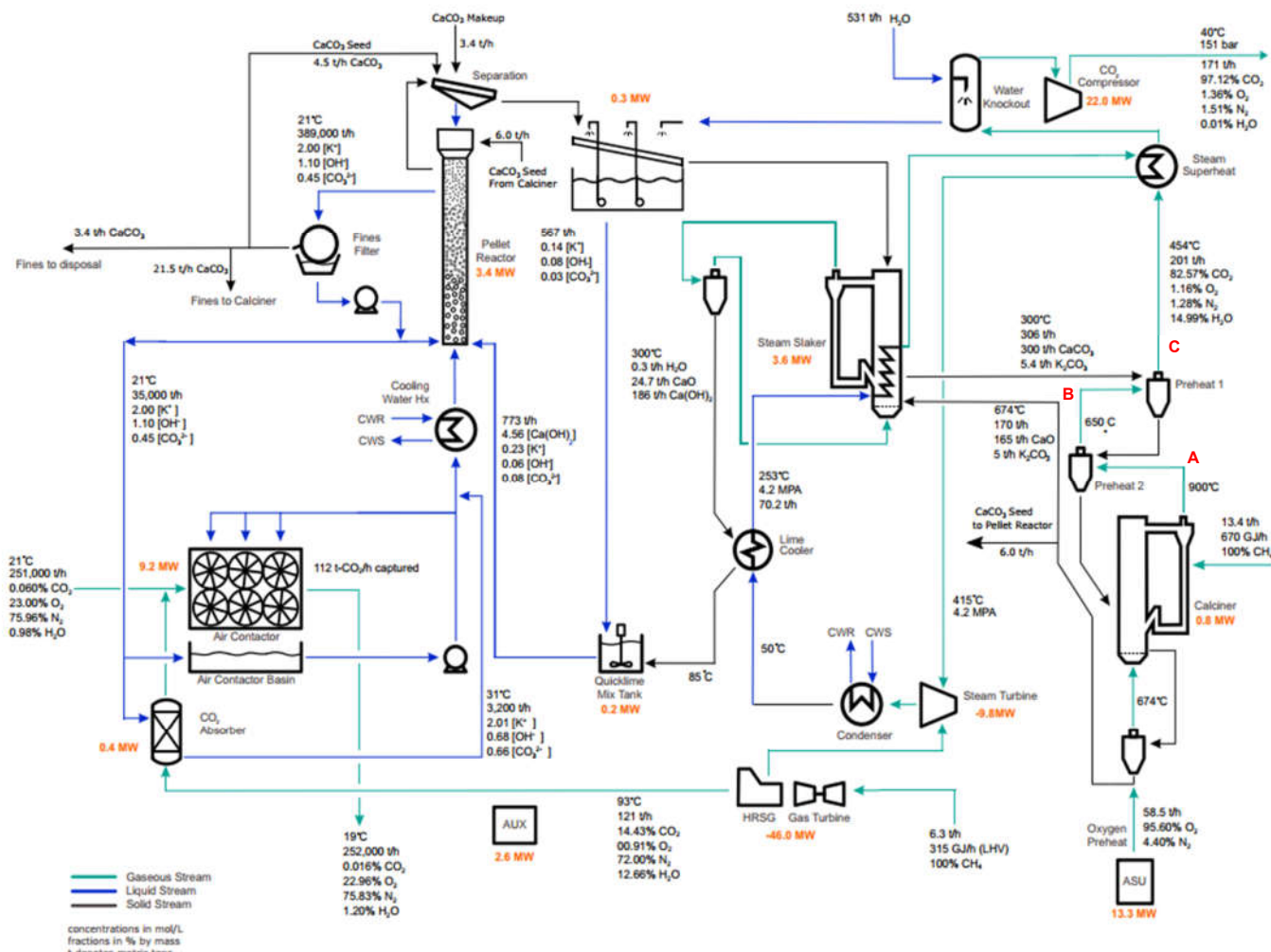


Fig.9 Carbon engineering DAC layout [2]

### Air Contactor

The air contractor can be considered as the lungs or heart of the system since it is responsible for pumping air into the system.

Contractors in aqueous DAC system usually can be represented as the collection cells with wetted structure inside that is equipped with power FAN that pushes air inside that in turn chemically reacts with the wetted solution. [Fig.10]



Figure 10. DAC air contractor [2]

Structured packing for years was one of the main topics that drove attention to research since the geometry of packing results in different pressure drops and efficiency. Moreover, the airflow configuration carries big importance. Usually, as a standard in many models of DAC systems the flow is modeled as counter-current [6] since DAC is being novelty itself, the first actual carbon capturing technologies were developed earlier, but for post-combustion application, where counter-current flow was mainly promoted. Whereas, the analysis conducted in [5] has shown that cross-flow can be more effective providing less pressure drop, consequently, less power requirement from FAN's side. In (Fig.9) the layout, the flow configuration is crossflow.

Conventional commercial packed towers have areas of  $100 \text{ m}^2$ , which resulted in hundreds of such towers to achieve  $1 \text{ Mt-CO}_2$  capture [4]. On the other hand, [2] proposed adopting the technology used in cooling towers and waste treatment plants, which have reduced the required number of towers to capture  $\text{CO}_2$  due to an increase in efficient volume which is at  $20000 \text{ m}^3$ , whereas conventional packed towers would provide for the same area only  $10000 \text{ m}^3$  [4].

The contractor is designed in collaboration with SPX Cooling Technologies (SPX).

### Pellet reactor

Pellet reaction, it is the part of DAC system, where solid particles of  $\text{CaCO}_3$  are being produced. Yet, as can be seen from the layout of the plant, the production of pellets is not straightforward, the pellets of specific sizes are directed into calciner.

For the reaction to happen, the fluidized bed reactor is used, adapted from water treatment technology developed by RHDHV.

Small-sized particles of 0.1-0.9 mm diameter are suspended, as their size increases the pellets sink, then directed into Calciner

In simple words, the idea behind this stage is to reduce the drying process, they are producing fine CaCO<sub>3</sub> pellet that can be easily dried out, rather than a slurry that would demand lots of thermal energy [4] to dry before going into calciner. This circulation using filters, pumps, and water treatment procedures is taking less energy rather than drying a very wet slurry substance.

### **Calciner**

It can be observed from [Fig.9], the pellets that are coming from the reactor, are first preheated using regenerated heat from the slaker, which effectively reduced the heat demand. The pellets exit the slaker heat up to 300 C.

After passing the slaker, incoming pellets pass through two pre-heaters, firstly, the pellets are preheated from 300 C to 450 C, then from 450 up to 650 C. Pre-heaters uses cyclone arranged in counter-current configuration

The design proposed by Carbon engineering includes additional preheating the pellets inside the calciner since the temperature of pellets is slightly lower than the required temperature to chemical reaction to activate.

The calcination chamber works at 1 atmospheric pressure, however, the calciner carefully sealed, which eliminates the contamination of captured Carbon gas.

The nominal energy required to drive the reaction is 3.18 GJ/t-CaO. However, the design proposed of Carbon engineering requires 4.07 GJ/t-CaO due to the fact that calciner besides the running the reaction consumes energy to preheat the pellets from 650 C to the required temperature, which is 900 C. Moreover, the kiln itself has its own efficiency of 89%, summing all up, it makes the Calciner 78% thermal efficient.

### **Steam Slaker**

Since the chemical reaction (eq.1.1) is exothermic, the heat can be recovered. The maximum temperature for slaking under 100 kPa is around 520 C, however, the design proposed by Carbon engineering operates at 300 C which offers faster kinetics [2].

Slaker in the layout [Fig.9], besides drying and preheating the pellets, vaporizes the water of the bottom cycles low pressure steam system.

Such an integration, helped to efficiently manage energy streams and optimize the system

### **CO<sub>2</sub> Compression and Cleanup.**

In the research done by Carbon Engineering [2], there is developed different scenarios with different economical outputs. One of the scenarios includes the compression of captured gas CO<sub>2</sub> up to 15 MPa.

For our thesis, the scenario with compression was chosen as the basement layout, therefore techno-economical assessment of the integration will include this equipment.

### ASU and gas power plant

Since our integration is mostly focused on the greenification of the DAC. Evidently, the part with gas power plant, where fossil fuels are used to run the plant will be omitted. As well as, ASU which Air separation unit.

In general, the application of ASU here is explainable since the energy is delivered to Calciner by burning methane, the ASU is used to purify the coming air, so the combustion of fuel to be Oxi-fired, which leads to release pure CO<sub>2</sub> after the oxidation reaction of methane, which is mixed the regenerated CO<sub>2</sub> from calcination reaction, therefore the resulted captured CO<sub>2</sub> is more than actual avoided CO<sub>2</sub>

Parameter	Value	Unit	Ref
<b>Contractor</b>			
Fan energy	61	kWh/t-CO <sub>2</sub>	[2]
Fluid pumping energy	21	kWh/t-CO <sub>2</sub>	
<b>Pellet</b>			
Fluid pump energy	27	kWh/t-CO <sub>2</sub>	[2]
<b>Calciner</b>			
Energy demand	4.05	GJ/t-CO <sub>2</sub>	[2]
Operating temperature	900	C	
Pressure	1	atm	
<b>Slaker</b>			
Operating temperature	300	C	[2]
Energy produced	77	kWh/t-CO <sub>2</sub>	
<b>ASU</b>			
ASU power usage	238	kWh/t-CO <sub>2</sub>	[2]

Table 1. Main parameters of DAC system

#### 4.1.2 Economics of DAC

Aqueous DAC	Capacity	Indicated time of cost	LCC	LCCA	Ref
	t-CO <sub>2</sub> /year	year	\$/t-CO <sub>2</sub>	\$/t-CO <sub>2</sub>	
(Keith, Ha-Duong, Stolaroff 2006)	280000	2005	376	-	[31]
(Holmes, Keith 2012)	1000000	-	258	-	[5][1]
(Socolow et. Al 2011)	1000000	2011	300-395	-	[32]
(Mazzotti, Baciocchi, Desmond, Socolow 2013)	1000000	2013	283-300	510-568	[6]
(Keith, Holmes, St. Angelo, Heidel 2018) Carbon eng.	1000000	2018	94-232	-	[2]

(National Academies of Sciences (U.S.) 2019)	1000000	2019	147-264	641-819	[4]
(Fasihi, Efimova, Breyer 2019)	1000000	2020	186	-	[1]

Table 2. Cost summary of the aqueous DAC

In [Table 2] can be observed the costs of DAC summarized from the specific sources. In fact, it's shown the cost of LCC resulting from the modeled plant [2], is in the range of 94-232 \$/t, certainly, showing that in ideal conditions 94 \$/t is achievable, moreover, the smooth decline in LCC with year is the sign of the improvement in the supply chain as well as achievements R&D in the field.

## 4.2 CSP

CSP, as the name suggests, is the system that generates solar heat by means of mirrors and lenses that are used to concentrate sunlight onto a receiver. Generally, CSP efficiency is higher than direct competitive PV technology and goes up to 40% [15].

CSP systems, in general, consist of the following elements [Fig.11]:

1. Heliostat field
2. Solar receiver
3. Power conversion block or also called Power Block (PB)
4. Electric generator
5. Thermal Energy Storage (TES), but may also not be included.

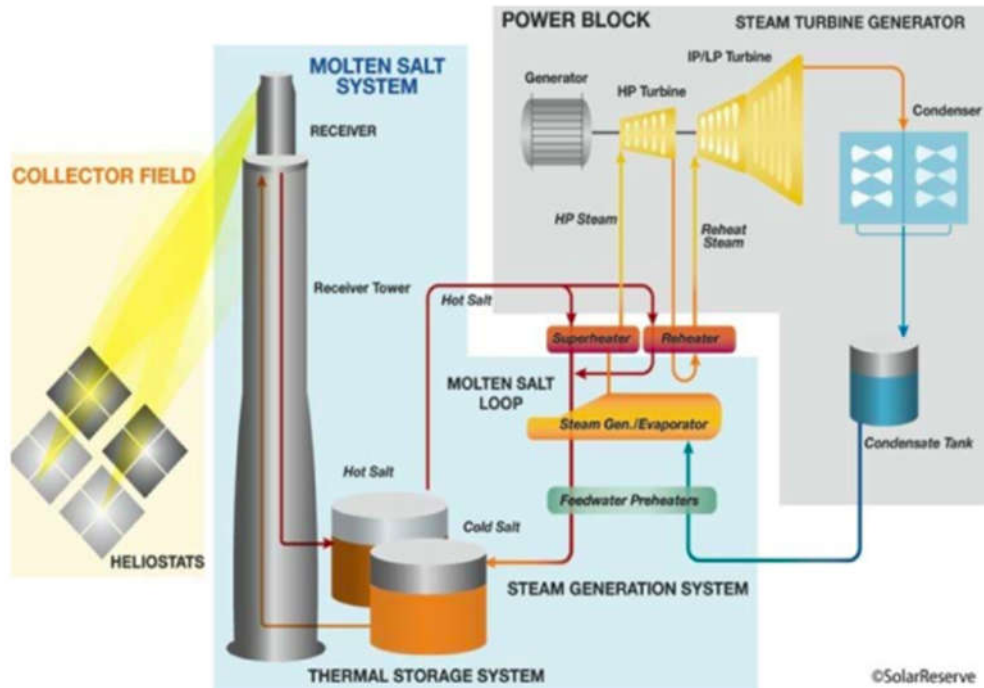


Fig.11 Concentrated solar power plant [33]

At the present time, four widely recognized types of CSP exist. The difference between is in the mechanism of capturing solar radiation, it can be observed in [Fig.12].

Parabolic Through Collectors (PTC) uses a parabolic mirror that concentrates the Sunray onto the focal tube, which is the receiver.

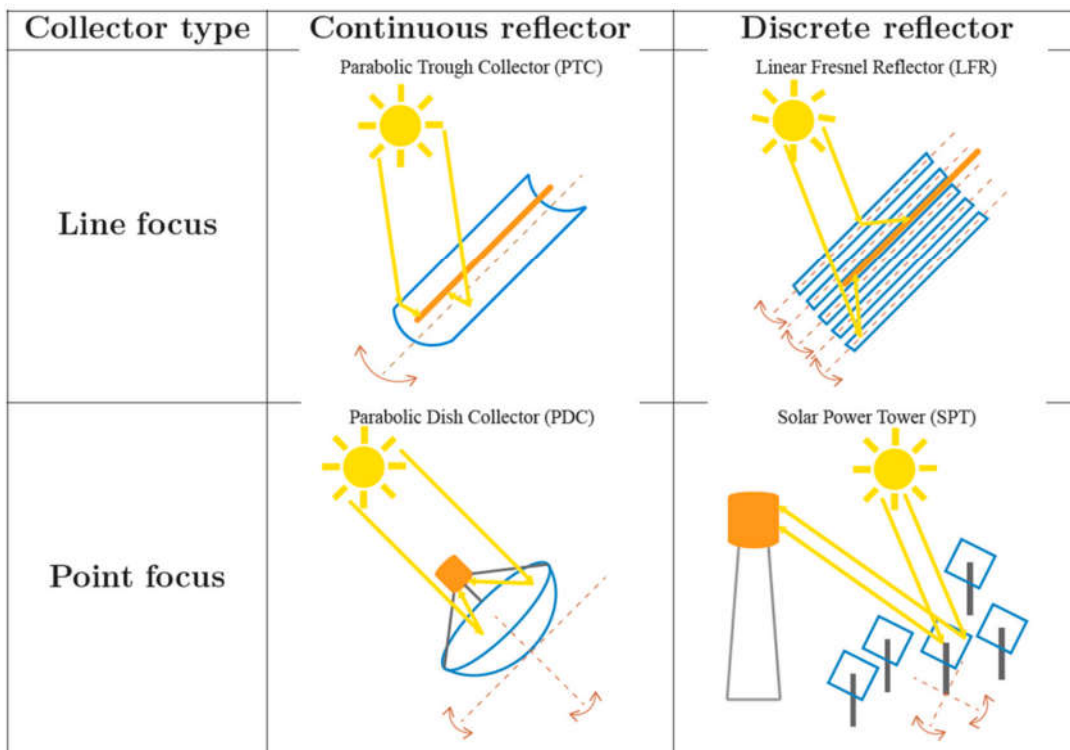


Fig.12 CSP types [15]

Linear Fresnel Reflectors (LFR) is also quite similar to PTC. However, here sunlight is being focused by an array of mirrors onto the focal line.

Parabolic Dish Collectors (PDC) is the type of CSP system where the solar ray is concentrated onto the focal point of the dish. This CSP is quite different from the perspective of power conversion. It uses Stirling engine rather than turbine technology to harness electricity.

Central Receiver System (CRS) or Solar power tower (SPT), the system where the heliostat field reflects solar radiation onto the receiver that is located on the top tower, therefore solar concentration becomes higher in this configuration.

On [Fig.13], you can see the different generations of CSP systems. It summarizes the main characteristics of systems of its generation.

As you find out, CRS is the only system that is capable of providing high-quality thermal energy, which is required by our DAC plant. Therefore, the scope of the current paper will be specifically about the integration of CRS and DAC system.

Generation	1 <sup>st</sup> gen.	2 <sup>nd</sup> gen.	3 <sup>rd</sup> gen.
Receiver outlet temp.	~250 - 450°C	~500 - 565°C	~720°C Expected to be >700°C
Typical plant or technology	PTC, SPT, LFR   	PTC, SPT, LFR   	PDC 
Heat transfer medium	Oil or steam	Steam or salt	Gas Salt Particle Gas
Thermal energy storage	Early designs: No or small Recent designs: Yes	Early designs: No or small Recent designs: Yes	No Yes
Power cycle	Steam Rankine cycle	Stirling	Brayton cycle
Peak temp. of cycle	~240-440°C	~480-550°C	~720°C Expected to be >700°C
Design cycle eff.	~ 28-38%	~ 38-44%	~38% Expected to be >50%
Annual solar-electric eff.	~ 9-16%	~ 10-20%	~ 25% ~ 25-30%

Fig.13 Generations of CSP plants [34]

Moreover, must be paid attention to the types of CRS. In fact, the CRS system also is divided into different types which are differentiated by the medium which is used to transfer the energy, heat transfer fluid (HTF), as well as on power cycle. Evidently, [Fig.13] gas Brayton cycle of CRS is the only option that is capable to fulfill the requirements of the DAC system [1]. CRS system that runs on Steam ranking cycle operates in the considerably lower temperature range from 200 to 550 C, whereas the third generation of CSP can provide the heat on the required temperature level.

#### 4.2.1 CRS receivers

The main part of CSP systems that assign or oppose the upper-temperature limit on a thermodynamic cycle of the plant is the receiver. Moreover, since our DAC system specifically requires energy around 900 degrees, the elaboration of the topic of solar receivers is vital for this thesis.

Next, it will be discussed the state of art in the field of CRS receivers, the types of them, temperature limits, materials, as well as commercial maturity.

CRS receivers are divided into 3 general types:

Tubular receivers

External receiver

Cavity receiver

Volumetric receivers

Open volumetric receiver

Pressurized air receiver

Solid particle receivers

Direct particle heating

Indirect particle heating

#### Tubular receiver

Tubular receivers are the most widely spread type of receivers [11]. Tubular receivers can be of two types: external and cavity. The external receiver is pictured in [Fig.14]. This type of receiver is usually shaped in cylindrical form, so the absorbing surface is to be seen from all directions.

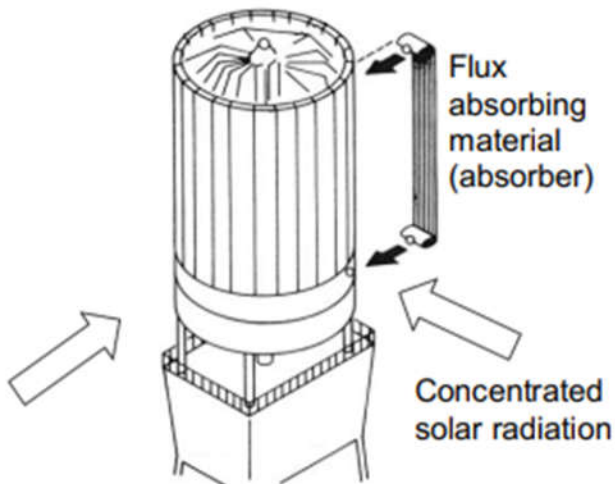


Figure 14. External tubular receiver [c]

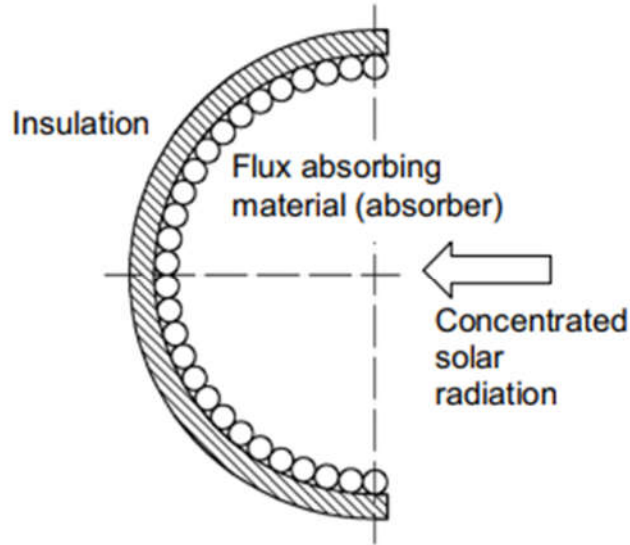


Figure 15. Tubular cavity receiver [c]

Whereas, cavity receiver types of receivers are characterized by absorbing surfaces to be located within a cavity [Fig.15].

Moreover, heat losses also differ very much in favor of cavity receivers.

Cavity receivers are most likely to play a role when the required temperature is very high ( $T>1000K$ ) [12]. Hence, it has great potential in solar Brayton systems [13][14]. In tubular receivers, it can be observed [Fig.14] [Fig.15], the wall works as an absorber. Therefore, the physical limitations of the absorber material are a crucial factor. It poses the limit for flux intensity, which in turn means the limitation on maximum temperature. In recent years, there has been a lot of research on allowable incident flux, as well as operating temperature [15][16][17].

On the other hand, the most recent works conducted in the field of cavity receivers are directed toward the optimization of flux distribution across the surface of the absorber and compete with the heat loss that happens due to convection. Moreover, except for the limitation opposed by the absorber material, another drawback of tubular and cavity receivers includes is a heat transfer effectiveness, when the temperature increases the heat

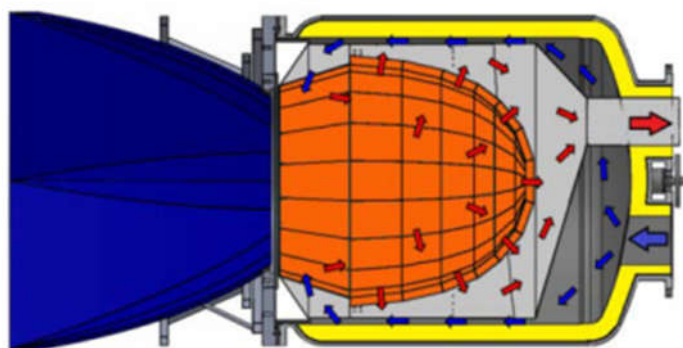


Figure 16. Volumetric air of Soltrec [17]

loss due to convection and radiation adds up as well, which makes it difficult to work under ultra-high temperature [16-17].

### Volumetric receiver

Presently, one of the best alternatives to tubular receivers is a volumetric receiver. Volumetric receivers offer a possible solution to overcome the limitation posed by tubular receivers and make it possible to decrease the heat losses by changing the concept of absorbing solar irradiation[16-17][Fig.16]. In volumetric receivers, the concentrated solar radiation is absorbed inside the volumetric foam material, as shown in [Fig.16]. The foam works as a trap [15] for solar radiation, as a result, it lessens the losses due to reflection and thermal losses. Consequently, its absorbance efficiency can be higher than 75% [20], whereas cavity receiver efficiency works in the region of 40-50% [. The volumetric foam is usually made of porous ceramic [Fig.17].

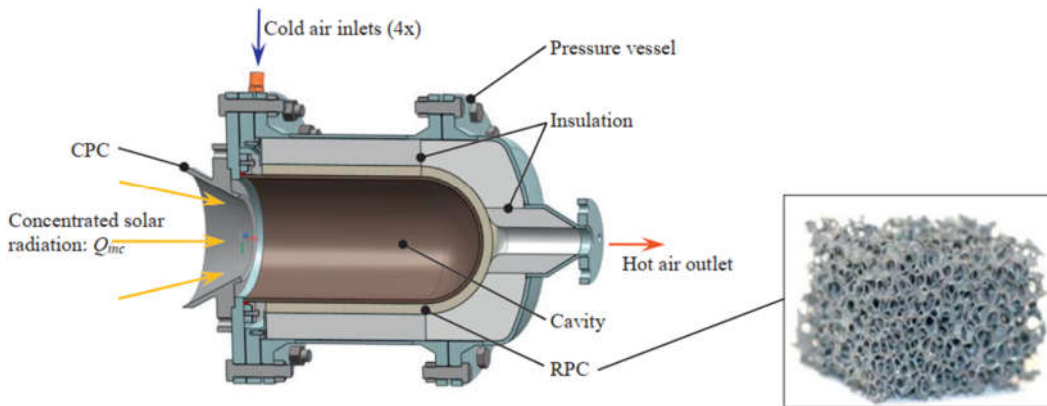


Figure 17. Section of solar volumetric air receiver made of SiC RPC foam [35]

The volumetric receiver can operate both at atmospheric pressure, this type of receiver is named an open volumetric air receiver. Alternatively, it can operate under pressure higher than atmospheric [17], such type of volumetric receiver is called a pressurized air volumetric receiver. To make it possible to work under higher pressure, they are equipped with a quartz window. The quartz windows have to be as thin as possible, but also they have to be strong enough to work under high flux and pressure.

Volumetric air receivers are capable to reach over 1000 C temperatures [35,17]

### Particle receiver

Another alternative solar receiver is named particle receiver. Unlike conventional solar receivers where Molten salt, water, or air operates as HTF that is being heated inside the receiver, the current receiver uses small solid particles that directly or indirectly are heated as it falls inside the receiver. Interestingly, the particle receivers can be integrated with thermal storage system [Fig.18]

In contrast to conventional receivers, solar flux density limitation almost doesn't exist in the case of direct particle receivers since sun ray is directly absorbed by heat transfer particles. The power capacity of a single tower ranges from 10-100 MW, mainly limited due to the technical challenges related with uplifting particles to very high towers [41].

In [Fig.20] can be observed indirect type of particle receiver. The receiver represents itself, a stack of tubes that are irradiated from inside, then particles falling and slides between the tubes are heated. Yet, small-scales tests were conducted, and it showed that heat transfer was limited by the locations, where particles lose contact with tubes. The advantages compared to free falling direct receiver, the issue with loss of particle through open aperture doesn't exist

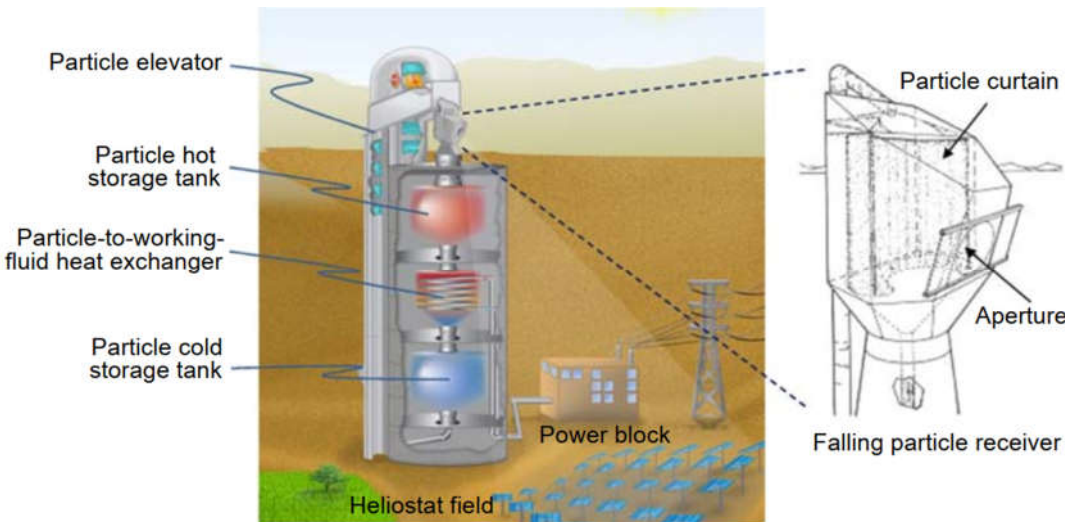


Figure 18. Falling particle receiver system with integrated storage and HEX [41]



Figure 19. Falling particle receiver testing. National Solar Thermal Test [41]

Another direct particle receiver is a fluidized bed particle receiver. As the suggests, the particles are fluidized by pumping gas into the receiver. In [Fig. 21], it is illustrated the testing conducted by the Chinese Academy of Sciences [41], where solid particles are placed inside the quartz tube and blown by air from the downside, so particles are suspended. The results are shown, that the temperature of air reached 600 C, and the difference between particles and air was 10 C, which shows a good heat transfer among solid particles and air.

Moreover, interestingly, another type of fluidized particle design exists, which is extremely relevant to the topic of this thesis. In [43], it is elaborated a new design of particle receiver where CaCO<sub>3</sub> particles, using a vortical flow of air, are fluidized in a conical-shaped receiver

[Fig.22]. The receiver is closed by a very thin quartz window that isolates pressurized air inside the receiver. Basically, the receiver functions as Calciner by activating the calcination reaction and heating the air. The temperatures gotten using this method are very promising exceeding 1300 Celsius [44]

[Table 3] shows the summary of particle receivers by their types, as can be seen in general operates at very high temperatures, and especially the fluidized bed receiver

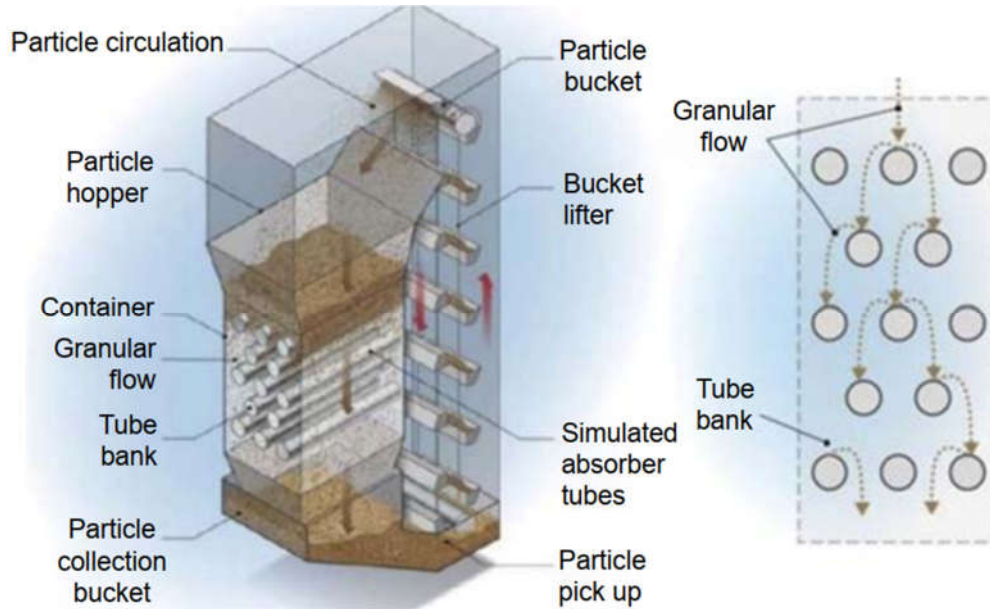


Figure 20. Indirect gravity-driven particle receiver [41]

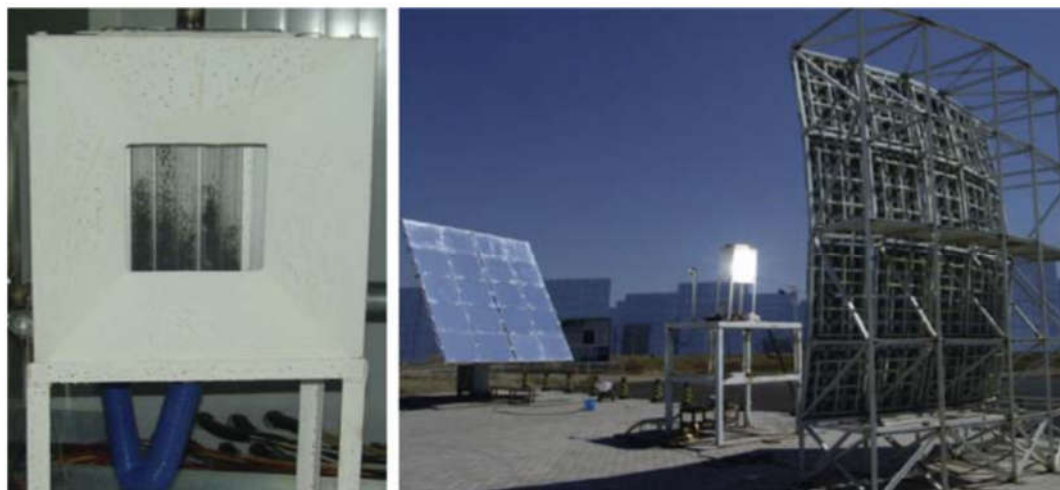


Figure 21. Images of testing of a quartz-tube particle air receiver [45]

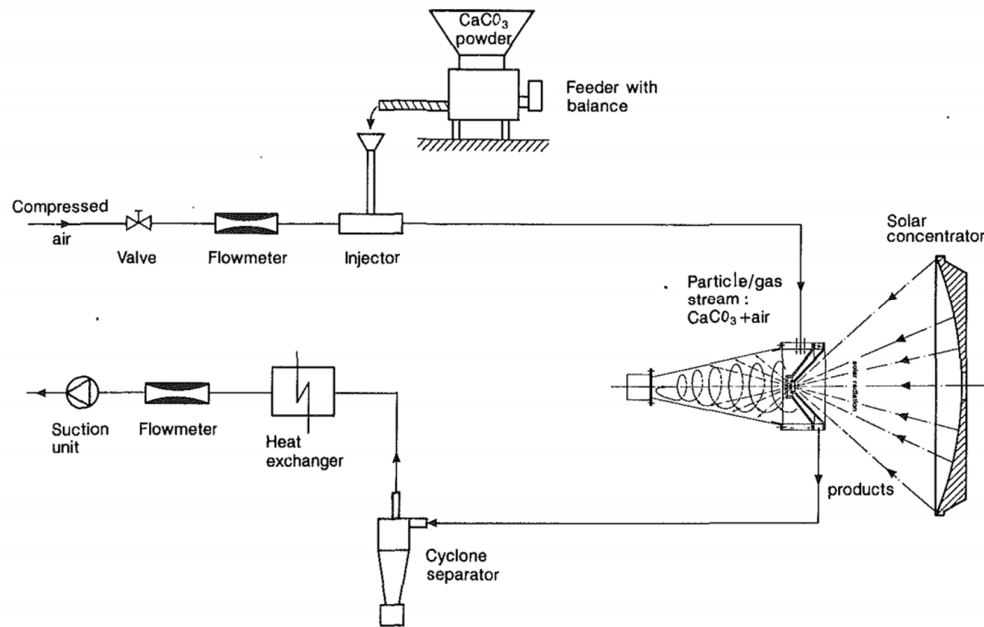


Figure 22. Canonical fluidized bed receiver [43]

Direct particle receivers	
Free-falling	>700°C/50–80%
Obstructed	>700°C/60–90%
Rotating kiln/centrifugal	900°C/75%
Fluidized bed	>1000 °C/20–40%
Indirect particle receivers	
Gravity-driven flow in enclosures	No data available
Fluidized flow in tubes	750°C/thermal efficiency not reported

Table 3. Particle receivers summary [41]

#### 4.2.2 Technical challenges with receiver and integration with DAC

The integration of CSP and DAC has raised some big challenges. Specifically, the delivery of heat using CSP or using fuels (coal, methane, etc.), from chemical and physical perspectives diverges very much. Whereas in CSP, HTF is used to deliver the heat, in the combustion of fuel, the heat is directly delivered to the point without any transferring media, moreover, the temperature of the flame when methane burns is over 1800 C [50].

Due to the limitations posed by the current state of CRS technologies, the possibility to raise the temperature over 1000 C, is a very big challenge.

Preliminary analysis has shown that to fulfill the requirement of the DAC plant to provide heat at temperature around 900 C, the HTF mass flow rate must be higher than 700 kg/s,

even in the most optimistic scenario, since the temperature difference that CSP may provide at such high temperatures is small. If we assume  $T_1$  = somewhat between 1000 and 900 C

$$Q_{csp} = m_{htf} * C_p * (T_1 - T_2) = m_{htf} * C_p * (T_1 - 900 \text{ C}); \quad (4.5)$$

$$m_{htf} > 700 \text{ kg/s}$$

Considering the height of solar towers, which sometimes reaches 200 meters, the delivery of such a big mass flowrate to 200 meters height 24/7, even not considering the sizes of pipes that have to be used to transfer such flowrate, it seems very doubtful.

Importantly, the absence of research articles studying the issue of delivering such a big flowrate into a receiver, and any mentions of such a flowrate in papers investigating the solar receiver [15], led to the conclusion of technical invalidity of building single tower CRS system with such technical parameters.

Considering the state-of-the-art of solar receiver, three solutions may be proposed:

1. To divide the HTF flow rate into smaller flows.
2. Increase the outlet temperature from solar receiver over 1000 C.
3. Integrate the Calciner inside the Solar receiver, run the calcination using Fluidized particle receiver [43-44][Fig.22].

Since this thesis seeks the ways to hybridize DAC/CSP system using commercialized technologies.

The 2<sup>nd</sup> and 3<sup>rd</sup> solutions are not possible achieve yet due to the *presence of quartz window* both in Fluidized particle receiver and pressurized volumetric receivers.

As we went through types of receivers, it may be seen that direct-irradiation receivers (pressurized volumetric air and direct particle air receiver) offer much higher thermal efficiency and higher outlet temperature (including the possibility of DAC inside receivers). It would be wise to consider these types of receivers for the integration. However, since the DAC system requires the isolation of captured CO<sub>2</sub> from the surrounding [2], a quartz window-equipped receiver will have to be the option to consider for the integration.

The quartz window as it has been discussed before is a very brittle component. Since quartz windows work under the ultra-high flux of solar irradiation (around 3000 suns [17]), the impurities and defects of the glass even in the micro-level are extremely harmful and significantly impact the life of the windows. Therefore, there is still a challenge in the commercialization of these types of receivers due to these manufacturing complexities [18]. Moreover, the economical and technical assessment of these receivers is hardly possible to find in public access, most of them in experimental laboratories, but not in commercial projects.

So, the 2<sup>nd</sup> and 3<sup>rd</sup> solution yet needs research and development, which doesn't comply with the aims of the thesis.

Finally, the 1<sup>st</sup> solution can the only option considering the current state of solar receivers.

Due to the problem with quartz window, the open volumetric air receiver will subsume the scope of this thesis. Therefore, the direct receiver integration for time being may not be possible with the current state of art of receivers, and it requires intensive research and development.

However, here as well another problem arises, the towers in single-tower CSP systems, are one of the most expensive parts of the CSP system [51]. The tower is very tall over 100 meters depending on the capacity of the CSP system, but usually, the systems of 100 MW and more are built with 150 meters and higher towers, which leads us to the complexities of building such towers, such high structures have to withstand the environmental variables such as wind, earthquakes. Due to that, such structures are very expensive to build and take more than 20% of CAPEX [51].

Therefore, modular CSP configuration is decided to be the optimum CSP configuration that would perfectly fit DAC requirements. It is the system, where small solar fields are built in combine with small-height cheap solar towers.

#### 4.2.3 Solar field and efficiency

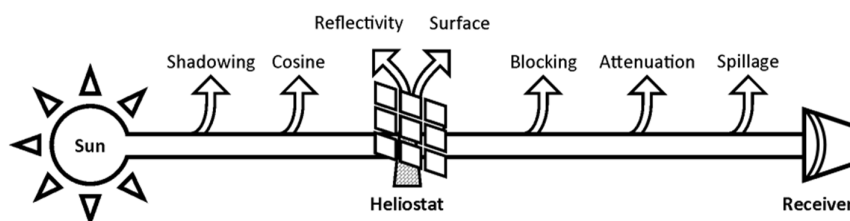


Figure 23. Efficiency flow of CSP system

$$\eta_{total} = \eta_{cos} \eta_{att} \eta_{spill} \eta_{block} \eta_{shadow} \eta_{refl}$$

- $\eta_{cos}$  – is produced when the mirror doesn't face the Sun
- $\eta_{att}$  – attenuation is caused by atmospheric scattering of light, in which light interacts with water vapor, dust, or other particulate matter and is reflected, refracted, or absorbed.
- $\eta_{spill}$  – spillage is caused when the reflected light does not reach a receiver, intercepted by something
- $\eta_{block}$  – caused when reflected light is blocked by a next mirror
- $\eta_{shadow}$  – caused when the coming sunray is blocked by a next mirror
- $\eta_{refl}$  – the power loss due to the dirtiness of mirrors

Depending on the type of receiver solar field varies. Since tubular external receivers are capable of receiving sunray from all sides [Fig.14], and cavity receivers and volumetric receivers are limited in angles, suitable solar fields will be distinct.

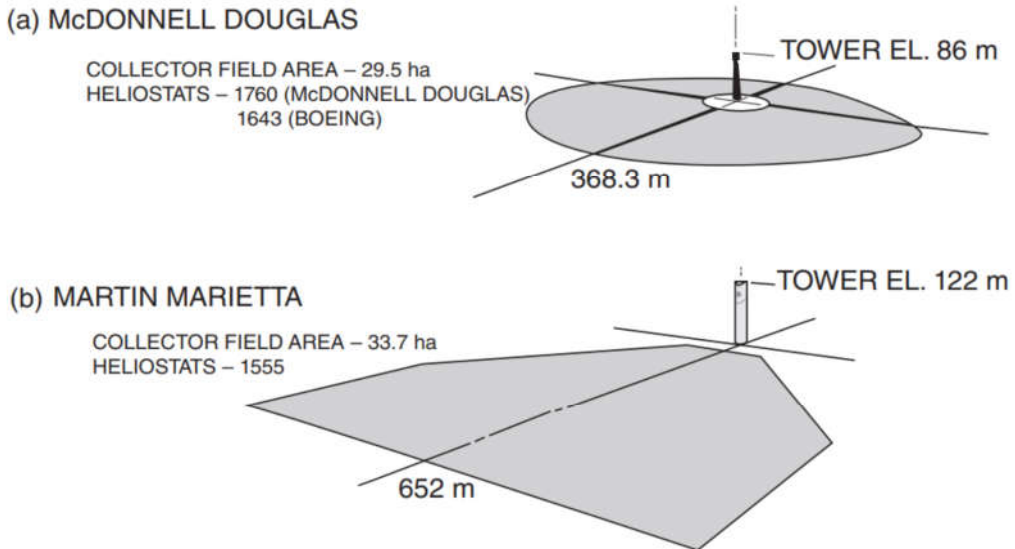


Figure 24. (a) SF for External tubular receiver, (b) SF for Cavity receiver [12]

#### 4.2.4 Modular solar plants

##### 4.2.4.1 Aora-solar

Modular CSP power plants are generally industrialized and developed by two companies: AORA-Solar, and 247Solar.

Aora-Solar is a company specializing in developing modular hybrid CSP plants. The CSP plant provided by Aora-solar is capable of using both solar and fossil fuels, to provide additional energy during the lack of sun radiation. Interestingly, the plant is able to work without TES 24/7 since it can use other fuels as well. The company's first two pilot plants were developed in Samar, Israel, and Almeria, Spain [7]. The plants are 100 kW in size and 170 kW accordingly.

The working principles of Aora-solar Tulip for 100 kW are as follows; The Tulip system concentrates solar radiation coming from an 800 square-meter field using heliostats, the air with the rate of  $88 \text{ m}^3/\text{min}$  [7] is heated up to the required temperature, to around 1000 Celsius, the inlet temperature is 600 degrees. When the coming air is not hot enough, it is heated by combusting fossil fuel.

Moreover, the plants of Aora can't operate until they are built for 100%, in contrast to conventional CSP plants. It can be explained by the specifics of the plant; Firstly, the plant is called the Aora-solar tulip for a reason, its power block, recuperator, and other components, including the firing chamber, are placed at the receiver. Also, the plant is quite

small and according to the developers, 10 units of 100 kW plant can be built every three months with 10 crews on the field, and only the limiting factor is the availability of the components.



Figure 20. Aora-solar Tulip

However, unfortunately, except for these two projects, there is not much available information about the company's advances in this field, including, also their official website is also inaccessible. However, the technical success of this concept suggests its feasibility, at least technical feasibility.

#### 4.2.4.2 247Solar

A more advanced modular CSP plant was presented by 247Solar. They stick to the conventional 3rd generation CSP.

In general, the CSP system of 247solar likewise conventional systems consists of a power block, solar receiver, and unlike Aora-solar they are also equipped with TES.

The design of the plant proposed by 247solar is for 400kW, which can be combined to get higher capacities. The thermodynamic cycle of the plant can be seen on [Fig.22]. One of the main advances of 247solar in their approach of using the high-temperature heat exchanger, which made it possible for the operation of CSP under different pressure levels.

247solar uses an open volumetric air receiver which operates under 1500 Suns. Since it is the open receiver, its operation pressure is 1 atm. The solar receiver can withstand temperatures up to 1200 degrees [8]. However, its design temperature is 970 C. Then, high-temperature air is transferred to HEX where heat is exchanged with compressed air. The compressed air then runs the turbine to produce electricity.

The tower where the receiver is mounted is a common truss tower of a height of 35 m [8][Fig.23].

Moreover, likewise Aora-solar, they are also equipped with combustor which enables to use of fossil fuels [Fig.22][8].

In February 2018, they has initiated a Collaborative Research and Development agreement with Masdar Institute in UAE to develop the first pilot plant [9].

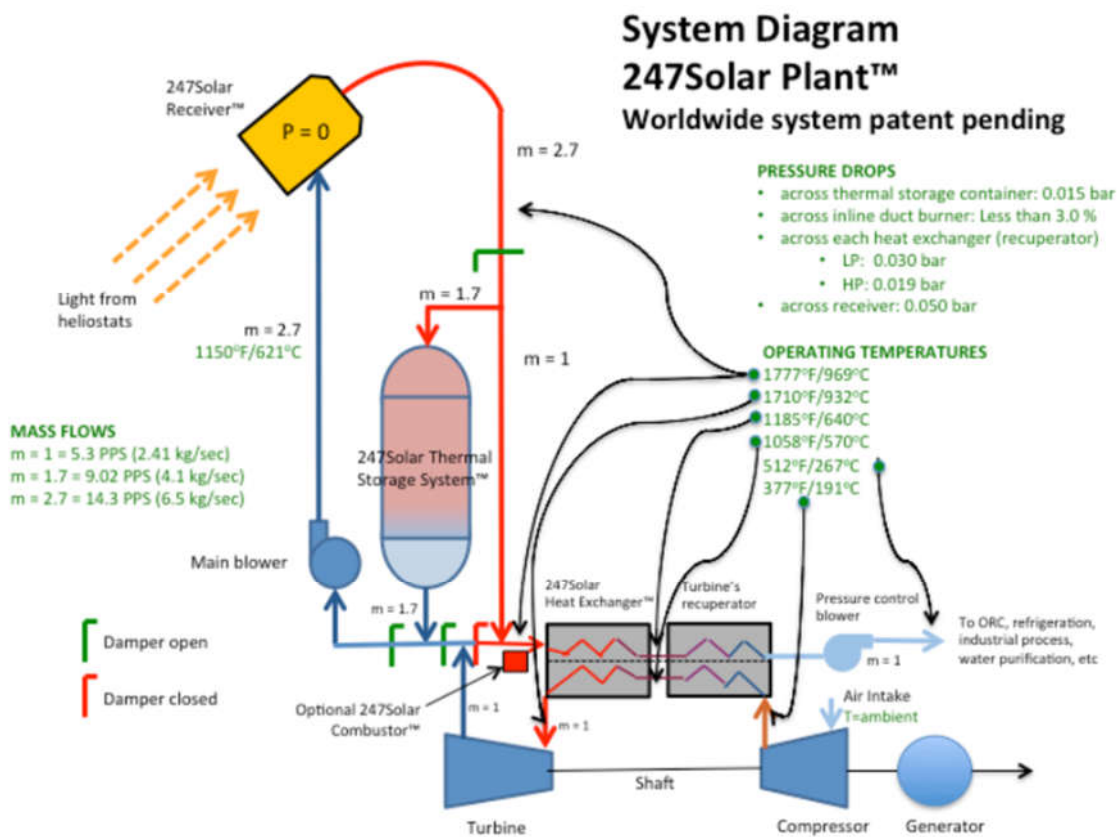


Figure 22. Scheme of 247solar

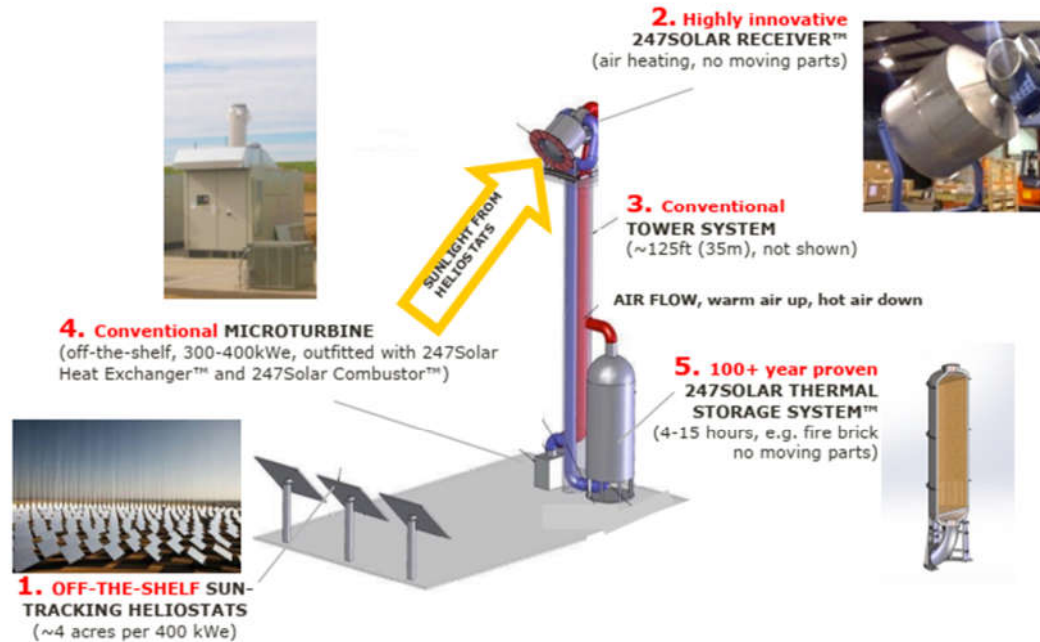


Figure 23. 247solar plant 3d model

#### 4.2.5 Heat exchanger

Initially, the heat exchangers were mostly applied in the low-temperature industry. However, the development of renewable energy technologies, and fields that utilize high temperature opened new prospects for heat exchanger applications.

Nowadays, heat exchangers can be categorized into two types by their industrial application: Low-temperature heat exchangers (LTHE), and high-temperature heat exchangers (HTHE).

As the name suggests, the temperature where these HEXs are applied is entirely different. Usually, LTHE is used for an application below 500-600 Celsius, whereas HTHE is above 600 Celsius.

Obviously, HTHE will be an objective choice considering the aims of the thesis.

HTHE technology recently regained attention. Therefore, this niche is still quite fancy, even though the technology of HEX is far more than mature.

To begin with, we go through the materials for HEX, elaborate on the state of the art of HTHE, then make the final selection choice for HTHE that will be used in our layouts.

Materials consideration:

- For HTHE, the thermal stresses during the work caused by the fluctuation in temperature can be considerable. Daily shutdown and startup may be a reason for the short life of the HEX. The material should be able to withstand thermal stresses
- Thermal capacitance [37] should minimal as possible to reduce the startup time
- High-temperature resistant, the material shouldn't degrade at high temperatures.

Usually, the most expensive part of HTHE is the high-temperature resistant material, the costs of material that can withstand over 675 Celsius increase dramatically [37].

Initially, HTHE was engineered using ceramic materials such as SiC. It is extremely thermal resistant, the working temperature is around 1600 [Table 5] Celsius. Yet, the behavior of such heat exchangers on commercial-scale production may be doubtful [8]. Therefore, high-temperature super alloys should be the option for HTHE.

On [Table 4], can be seen the details how the composition of super alloy affects its temperature range. Studying Table 4,5, it may be concluded that at least our HEX should be Nickel based, to fulfill the requirements of our thesis

In [8], 247Solar give special attention to its high-temperature HEX, noting that it is the key modification they have done to the conventional Brayton cycle CSP. As I mentioned before, HTHE is developing technology, and there is a big lack of available papers that studies this topic.

Interestingly, the application and scheme of how HEX is used in 247Solar plants precisely comply with the aims of this thesis. They used Haynes 214 for their HEX. However, unfortunately, 247Solar haven't disclosed the details of the methodology they used in sizing and quantifying it.

In their [8] white paper, they have provided HEX costs for specific powered CSP system, but the flow rate on which the system operates strongly differentiate from our system. Their system operates at 8.73 kg/s, under design condition, which makes it impossible to use their numbers in the economic analysis.

Therefore, for calculating the HTHE methodology from [37] was used. In fact, the studied topic is about recovering heat from a flue gas that is produced during calcination.

Consequently, HTHE configurations [Table.6] from [37] will be used in the economical assessment.

Temperature Range	Alloys
Up to 1202°F (650°C)	Carbon steels having <1% Cr, or steels having 1%–12% Cr and Mo up to 1%.
1202°F–1472°F (650°C–800°C)	Carbon steels and low-alloy steels, Cr–Ni–Mo steels that can contain 12%–25% Cr and 5%–25% Ni, e.g., AISI type 310.
1472°F–1832°F (800°C–1000°C)	Steels with 17%–27% Cr and Mo addition, or higher Cr–Ni–Mo steels having more than 8% Ni.
1832°F–2192°F (1000°C–1200°C)	Higher alloyed nickel- or cobalt-base alloys with 18%–35% Cr; Al additions to these alloys improve resistance to high-temperature oxidation and cyclic oxidation.
>2192°F (1200°C)	Advanced ceramics and other highly refractory material.

Source: Compiled from Kane, R.D. and Cayard, M.S., *Hydrocarbon Process.*, November, 129, 1995.

<b>Material</b>	Metallic Ni Alloys (Inconel 718)	Ceramics oxides of Al, Si, Sr, Ti, Be, Zr, B, SiN, AlN, B4C	Carbon fiber – SiC composite	Haynes 214
<b>Temperature range</b>	1200-1250 C	1500-2500 C	1400 – 1650 C	1260 C
<b>Ref</b>	[37]	[37]	[37]	[46]

Table 5. High temperatures materials

HTHE			Ref	
Allowed CO <sub>2</sub> flow	4.65	Kg/s	[37]	
Allowed air flow	4.93	Kg/s		
Maximum temp.	1200	C		
HEX type	STHE 2-4			
Material	IN 718			
Eff.	0.9		[24]	

Table 6. HTHE configuration

Since our system's flow rate is much higher than in [Table 6], HTHE will be scaled up by increasing the number of heat exchangers

#### 4.2.6 Thermal Energy Storage System (TES)

In the field of CSP, there are two types of TES that the most commonly used:

Solid media and Liquid media storage.

Liquid media storage, is sensible heat storage, which means the temperature of the medium either increased or decreased during the discharge and charge.

Usually, the storage is divided into two tanks, 1<sup>st</sup> for hot fluid that comes from CSP, and the 2<sup>nd</sup> for cold fluid, which comes from a thermal load. In such a simple way, thermal stratification is accomplished.

The medium that are used [12]:

- Saturated water (max temperature 250 C, 40 bar)
- Mineral oil (<320 C)
- Synthetic oil (<400 C)
- Nitrate salt (Molten salt) (220 C < T < 570 C)

The molten salt TES is being the widely prevalent due its conveniences. It is very cheap, works under atmospheric pressure, operates as HTF, unlike Oils very safe not flammable.

Another alternative is solid media thermal storage.

Compared to liquid mediums, rocks that are used in solid media thermal storage, have twice or thrice less thermal capacity [48]. However, the possibility to heat up to 1200 C, make this type of sensible TES, which is also named packed bed especially unique.

In packed bed, rocks or concrete is layered inside the container, HTF passing through the rocks charges and discharges the TES [Fig.24].

After all, the packed bed TES will be the objective choice for the CSP/DAC system, due to the temperature allowance and easy handling.

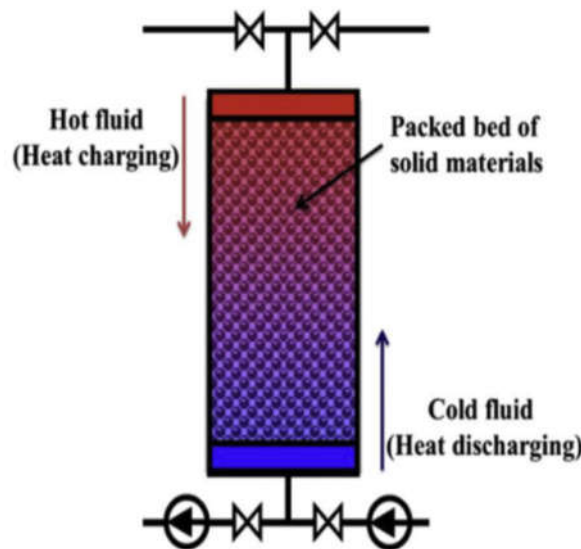


Figure 24. Packed bed TES [49]



Figure 25. Concrete storage module (400 kWh) [12]

## 5 Layouts

This section will show finished layouts and explain the approaches that were used to create layouts.

Since we are integrating modular CSP with DAC system, two approaches may be applied:

1. Using one large DAC plant and power it up with multiple modular CSP plants [Fig.26a]
2. Using small-scale DAC, building modular CSP/DAC plants [Fig.26b]

From a technical perspective, the modular approach has to be a more valid one, since a large DAC approach including pumping and merging huge mass flow-rate HTF that comes from modular CSP, that may be technically very hard to accomplish or very cost ineffective and risky.

But again, posed boundary conditions posed by publication [2], does not give such an option to rescale the DAC system. In fact, we can rescale it, yet the economical part won't give such an option. All the economics done by paper including [2], are based on 1 Mt/y boundary condition, so it isn't possible to assess the economical side of modular CSP/DAC system, for now at least.

Hence, in this thesis Large-DAC approach is used.

Next, it will be shown three different layouts of the Hybrid DAC/CSP system.

The layouts were built following the criteria:

1. The simplest system, sole CSP and DAC [Fig. 27]
2. Maximum solar fraction scenario, that will be CSP + TES (Thermal storage) + DAC [Fig.28]
3. An autonomous system, to fulfill the electrical demand of the DAC system, CSP + DAC + PB (Power block) [Fig.29]

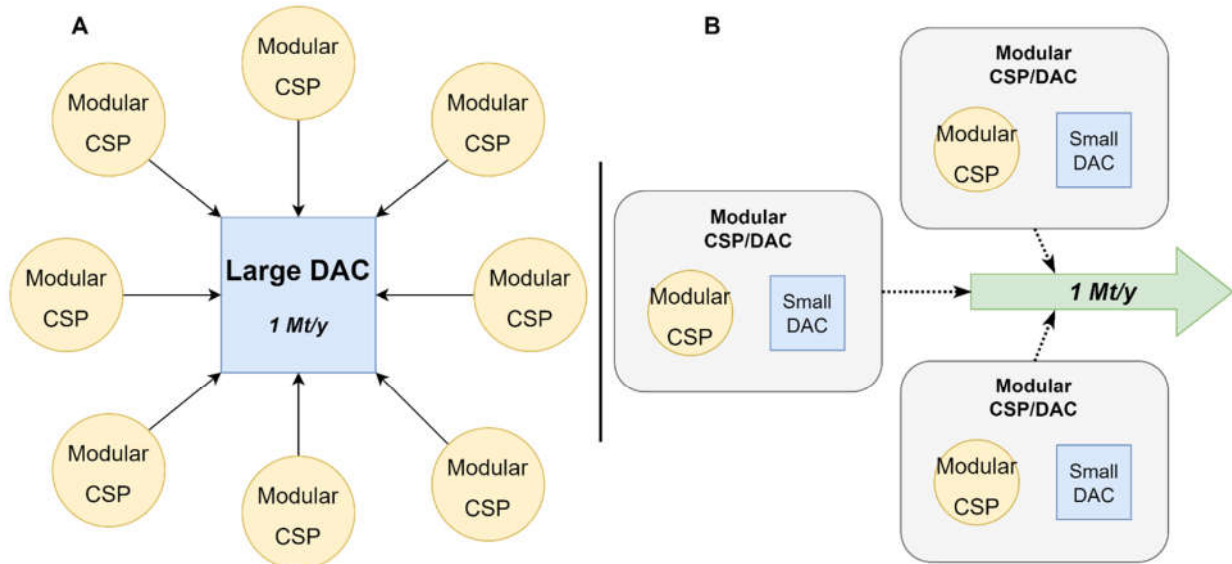


Figure 26. Integration approaches (A) large DAC, (B) Modular

## 5.1 Sole CSP (Layout A)

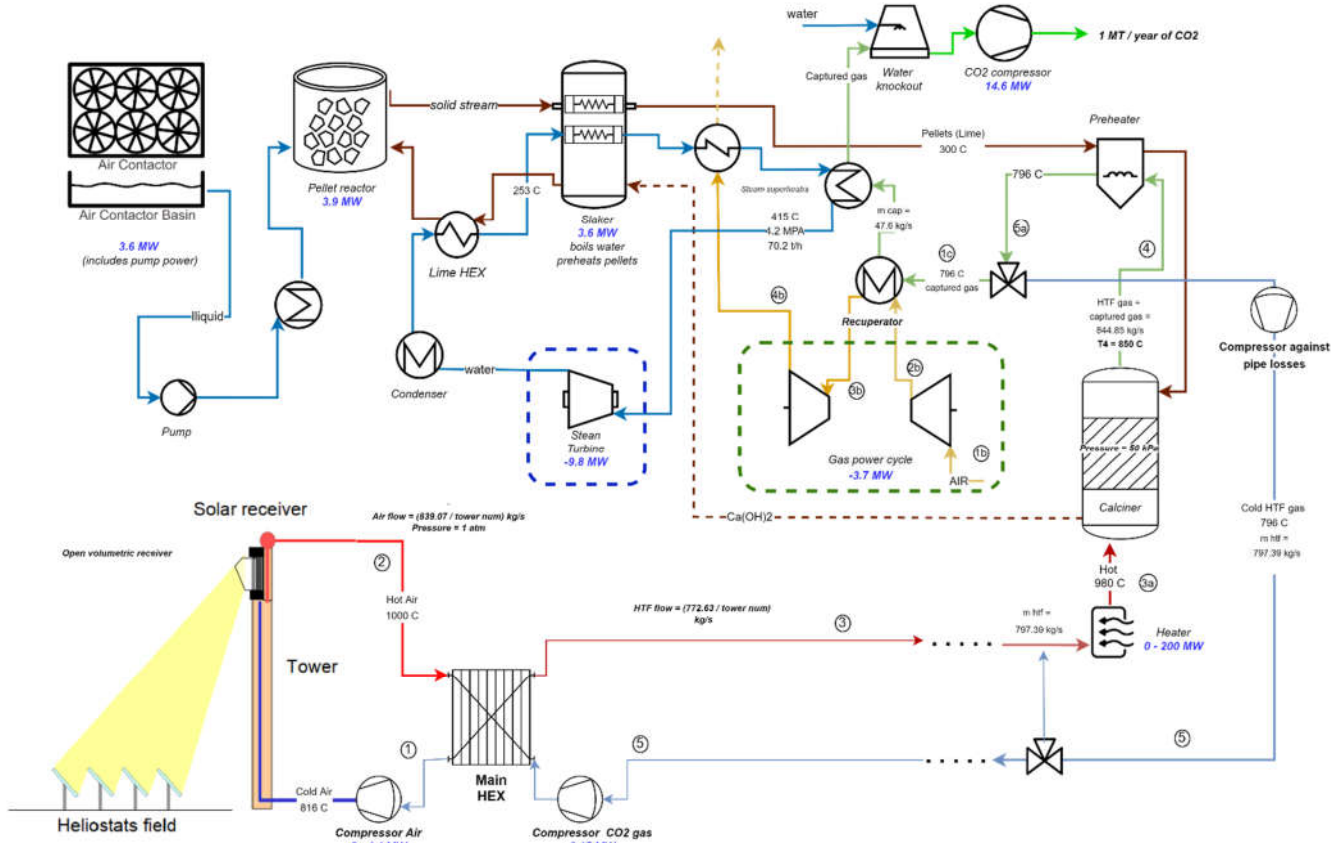


Figure 27. Layout A

In [Fig.27], it is illustrated the layout for the simplest system that doesn't include any optional parts, and solely directed to see the impact of CSP on the DAC system.

All the layouts work under a very high-temperature CSP system of 1000 C.

Heat transfer fluid in the CSP system, the air, and DAC system are isolated. To reach the isolation between the DAC and CSP system is installed HTHE, which is named Main HEX. It isolates air from the HTF flow (carbon dioxide).

This approach helped to preserve the purity of captured gas since the heat to the pellets is assumed to be delivered by direct cyclone method [52]. This option of heat delivery is considered to be the most effective as pellets are solid particles.

The dashed line on the scheme of the system on the place of integration is positioned on the place where modular CSP HTF flows' are merged.

For that reason, mass flow rates before the dashed lines are represented as  $m_{HTF} = \frac{772.63}{\text{number of towers}} \frac{\text{kg}}{\text{s}}$

As for the heater, in the original layout [2], the Calcination reaction is powered by natural gas, therefore, for the sake of simplicity, the heater will be assumed to be able to operate as a burning chamber using fossil fuels, as well as electric heater using electricity.

The valve placed below the heater operates as a by-pass that allows skipping the pressure drop when there is no solar energy. For example, at night, when the solar station doesn't work

The rest of the assumptions and technical validations will be covered in the upcoming chapter.

Moreover, in comparison to the original layout [Fig.9], some equipment are extracted from the system: ASU (air separation unit), and gas power plant with its carbon capture mechanism.

On the other hand, a new GT bottoming cycle is added to the system since the flow after pre-heater in comparison to [Fig. 9] has a higher temperature, 796 C.

Technical details, how power blocks were integrated, and how temperature distribution was calculated are covered in the next chapter.

## 5.2 CSP/DAC + TES (Layout B)

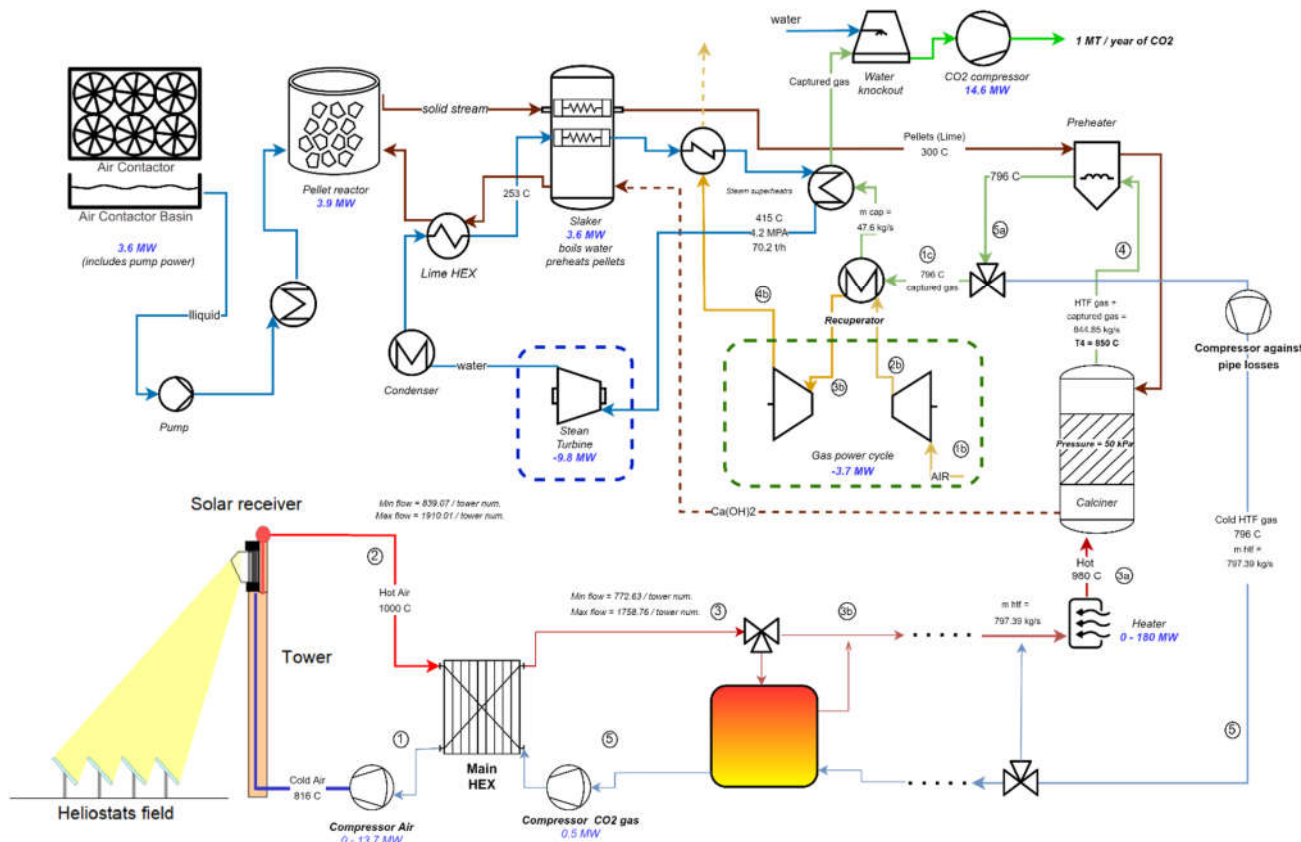


Figure 28. Layout B

This layout is very similar to Sole CSP system, except the flow rate.

The flow rate [Fig. 28], is described with maximum and minimum flow both for air and HTF because the system has TES to charge it up.

The extra solar power, is being captured by adding extra mass flow rate, which in turns is being transferred to TES via valve located above the TES. During the night or when required, cold flow passing by-pass valve enters TES and going upward discharges the TES, and when TES is discharged uses by-pass to escape the optional pressure drop from TES and HEX

As can be seen, TES is located before the dashed line, which means each modular CSP will have its own small TES.

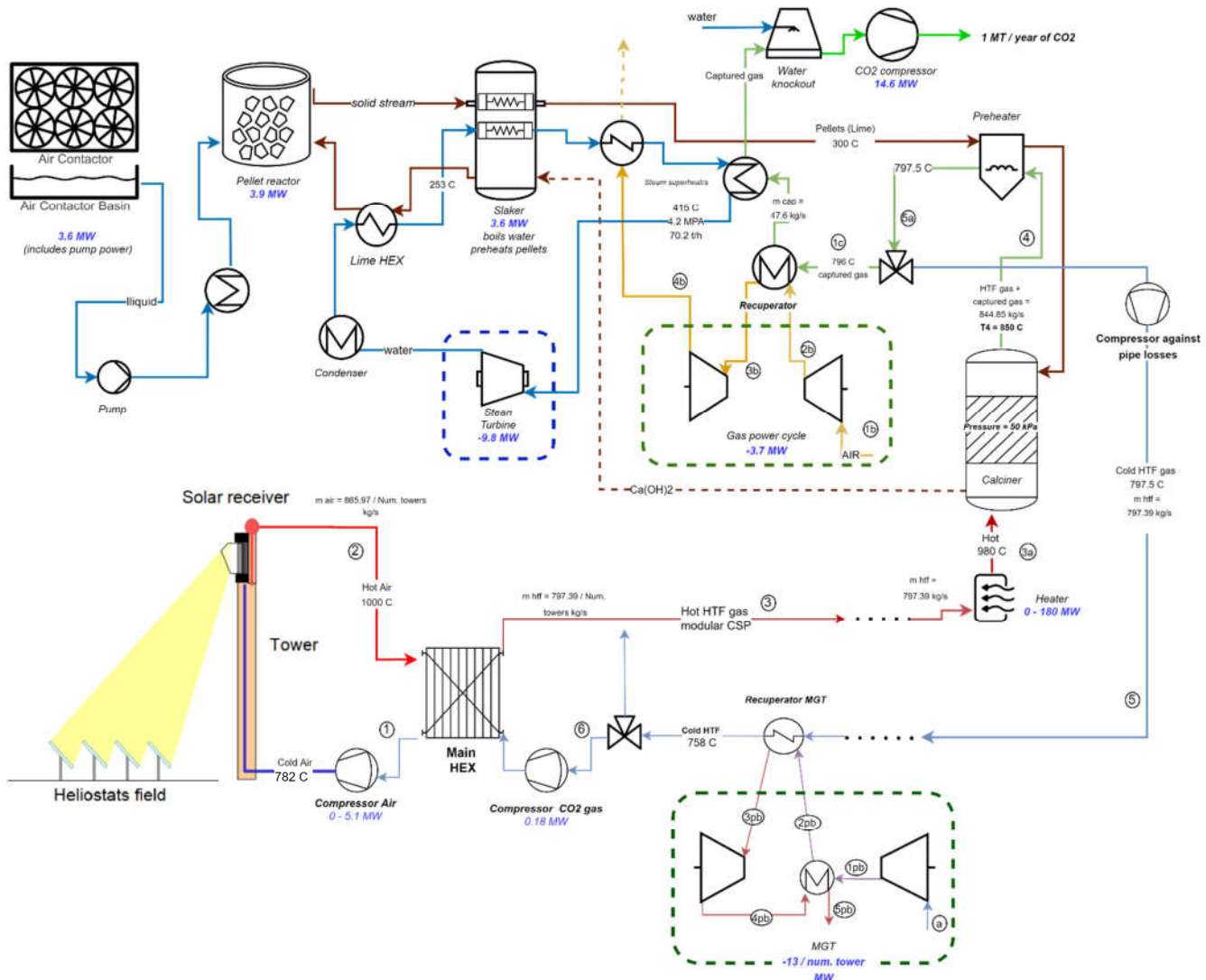


Figure 29. Layout C

### 5.3 CSP/DAC + PB (Layout C)

This layout is a bit distinct from the former layouts. Mainly, it can be found the temperature difference across the Main HEX is different. Whereas the outlet temperature is the same 1000 C, the inlet temperature of the air is lower from the former layouts.

Moreover, since the energy from CSP is also covering Power block heat demand, naturally that leads to lower temperatures for HTF. Consequently, higher mass flow rates [Fig. 29].

The power block is located inside the modular CSP system. Such an approach was taken, for the following reasons:

1. The merged flow rate is huge, which means an expensive huge Heat exchanger had to be used to power up the power block
2. The practice has shown, that the temperature of incoming HTF is not very high, therefore, a small pressure ratio GT is more efficient. Small pressure ratio gas power turbines usually are similar in technical aspects to Micro gas turbines (MGT). MGT is usually a turbine with power up to 300 kW, whereas our PB works on MW scale.

### 5.4 Operation strategy

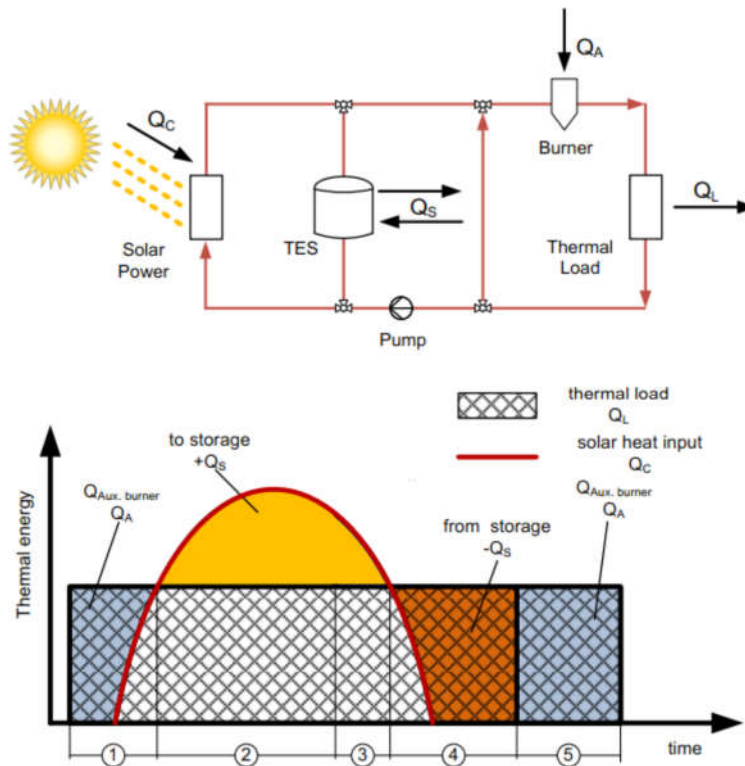


Figure 30. Operation strategy for Layout B

The operation strategy can be observed in [Fig.30]. It is assumed that the DAC plant will work 100% capacity. So during the lack of thermal energy, at night, energy is taken from

TES, and the rest is covered by the energy for an external. In the case of Layouts A and C, all the parts outside the dome will be covered by an external energy source.

## 6 Model description

This chapter discusses the challenges that may occur with hybridization the DAC with CSP, and their possible technical solutions based on the state of art of CSP technology, providing the relevant technical validation from recent researches done in that specific fields.

The chapter is structured as follows:

- Integration
  - Heat delivery analysis (*discusses the distinction between solar heat and combustion chamber*)
  - Temperature analysis (*the calculation procedure of the temperature distribution*)
    - For Layouts without PB
    - Layout with PB
  - Power island (*discusses the inclusion of bottoming cycle*)
- Model preparation (Introduces the assumptions used for modelling)
- Modular CSP (*discusses the steps done to optimize the modular CSP system*)
  - Receiver and Solar field
  - Tower and final CSP plant

### 6.1 Integration

#### 6.1.1 Heat delivery analysis

In [Fig. 31], it is illustrated the part of DAC layout that will be modified to fit the requirements of a CSP plant.

Determination of the temperature difference for the CSP system can't possibly be straightforward because the delivery of heat in [2] is done by burning natural gas, which we have briefly discussed in the literature review.

Moreover, since there are pellets in [2] coming from the pre-heater with temperature of 650 degrees. Since the pellets become chemically active reaching only 900 C, the pellets indeed heated up to 900 C, which is emphasized in the publication, yet they are including it as the efficiency of the calciner.

For that reason, it was supposed to be wiser to consider only the nominal energy of the calcination reaction for integrating with CSP.

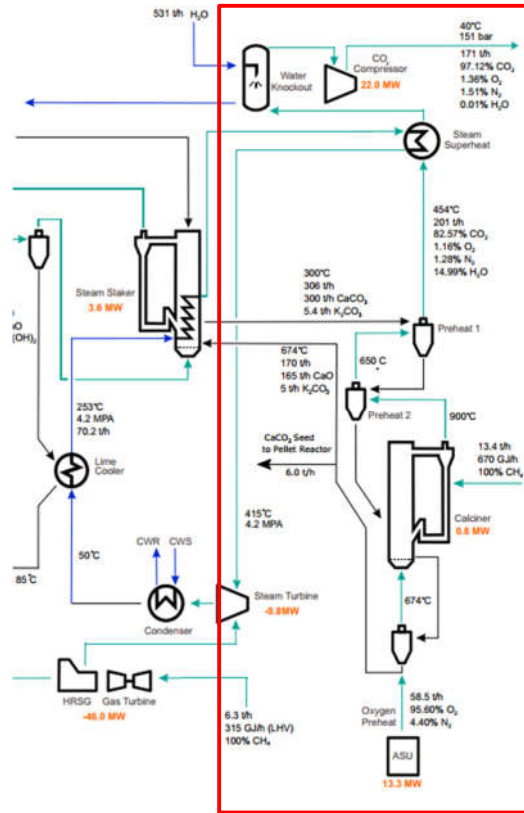
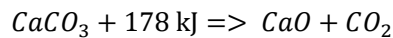


Figure 31. Part of DAC system that is modified [2]

The chemical reaction in the calciner is described by the equation (4.3), for convenience it was repeated below:



To produce 1 mole of quicklime and carbon dioxide from limestone, it is required under ideal conditions to deliver 178 kJ. In other words, since the molar mass of limestone = 100 g, it is  $1.78 \frac{\text{kJ}}{\text{g}(CaO_3)}$

Similarly, it can be converted to the following values:

$$\begin{aligned} Heat &= 1.78 \frac{\text{kJ}}{\text{g}(CaO_3)} = 3.178 \frac{\text{kJ}}{\text{g}(CaO)} = 4.04 \frac{\text{kJ}}{\text{g}(CO_2)} \\ Power &= \frac{4.04 \frac{\text{kJ}}{\text{g}} * 1 \text{ Mt}}{8760 \frac{\text{h}}{\text{y}} * 3600 \frac{\text{s}}{\text{h}}} = 128 \text{ MW} \end{aligned}$$

The quick lime application in the industry is widespread, from cement production to the food industry. Consequently, the chemical reaction of limestone decomposition is very well studied.

Usually, in the industry, rotary kilns [Fig. 32], fluidized bed reactors, and furnaces [23] are used for calcination.

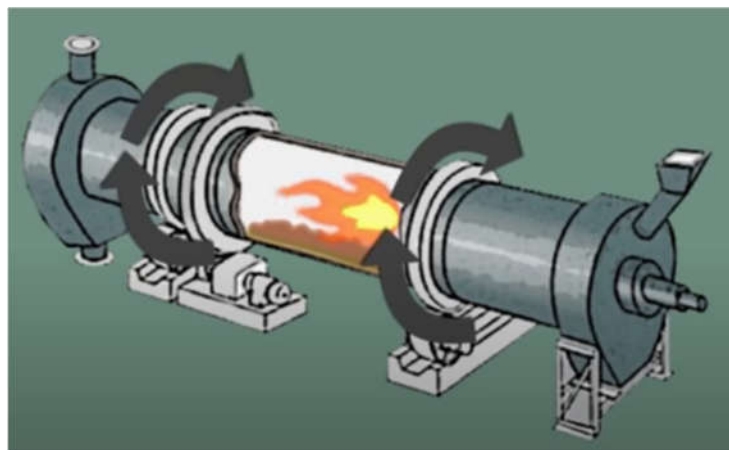


Figure 32 Rotary kiln used for calcination [38]



The furnaces and kilns can operate with different kinds of fuels. However, the layout proposed [2] assumes to work methane or also named natural gas

The burning of methane, it can be observed, produces a huge amount of energy under the remarkably high temperature of over 1600 Celsius [25]. Moreover, besides the temperature, as we emphasized methane releases a huge amount of energy, and it happens momentarily, therefore, the power density of the reaction is huge and it is under desired temperature level for calcination to proceed. Hence, for conventional kilns, the elaboration of the specifics of the calcination chemical reaction does not carry much significance.

Yet, for CSP it is important since the temperature difference, as well as the power density, matters much because power requirement directly affects the parameters of the system.

In fact, the mass flow rate may become immensely huge if we consider several degrees of temperature difference. For example, for 850 - 905 temperature difference. In other words, HTF comes enters the Calciner at 905 C and leaves at 850 C, in this range of temperature the required energy for the reaction is delivered

Delivering the 128 MW power would lead to an air mass flow rate of several tons per second, which is economically and importantly technically infeasible.

$$\text{mass flow rate air} = \frac{128 \text{ MW}}{h_{905} - h_{850}} = 1994.3 \frac{\text{kg}}{\text{s}}$$

Fortunately, the calcination reaction does not require specifically the heat of 900 Celsius. As it turns out, actually the temperature threshold posed in papers is somewhat misleading [21].

In [Table 7], it can be observed that the reaction may proceed under different temperatures [22]. The partial pressure of CO<sub>2</sub> above 550 Celsius increases reaching the atmospheric pressure at 898 Celsius and getting even higher as the temperature increments. In other

words, the temperature of activation decreases as pressure decreases similar to the boiling of water.

As can be seen in [Table 7], the calcination reaction may follow under different temperatures, even at 750 Celsius. However, the pressure of the chamber has to be vacuum pressured down to 9.3 kPa, which is technically hard to accomplish.

Taking into account all the facts, our layout was decided to operate being under-pressured down to **50 kPa**. So the required temperature for calcination reduces down to **850 Celsius** and onwards. That considerably diminished the mass flow rate.

P (kPa)	9.3	14	24	34	51	72	80	91	101	179	901
T (°C)	748	777	800	830	852	871	881	891	898	937	1082

Table 7. Activation temperature of Calcination with partial pressure [22]

### 6.1.2 Temperature analysis

In [Fig. 27] can be observed, the DAC system and CSP system are isolated from one another

It might be explained by the following motives:

1. The preservation of the purity of captured Carbon dioxide gas. HTF of CSP, which is air, should flow in separate cycles as for the possibility of mixing to be nonexistent. Moreover, the HTF of the DAC system has to be the content as captured gas.
2. The usage of a single HTF inside the CSP and DAC is impossible due to the fact:
  - The receiver has to be closed, and a quartz window is required, which is infeasible for this moment, as was covered in the literature review.

Identifying the temperature distribution across the system, can't be straightforward from now on, due to the requirement of HEX implementation that would isolate two HTF flows.

As for determining the temperature at points of layouts A-C, the following [Table 8] HEX is being used that is validated using the shown references.

Main HEX specification		Ref
Mass flow CO <sub>2</sub>	4.65 kg/s	[39]
Mass flow Air	4.93 kg/s	[39]
Efficiency	90 %	[19,24]
Pressure drop hot side	2.7 %	[24]
Pressure drop cold side	1.3 %	[24]

Table 8. Main HEX parameters

$$eff = \frac{Q_{actual}}{Q_{max}}; \quad (6.2)$$

$$Q_{actual} = m_{air}c_p \text{air}(T_2 - T_1) = m_{gas}c_p \text{gas}(T_3 - T_5); \quad (6.3)$$

$$Q_{max} = C_{min}(T_2 - T_5); \quad (6.4)$$

Since this thesis includes the modeling of several layouts of DAC/CSP system. The mass flow rate regulation method has to be defined too. For example, layouts A and C work under a constant flow rate, whereas layout B includes TES, hence, for TES to be charged, which draws an additional mass flow, hence, pumping more HTF into the system.

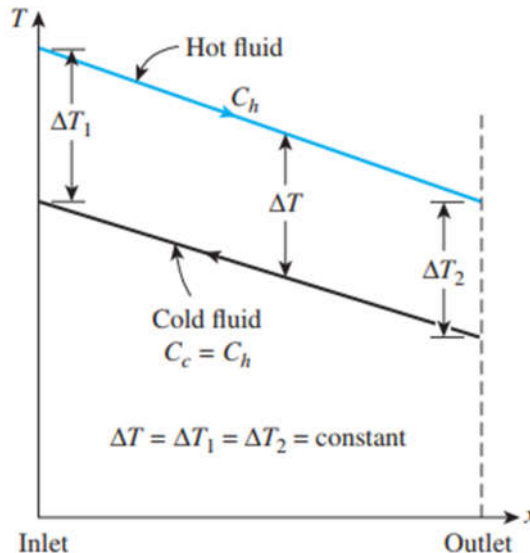


Figure 33. Heat exchange under constant capacity rate

As the heat-exchanging fluids are different substances, their enthalpies act to the temperature change in a different way.

In ideal, it had to be used LMTD method to calculate the temperatures. However, to simplify the process, the following assumption was made:

- Capacity rates (C) of both of the HTF fluids (**air** and **HTF** (of DAC)) [Fig.m1] to be identical.

$$C = c_p \text{air} m_{air} = c_p \text{HTF} m_{HTF}; \quad (6.5)$$

Under such condition, the temperature change in both fluids will be constant [Fig.14]

$$T_5 = T_1 + T_{pitch} \quad (6.7)$$

$$T_6 = T_1 + T_{pitch} \quad (6.7a) \text{ (Layout C)}$$

$$T_3 = T_2 + T_{pitch} \quad (6.8)$$

Hence, the efficiency of HEX (can be expressed as follows:

$$eff = \frac{Q_{actual}}{Q_{max}} = \frac{T_3 - T_5}{T_2 - T_5} = \frac{T_2 - T_1}{T_2 - T_5};$$

$$T_2 = 1000 \text{ C}; \quad 0.9 \geq \frac{T_3 - T_5}{1000 - T_5};$$

$$0.1 T_5 \geq T_3 - 900; \quad (6.9)$$

$$0.1 T_6 \geq T_3 - 900; \quad (6.9a)$$

This equation (eq. 6.9) can't be solved analytically. Hence, the iterations should be done to find the roots of the current equation. For that, the python language has been applied.

Before going into coding, another crucial part of the DAC have to be investigated, the Pre-heater.

### 6.1.3 Pre-heaters

The temperature at points T5 (and T6 for layout C) and T3 are codependent as was shown by equation (eq. 6.8). Therefore, here is described the used methodology for the calculation of the temperature at points 1, 3, and 5 [Fig. 27]

First of all, according to our layout A-C [Fig. 27-29], the pellets that are coming from the slaker should be pre-heated up to 850 C. Yet, we don't know the efficiency of the pre-heaters.

In [2], the efficiencies of pre-heaters are not mentioned, so it has been manually calculated. If we remember pellets in [2] are preheated by outgoing gas from 300 to 650 C.

$$Q_{preheat} = C_{pellet}(650 - 300); \quad (6.10)$$

The content of the flow that is coming from the Slaker is following [Fig. 9]:

Tc	300	C	[2]
m CaCO <sub>3</sub>	83.33	kg/s	[2]
m K <sub>2</sub> CO <sub>3</sub>	1.5	kg/s	[2]
m all	84.83	kg/s	[2]
C <sub>p</sub> CaCO <sub>3</sub>	834.3	J/kg K	[25]
C <sub>p</sub> K <sub>2</sub> CO <sub>3</sub>	827.7	J/kg K	[26]

Table 9. Flow content coming from the Slaker

Since the flow is mostly solid, the specific capacities are assumed to be constant in the range of 300 C - 850 C.

$$C_{pellet} = c_{p\ CaCO_3} * m_{CaCO_3} + c_{p\ K_2CO_3} * m_{K_2CO_3} = 70763.77 \frac{J}{K} \quad (6.11)$$

Outgoing gas content:

CO2	97.13%
O2	1.36%
N2	1.51%
TA	900 C
TB	650 C
TD	454 C

Table 10. Captured gas content

$$h_x = \%_{CO_2} * h_{x CO_2} + \%_{O_2} * h_{x O_2} + \%_{N_2} * h_{x N_2}; \quad (6.12)$$

The enthalpies at points [Fig.9] A,B,D were calculated using CoolProp plugin in excel and applying the equation (eq. 6.12):

hA	1914192	J/kg
hB	1562974	J/kg
hD	1303487	J/kg

Table 11. Enthalpies of captured gas

For simplification, the efficiency of pre-heaters is calculated using the following equation (eq. 6.13), rather than using HEX efficiency equation:

$$eff_{in} = \frac{Q_{pellet}}{Q_{gas}}; \quad (6.13)$$

$$eff_{in1} = \frac{C_{pellet}(450 - 300)}{H_B - H_D} = \frac{10.61 \text{ MW}}{14.41 \text{ MW}} = 0.736 = 73.6\%$$

$$eff_{in2} = \frac{C_{pellet}(650 - 450)}{H_A - H_B} = \frac{14.15 \text{ MW}}{19.51 \text{ MW}} = 0.725 = 72.5\%$$

Finally, the energy efficiency for cyclone pre-heaters will be assumed to be 70%.

#### 6.1.4 Layouts A,B (without PB)

To begin with, it was revealed that the iteration must be done to solve the (eq. 6.8). Moreover, in [Fig. 27] can be noted and in [Fig. 31] as well, that pre-heaters are using exhaust gas from calciner to heat up the pellets, in our DAC system from 300 to 850, in Carbon engineering DAC from 300 to 650.

Layouts A-C have the same nominal power requirement from the DAC side.

$$Q_{DAC}, Q_{preheat} = \text{const.}$$

However, T5 for layouts A, B, and C is distinct. In layouts A-B mass flow rate of HTF is the same at point (3a) [Fig. 27, 28], whereas in Layout C is not.

For the pre-heater, the efficiency is assumed to be 70% as was mentioned and validated in the previous section.

$$Q_{preheat} = \frac{C_{pellet} (850 - 300)}{0.7} = 55.6 \text{ MW}$$

$Q_{dac} = 128 \text{ MW}$ ; the energy needed for calcination

$$Q_{req} = Q_{DAC} + Q_{preheat} = 183.6 \text{ MW}$$

The mass flowrate participating in preheating the pellets, the sum of HTF and released Carbon gas.

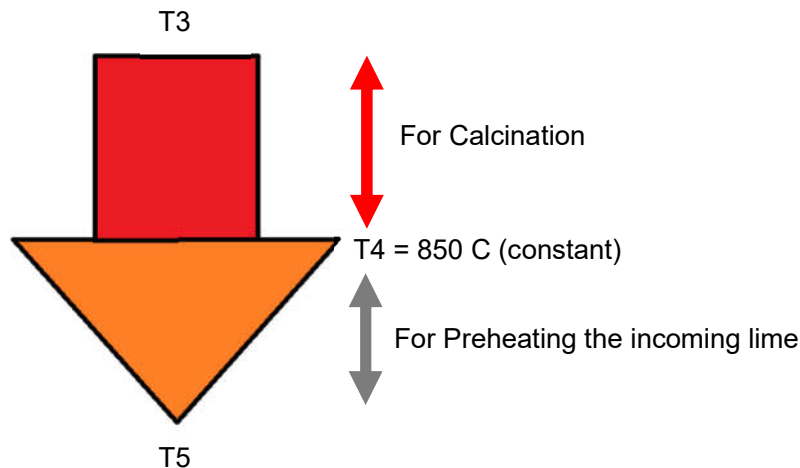


Figure 34. Temperature difference for layouts A and B

The mass flow rate for preheating will be  $m_g = m_{htf} + m_{cap}$

Using these data, it was built a script in python to solve the equation (eq. 6.8)

A short workflow for the code can be observed in [Fig. 35], the code can be found in (Appendix 1) with more detailed workflow.

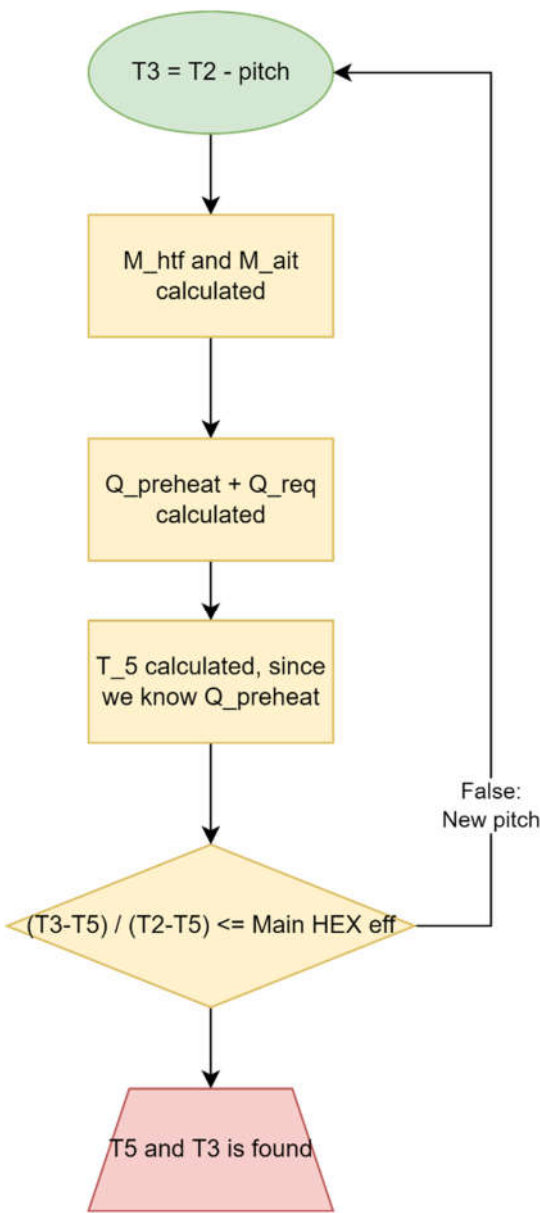


Figure 35. Workflow of the python script for layouts A, B

At last, using the code, it was concluded that  $T_3$  and  $T_5$  will be 980 and 796 accordingly. Moreover, since our system's capacity rate either for air and CO<sub>2</sub> gas is the same, using (eq. 6.6) and (eq. 6.7),  $\text{pitch} = T_2 - T_3 = 20$ ; and  $T_1 = 796 + 20 = 816$  C

$$m_{htf} = \frac{Q_{dac\ nom}}{C_{htf} (T_4 - T_3)} \quad (6.13)$$

Layout	B	A
m htf	772.63 kg/s	772.63 - 1758.76 kg/s
m air	839.07 kg/s	839.07 - 1910.01 kg/s
m cap		47.46 kg/s
T1		816 C
T2		1000 C
T3		980 C
T5		796 C
Q nom		183.6 MW

Table 12. A and B layout's main parameters

### 6.1.5 Layout C (with PB)

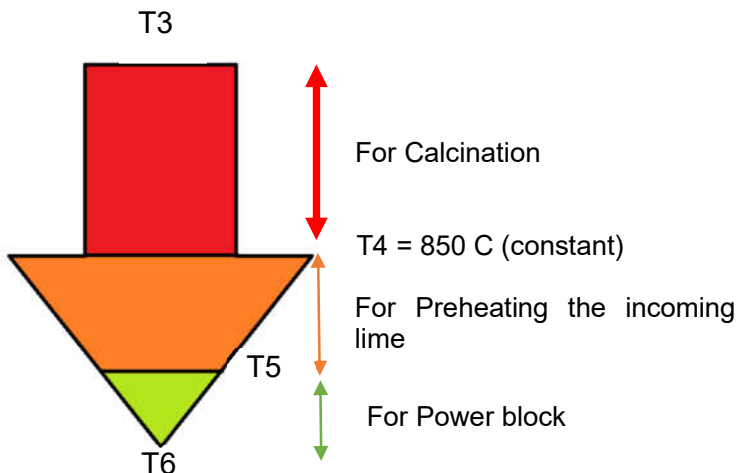


Figure 36. Layouts C's temperature difference

In layout C, the presence of the Power block completely changes the methodology and the condition (eq. 6.8a) is not enough to satisfy in order to find the temperatures since the system also drives the power block.

As usual modular CSP systems are equipped with micro gas turbines, which work under a lower pressure ratio in comparison to conventional gas turbines that enables to provide higher efficiency.

The Power block capacity was decided to fulfill the electrical demand of the DAC plant excluding the compressors' power, which will come from grid. Therefore, summing up the power demands from [Fig. 27], the electrical demand was calculated to be 12.2 MW, then it was rounded up to 13 MW.

It can be observed that the GT turbine in [Fig. 29] is located in a modular CSP site, since according to the layout the GT cycle is before the dashed line.

Therefore, assuming that the number of CSP plants will be in the range of 10-15, the capacity of a singular GT cycle in the modular CSP site may be assumed to be in the range of 1 MW. Such a capacity for GT is treated as low-pressure turbines [40], the pressure ratio is around 4

Compressor ratio	4	[39,19]
Compressor isentropic eff	0.81	
Mechanical eff	0.98	
Turbine isentropic eff	0.81	
Recuperator eff	0.895	
Regenerative HEX eff	0.895	
Generator eff	0.96	
Inverter eff	0.96	

[39]

Table 13. PB system specification

The power block is designed is to efficiently use the exchanged heat. It includes 2 recuperation systems, first, exchange heat from CSP flow, and the second regenerates heat exhausted from the turbine.

In order to solve the temperature points across the PB and DAC/CSP system, the (eq. 6.14 and 6.8a) have to be satisfied

$$0.895 \geq \frac{T_5 - T_6}{T_5 - T_{2pb}} \quad (6.14)$$

In [Fig. 37], the logic of the code is illustrated, and the code itself can be observed in [Appendix.1.2].

$T_{ambient} = T_a = 9 \text{ C} = \text{constant}$  (*annual average  $T_{ambient}$  of the location*)

Layout C	
m htf	797.39 kg/s
m air	839.07 kg/s
m cap	47.46 kg/s
T1	780 C
T2	1000 C
T3	976 C
T5	797.5 C
T6	756
Q nom	183.6 MW

Table 14. Layout C parameters

Power block	
m pb	111.9 kg/s
T1 pb	180 C
T2 pb	474.99 C
T3 pb	792.5 C
T4 pb	522
T a	9

Table 15. Layout C's power block parameters

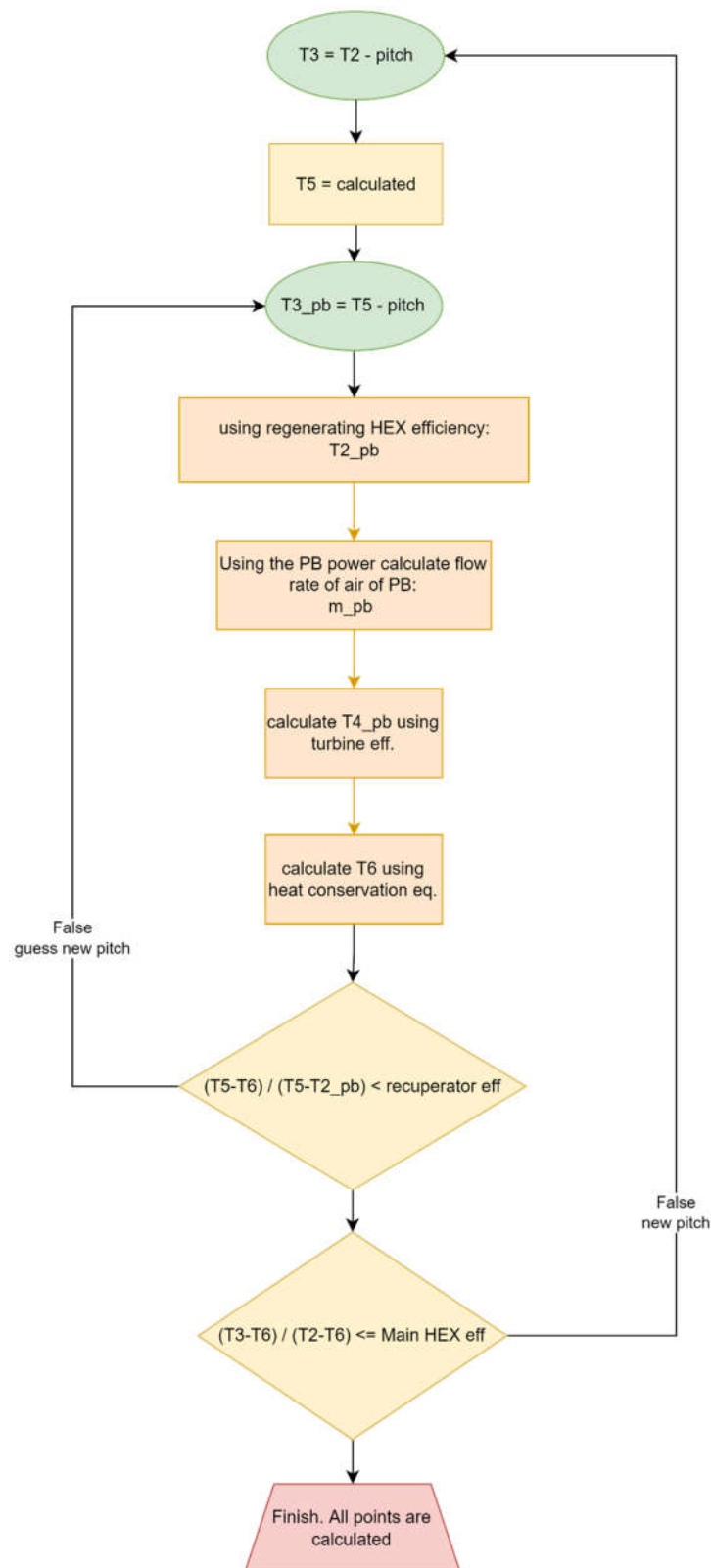


Figure 37. Workflow of the script for layout C

### 6.1.6 Power Island

In [Fig.9] can be observed that the DAC layout provided in [2], includes bottoming low-pressure steam cycle. The temperature that superheats the steam of the cycle is 454 Celsius.

However, the Layouts A-C provides higher temperature flue point  $T_{5a} = 796$  C. Consequently, it is an opportunity to integrate another bottoming cycle.

Since the temperature is quite high, it was decided to use Gas brayton cycle as the first bottoming cycle. As and turbine it was selected to use SGT-100 [39]

Compressor ratio	14	[ml2]
Compressor isentropic eff	0.81	
Mechinical eff	0.98	
Turbine isentropic eff	0.81	
Recuperator eff	0.9	
Generator eff	0.96	
Inverter eff	0.96	

[19]

Table 16. Gas power cycle assumptions

Temperature after Gas power cycle [Fig. 27] at point 2c will be 430 Celsius.

Calculation:

To calculate the temperatures, the efficiency of the recuperator was used:

$$T_{ambient} = T_{1b} = 9 \text{ C} = \text{constant (annual average } T_{ambient} \text{ of the location)}$$

T1b	9	C
m_b	47	kg/s
$C_{cap} = C_b$		

Table 17. Assumptions power cycle

T1b	9	C
h1b	408188.1505	J/kg
S1b	3824.462075	J/kg

T3b	787.712489	C
h3b	1242955	J/kg
s3b	4463.01223	J/kg

h2b is	726757.0171	J/kg
h2b	801483.0476	J/kg
T2b	391.2139754	C

h4b is	659258.539	J/kg
h4b	752649.972	J/kg
T4b	345.260862	C
W	3.77725982	MW

Table 18. Results of Bottom cycled GT system

$$\text{assuming } C_{cap} = C_b; \quad 0.9 = \frac{T_{1c} - T_{2c}}{T_{1c} - T_{2b}}; \quad T_{2c} = 796 - 0.9 * (796 - 391.2) = 431.68 = 430$$

$$Q_{heat} = C_{cap}(T_{1c} - T_{2c}) = C_b(T_{3b} - T_{2b}) = 20.74 \text{ MW}$$

$$h_{3b} = h_{2b} + \frac{Q_{heat}}{m_b}; \quad T_{3b} = 787.71 \text{ C}$$

In the original layout the temperature of the flue gas to heat Steam cycle is 454, whereas in our layout the temperature  $T_{2c} = 430$  C. The lower temperature is compensated with exhaust flow that comes from the gas power cycle which preheats the steam [Fig. 27], therefore the steam cycle is going to work on the same manner as it was before modification.

## 6.2 Model preparation

As was discussed in the methodology, this thesis firstly technically validates the used specifications for parts of the system that is unique, i.e. which is not commercialized due to its nonnecessity, but technically is possible to commercialize since there are already existing projects and companies that uses that specifics. For example, allowed mass flow rate for solar receiver, what is maximum flow rate that can be used for modelling, and is it technically feasible.

The references for each assumption that is made will be supported by the references to existing projects or research papers.

### 6.2.1 Modelling assumptions

- Pressure loss:  
During the modeling of the systems, several assumptions were made concerning the pressure drops. This model neglects pressure drops caused by the following activities:
  - Piping, valves (Minor and major losses)
  - Pressure drop inside the Calciner
  - Pre-heater pressure drop
- Power block:
  - Ambient temperature is assumed to be constant, which enables to suppose power blocks provide constant electric power.
  - Electrical energy losses during the transfer (Cabling losses)
- Heater:  
The heater is assumed to work as an electric heater and combustion chamber. However, the economic analysis only considers the heater as a burning chamber cost. In other words, DAC system economics in default includes burning chamber cost, whether the system is power by electricity or fuel.  
The efficiency of the heater is assumed to be 90%, slightly higher than [2] DAC plant.

### 6.2.2 Cost

- **DAC:**  
The cost for DAC is taken from [2] plant

Module	Value	Unit	Ref
Air contractor	212.2	mln \$	[2]
Pellet reactor	130.7	mln \$	
Calciner	77.7	mln \$	
Compressor	19.9	mln \$	

Steam power plant	7.51	mln \$	
Filter	30.9	mln \$	
other	102.9	mln \$	
Site preparation and installation	6.7	mln \$	
Transformer	19.8	mln \$	
OPEX	42	Mln \$	

Table 19. The DAC system costs

WACC = 8 % [2]

Life = 30 years

- **CSP system**

## 1. Compressor

$$C_{compr} = 1.23 \cdot 10^6 \cdot W^{0.3992} \quad (6.15)$$

Nominal compressor work in [MW]

Cost function is based on the work [54].

## 2. Main heat exchanger

$$C_{HTHE} = 378.15 * 19.26 * \frac{m_{HTF}}{4.65} * 1000 * (\text{exchange}_{\text{nok to usd}}) \quad (6.16)$$

Or

$$C_{HTHE} = 378.15 * 19.26 * \frac{m_{air}}{4.98} * 1000 * (\text{exchange}_{\text{nok to usd}}) \quad (6.17)$$

Based on [39], exchange rate was taken for (May 2022, 1 NOK = 0.1 USD)

## 3. TES

$$C_{TES} = c_{\text{found}} \cdot N_{TES} \cdot A_{TES} + \sum_{i=1}^n c_i V_i \quad (6.18)$$

Parameter	Meaning	Value	Unit
c_found	TES foundation cost	1210	\$/m^2
c_i	Natural Rocks cost	66	\$/m^3
	High T Insulation cost	4269	
	Low T insulation cost	616	
	Steel cost	42354	
V_i	volume of specific material	---	m^3

Cost function is based on the work [53]

Sizing is done using [65]

#### 4. Gas power plant

GT system = 655.2 \$/kW [19]

This cost includes all the recuperators and compressors costs, only suitable for low pressure gas turbine

#### 5. Modular CSP

Module	Value	Unit	Ref
Heliostat field	169.2	\$/m <sup>2</sup>	[55]
Land and site	15.6	\$/m <sup>3</sup>	[56]
Tower and foundation	1105.2	\$/m	[19]
Receiver	162	\$/kW	[57]
Balance of plant	15%		[2]
OPEX	3%		[58]

Table 20. The CSP systems costs

OPEX for CSP part considers only expenses from CSP equipment including gas power plant.

WACC = 7.4 % [58]

Life = 30 years

Degradation = 0.4 % [58]

- **Emission and energy prices:**

Electricity	Value	Unit	Ref.
Carbon emission	0.82	t CO <sub>2</sub> /MWh	[62]
Electr. Price Chile	0.105	\$/kWh	[64]
LCOE_PV	0.04-0.24	\$/kWh	[65]
Natural gas			
Price	0.016	\$/MJ	[59]
Energy density	36.4	MJ/m <sup>3</sup>	
Carbon emission	1.9	kg/m <sup>3</sup>	[63]
Coal			
Price	0.0046	\$/MJ	[60]
Carbon emission	2.85	t CO <sub>2</sub> /t coal	[63]

Table 21. energy prices and inherent emissions

### 6.3 Modular CSP

In this section, will be covered the modeling of Modular CSP and optimization of configurations for modular CSP system, which will be applied in the final layouts.

#### 6.3.1 Location

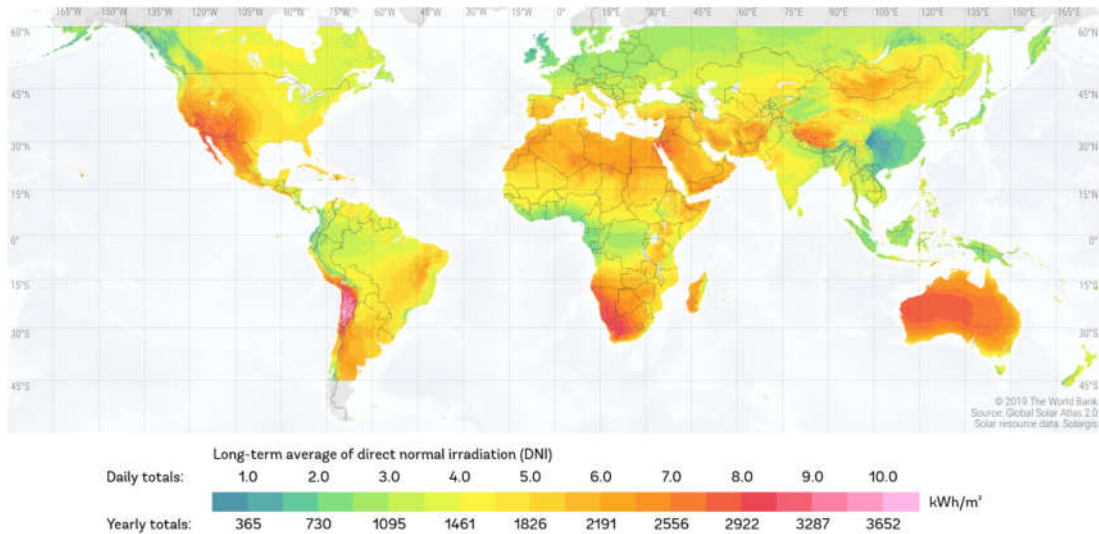


Figure 38. DNI map [Global Solar Atlas]

As for location was selected country Chile. As you see [Fig.38], Chile is considered to be the most DNI-rich location. Considering that CSP technology is dependent on DNI the most. Chile was an obvious choice. Location coordinates: -19.4 (Lat), -67.6 (Lon)

#### 6.3.2 Receiver

SolarPilot is a very great tool to use for modeling CRS systems. However, the lack of capability to simulate exactly the air volumetric receiver is its disadvantage. Hence, the option for modeling a Flat plate receiver is the best approximation, and it was used to build our CSP system.

The technical parameters of the receiver are presented in [Table 22]

Receiver			
Parameter	value	unit	Ref
Pressure drop	20	%	[2]
Allowed peak flux	1000	kW/m²	[42]
Allowed mass flow rate	0 - 250	Kg/s	[20]
Absorptance	0.995		
Thermal loss	40	kW/m²	
Height	to be decided	m	
Width	to be decided	m	

Table 22. Receiver parameters

As it can be seen, the dimension of the receiver yet is an open question. Dimension of the receiver is a very tricky side of CSP plant, oversizing and undersizing the receiver may lead to problems.

The CSP system efficiency is directly affected by the size of its receiver dimension. Equation (4.6) illustrated the components that affect the efficiency.

Oversizing the receiver reduces spillage, but the size of a receiver should be in a logical range that does not allow the peak flux to be higher than 1000 kWh/m<sup>2</sup> due to limitations of material [42], to be in logical scale compared to the tower height.

The reference input for optimization presented in [Table 23].

DNI	900	W/m <sup>2</sup>
Designed power	15	MW
Tower	40	m

Table 23. Reference values used for optimization the receiver

The parametric optimization in SolarPilot [Fig. 39],

Initial step size	0.06
Maximum iterations	1000
Convergence tolerance	0.0001
Power shortage penalty	2

Figure 39. Receiver optimization tool in SolaPilot

The optimization in SolarPilot is designed so that it iterates different dimensions of the receiver and validates does this receiver exceeds the allowed flux. For the reference input [Table 23], SolarPilot has given the result to be around 4.8x4.8 m in dimension.

From the given result, the assumption was made that the dimension that would allow flux to be below 1000 kWh/m<sup>2</sup> lies in the range of 3x3 m and 6x6 m, for 5 MW and 30 MW CSP systems accordingly.

Which was validated by conducting the simulation [Fig. 40]

Des. Power	Tower height	Rec. height	Rec. width
5 MW	40 m	4 m	4 m
10 MW		4.5 m	4.5 m
15 MW		4.8 m	4.8 m
20 MW		5 m	5 m
25 MW		5.2 m	5.2 m
30 MW		5.5 m	5.5 m

Table 24. Receiver dimensions

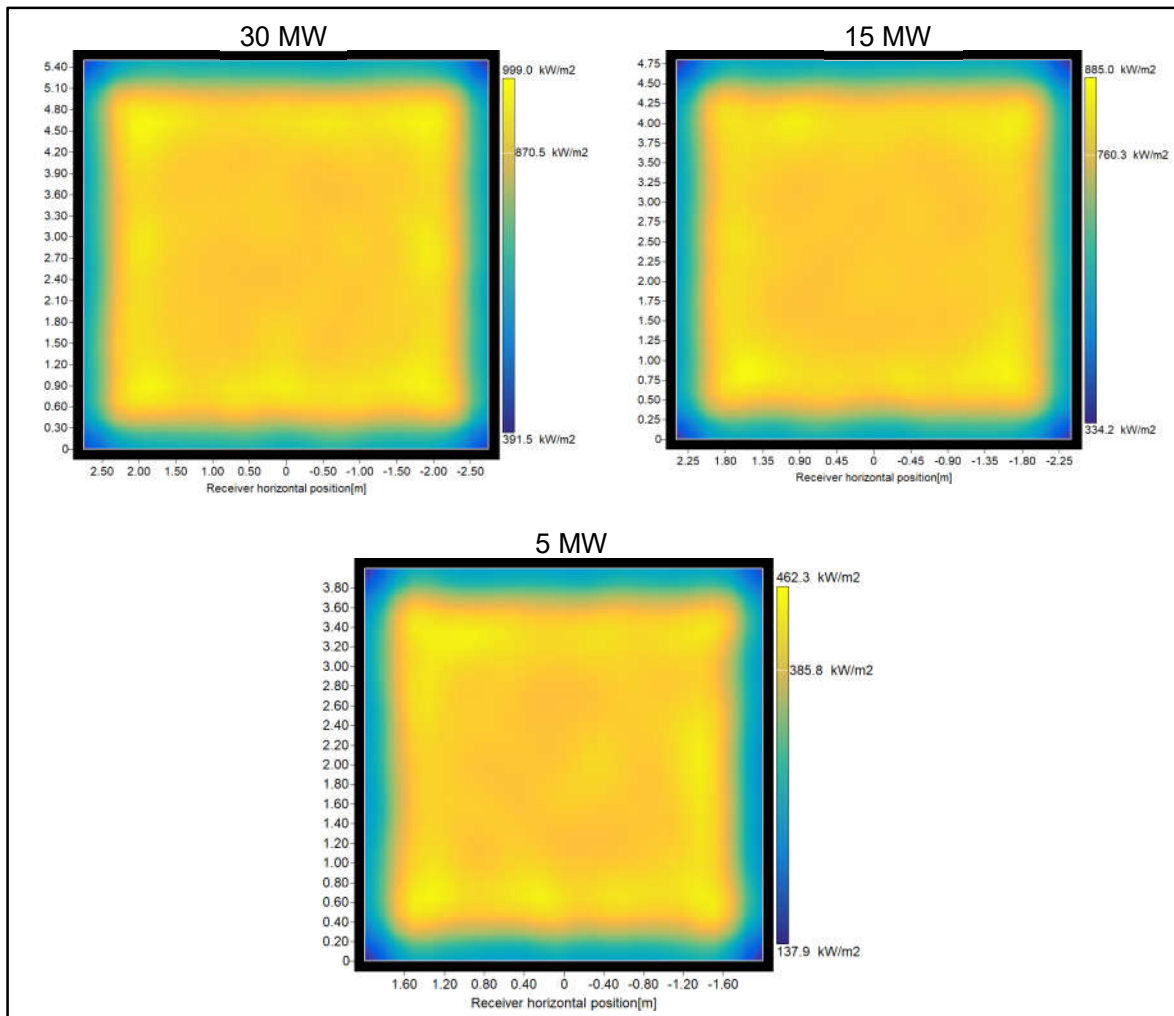


Figure 40. Resulted flux distribution

### 6.3.3 Heliostat field

In [Table 25], it is illustrated the main parameters of the heliostat field on which it will be designed. Since our system is modular and tower is low-height, for mirrors to be able to track properly the receiver, they had to be small, the dimensions were taken as in [19]. Designed DNI is being crucial parameter which defines the size of heliostat field, it was taken DNI at noon equinox (March 21, 12 pm), since the intention to be able to provide stable solar energy across the year, not to be undersized so it wouldn't provide enough energy in summer (Chile is located in southern hemisphere, so conventional "winter" is in summer).

Heliostat field				
Parameter	value	unit	Ref	
Designed DNI	900	W/m <sup>2</sup>		
Heliostat width	4	m	[19]	
Heliostat height	4	m	[19]	
Horizontal panels	2			
Vertical panels	8			

Table 25. Heliostat field parameters

In [Fig. 42], it is illustrated the solar field for 10 MW CSP station with 40 m tower, as was noted Chile is southern hemisphere country, therefore solar field must be oriented due north. In the same manner, solar field in is oriented due north.

As for the efficiency of solar field, since the efficiency of the solar field changes continuously across the year, the interpolation using excel helped to precisely identify the specific efficiency at specific time and day [Fig. 41].

		Elevation Angle (90°: Zenith)							
		5	15	30	45	60	75	90	
Azimuth Angle (0°: North)	-180	29.5	53	57.7	57.8	56	53.3	49.9	
	-135	26.2	48.1	54.4	54.9	53.8	52.2	49.9	
	-90	22.1	38	45.1	47.3	48.4	49.3	49.9	
	-45	16.3	26.8	34.2	38.7	42.7	46.6	49.9	
	0	15.2	22.8	29.3	34.9	40.2	45.4	49.9	
	45	16.3	26.8	34.2	38.7	42.7	46.6	49.9	
	90	22.1	38	45.1	47.2	48.4	49.3	49.9	
	135	26.2	48.1	54.4	54.9	53.9	52.2	49.9	
	180	29.5	53.1	57.7	57.8	56	53.3	49.9	

Figure 41. Interpolation of efficiency

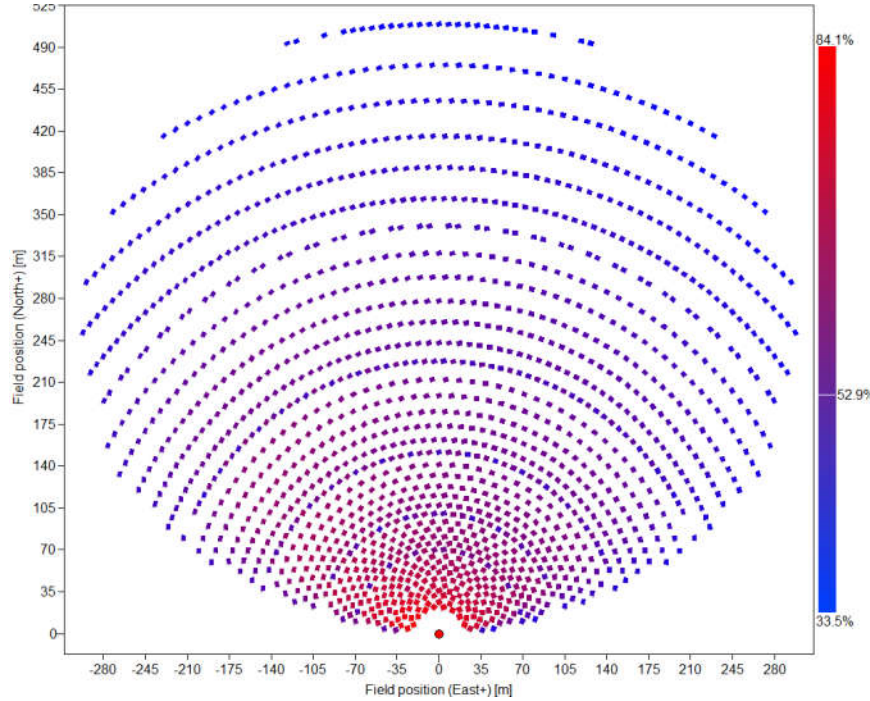


Figure 42. Efficiency map of 10 MW CSP

### 6.3.4 Compressor

As was noted in assumptions, the pressure drop related to Minor/Major head losses, and Calciner are neglected in this model.

The compressor power is calculated as follows:

$$W_{compressor} = \frac{(\rho gh + \Delta p) * V_{air/htf}}{\eta_{compressor}}; \quad (6.18)$$

$h$  – tower height

$\eta_{compressor}$  – efficiency of compressor

$\Delta p$  – pressure drop across HEX/receiver/recuperator/TES

$V_{air/HTF}$  = flow rate of air and HTF gas

### 6.3.5 Tower

Knowing the dimension of the receiver for design powers, it is time to define and validate what tower height and design power is optimum for our Layout.

As for defining the optimum modular CSP system, Layout A [Fig. 27] is used.

To compare the systems the following KPI were used (from chapter 3.2):

- LCCA
- Solar fraction
- Net CSP exp. (NCE)
- Energy yield

Required power from DAC system = 186.3 MW.

The number of modular CSP system should cover this demand.

The number of modular CSP systems were calculated using equation (6.19)

$$\text{number of CSP} = \frac{186.3 \text{ MW}}{\text{designed power}}; \quad (6.19)$$

- For example, for designed Power = 10 MW, number of CSP = 19

According to the operation strategy [Fig. 30], the uncovered energy demand is covered by external sources.

For this model, we will assume that the uncovered heating demand is satisfied by burning natural gas [Table 21], and the electrical demand from the grid.

To validate the optimum tower height and designed power, 4 distinct heights for tower are simulated (20, 30, 40, 50 m), and the designed powers (5, 10, 15, 20, 25, 30 MW)

[Fig. 43] illustrates the LCCA (from natural gas) for each configuration of modular CSP, from the graph can be seen the tendency of LCCA reduction with height increment and power increment.

Whereas in [Fig. 44], the behavior is not straightforward, that can be explained by the number of CSP stations.

Since 186.3 MW is not divisible by 30 MW,  $186.3/30 = 6.21$ , due to the decimal we are building one extra station to cover the energy demand. Therefore, naturally, smaller scale modular CSP plants are more flexible in that sense, one extra plant doesn't cost that much in comparison to 30 MW plant.

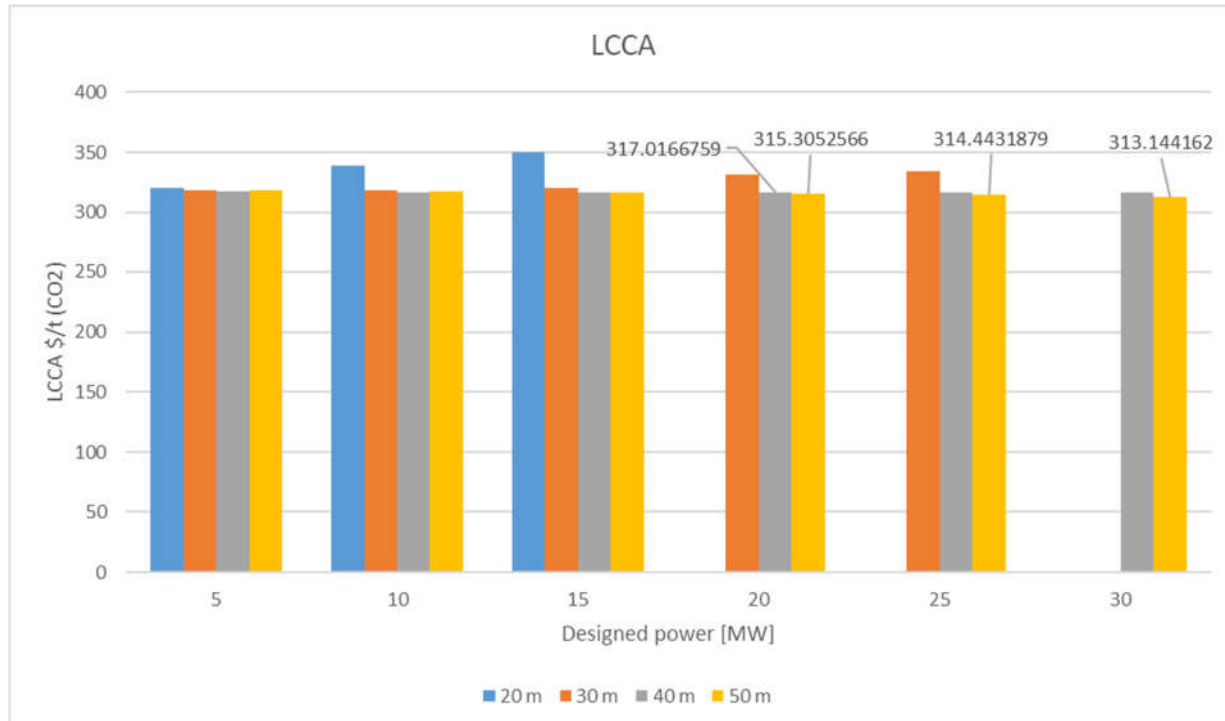


Figure 43. LCCA vs Designed power

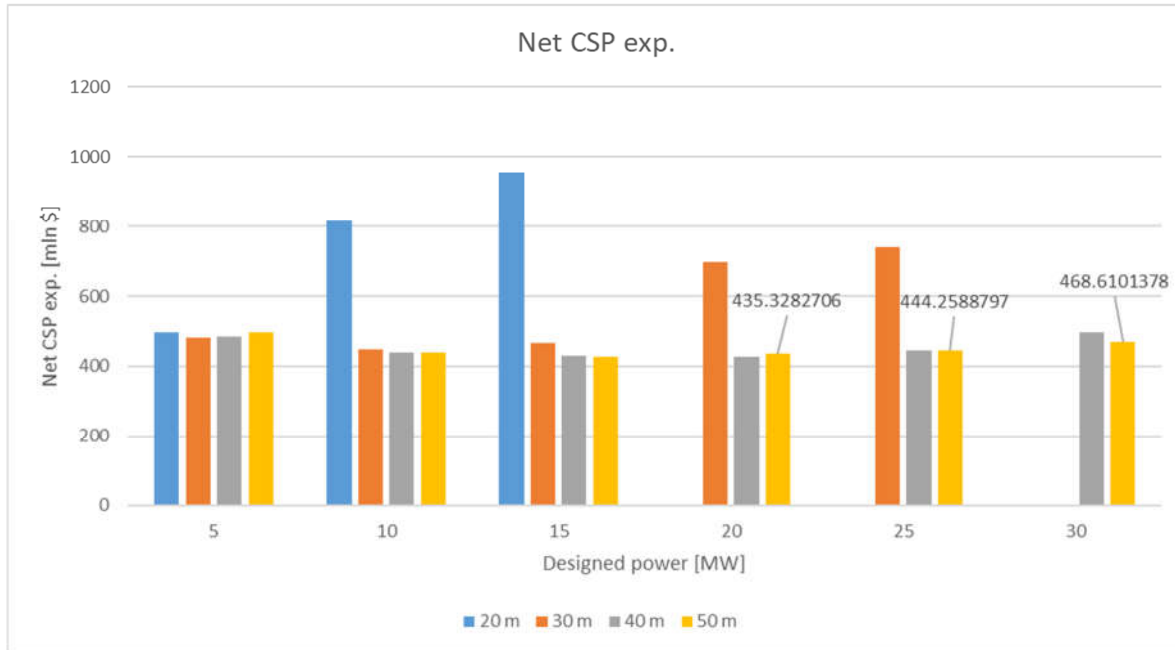


Figure 44. Net CSP exp. vs Designed power

For that reason, the behavior of LCCA becomes even more interesting, the question arises, why is LCCA diminishing while NCE grows?

The answer to that can be observed from the [Table. 25]. Energy yield, solar consumption are naturally decreasing because higher designed power leads to the bigger solar field, hence, less efficient field and energy yield.

Whereas the effect of “decimal” on bigger designed power is high, more energy is lost, consequently, SC declines. However, it can be observed that Solar fraction is increasing, because of the “decimal effect”, the system is designed to produce more energy, when a smaller CSP system is not. From the results can be concluded, that the most important technical KPI that affects the LCCA is SF.

In addition, from [Fig. 43,44] can be found for the designed power of 30, 25, 20 MW; 20-30m height configurations are dropping out.

It is happening because of efficiency loss, the impossibility to build a solar field for larger scale can be explained by attenuation and spillage that is becoming too huge.

In the end, the vote was given in favor of the largest station, **50 m with 30 MW**. Mainly, the number of CSP stations will be in the logical range, and as we observed, the LCCA is not affected that much after 20 MW. However, a larger modular CSP system may reduce the complexities of piping and the delivery of HTF to the DAC system.

Power MW	En. Yield [kW/kWh]	SC	SF	Num CSP	LCCA [\$/t CO <sub>2</sub> ]	Net exp [mln \$]
20	0.371682	0.733496	0.362767	12	315.3053	435.3283
25	0.364446	0.725297	0.366398	10	314.4432	444.2589
30	0.362124	0.688978	0.373485	9	313.1442	468.6101

Table 25. Results table Modular CSP

## 7 Results

### 7.1 Layout A

SM	SC	SF	Num	Coal			Natural gas			Only electricity				
				LCCA \$/t	LCC \$/t	EE mln \$	LCCA \$/t	LCC \$/t	EE mln \$	LCCA \$/t	LCC \$/t	EE mln \$	NDE mln \$	NCE mln \$
1	0.76	0.36423	8	<b>521.06</b>	109.23	1755.55	<b>324.845</b>	155.113	3132.10	<b>-907.925</b>	208.11	4721.98	1083.561	437.7186
1.2	0.69	0.37348	9	<b>507.84</b>	109.98	1747.48	<b>322.965</b>	155.201	3104.03	<b>-960.779</b>	207.43	4670.82	1083.561	468.4367
1.4	0.58	0.38605	11	<b>494.1</b>	111.66	1736.54	<b>321.798</b>	155.971	3065.99	<b>-1047.07</b>	207.15	4601.46	1083.561	529.5849
1.6	0.54	0.39114	12	<b>489.81</b>	112.53	1732.32	<b>321.769</b>	156.479	3050.77	<b>-1087.44</b>	207.24	4573.55	1083.561	560.0398
1.8	0.47	0.39965	14	<b>484.13</b>	114.31	1724.92	<b>322.312</b>	157.645	3025.04	<b>-1164.47</b>	207.7	4526.64	1083.561	620.7553
2	0.45	0.40301	15	<b>482.82</b>	115.22	1721.98	<b>322.945</b>	158.314	3014.82	<b>-1199.26</b>	208.09	4508.01	1083.561	651.0289

Table 26. Results layout A



Figure 45. Layout A performance graph (SM = 1.4)

As can be seen [Table 26], LCCA perspective, the best result is shown by natural gas fired DAC plant. Which is quite predictable since the emission produced by natural gas is less than other sources. Even though Energy exp. (EE), is much higher than coal fired plant [Fig.48], it is leading in LCCA

However, LCC perspective, coal is in leading place because coal is cheaper [Fig.48] than other fossil fuels, since it doesn't include carbon emission, the LCC will be lower.

Moreover, it can be noticed that when the plant is only provided by electricity, i.e., the burner works as an electrical heater, the LCCA becomes negative, that means electrical heating using grid is economically feasible. LCCA is becoming negative since the emission of CO<sub>2</sub> caused by the utility electricity of Chile is higher than 30 Mt [Fig.48] as electricity in Chile mostly produced by Coal. The system's lifetime is 30 years, it captures 30 Mt of CO<sub>2</sub>, overall in lifetime.

In [Fig. 46,47], can be observed the distribution of CAPEX for CSP and DAC system, for the winner configuration, where LCCA is lowest of Solar Multiple = 1.4.

[Fig. 45] illustrates the performance of the plant at March 21 and December 18, the were specifically chosen to show that plant behaves properly to the fluctuations of DNI. As we can see, the heat demand from DAC side, is being subsidized during the day, which is the right sign. Moreover, compressor power is much higher during the day, that's also predictable since installed by-pass valve relocates HTF to the Calciner reducing and minimizes the pressure drop, moreover, air compressors are being turned off at nights, these processes considerably affecting the electrical demand.

In general, the results are in valid range of LCC, when compared to [Table 2]

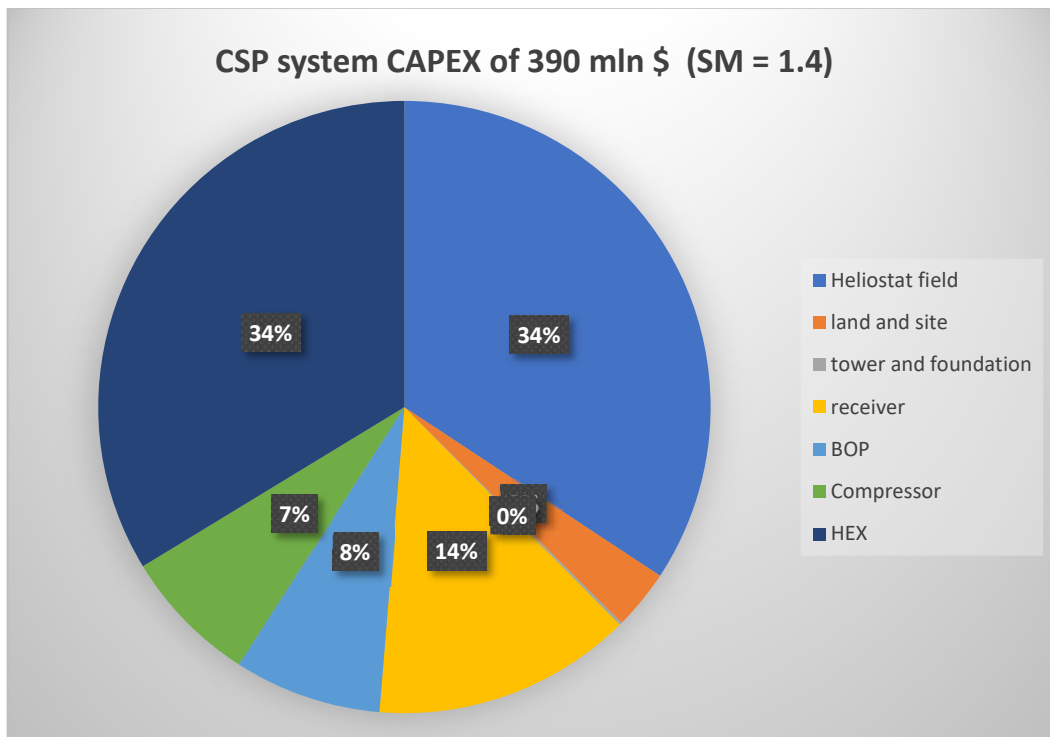


Figure 46. CAPEX distribution of the CSP system

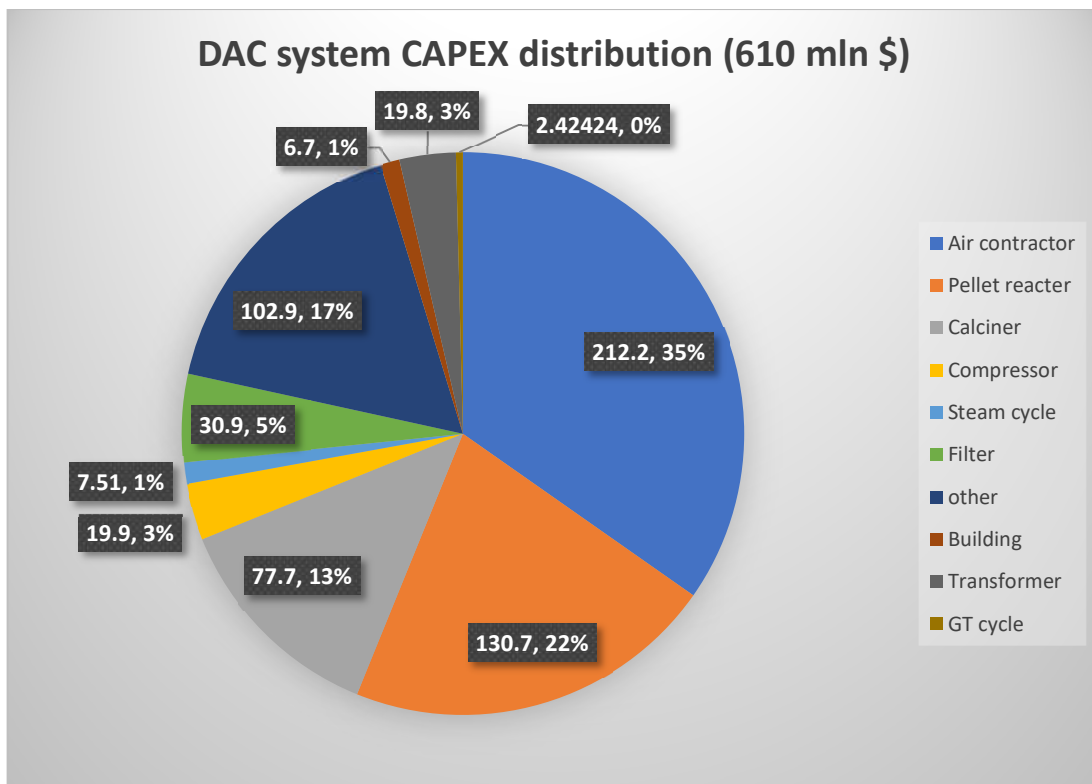


Figure 47. CAPEX distribution of the DAC system  
(Same for Layout A, B, C since the DAC system doesn't change with layout)

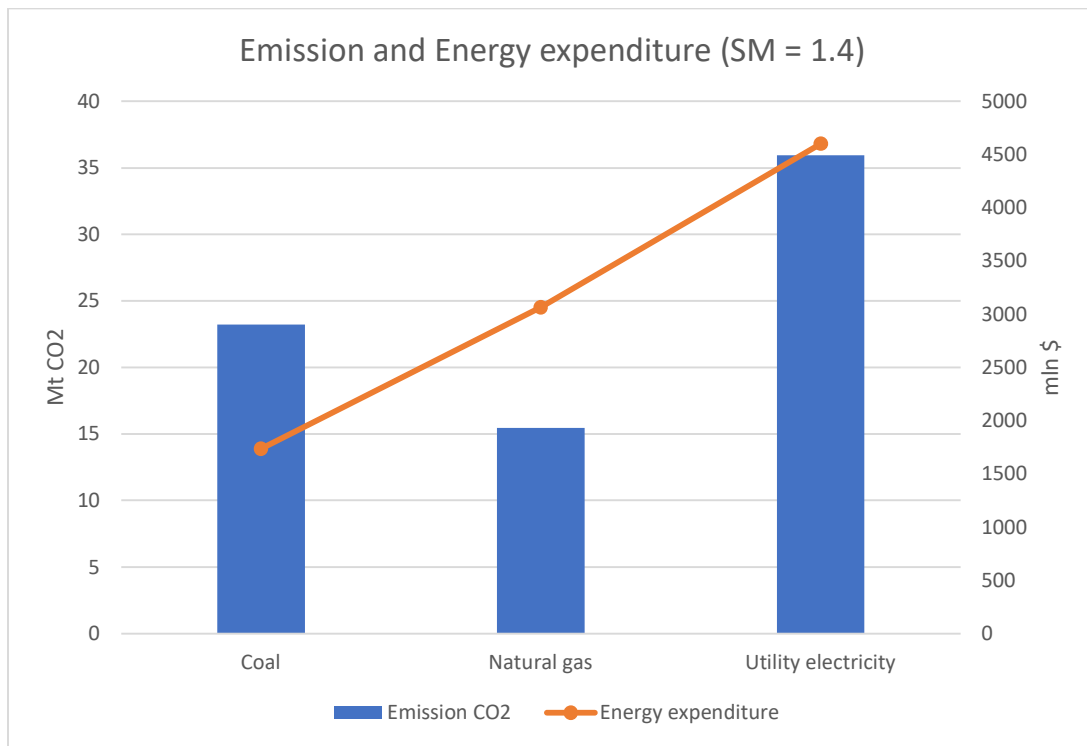


Figure 48. Emission and Energy expenditure produced in 30 years

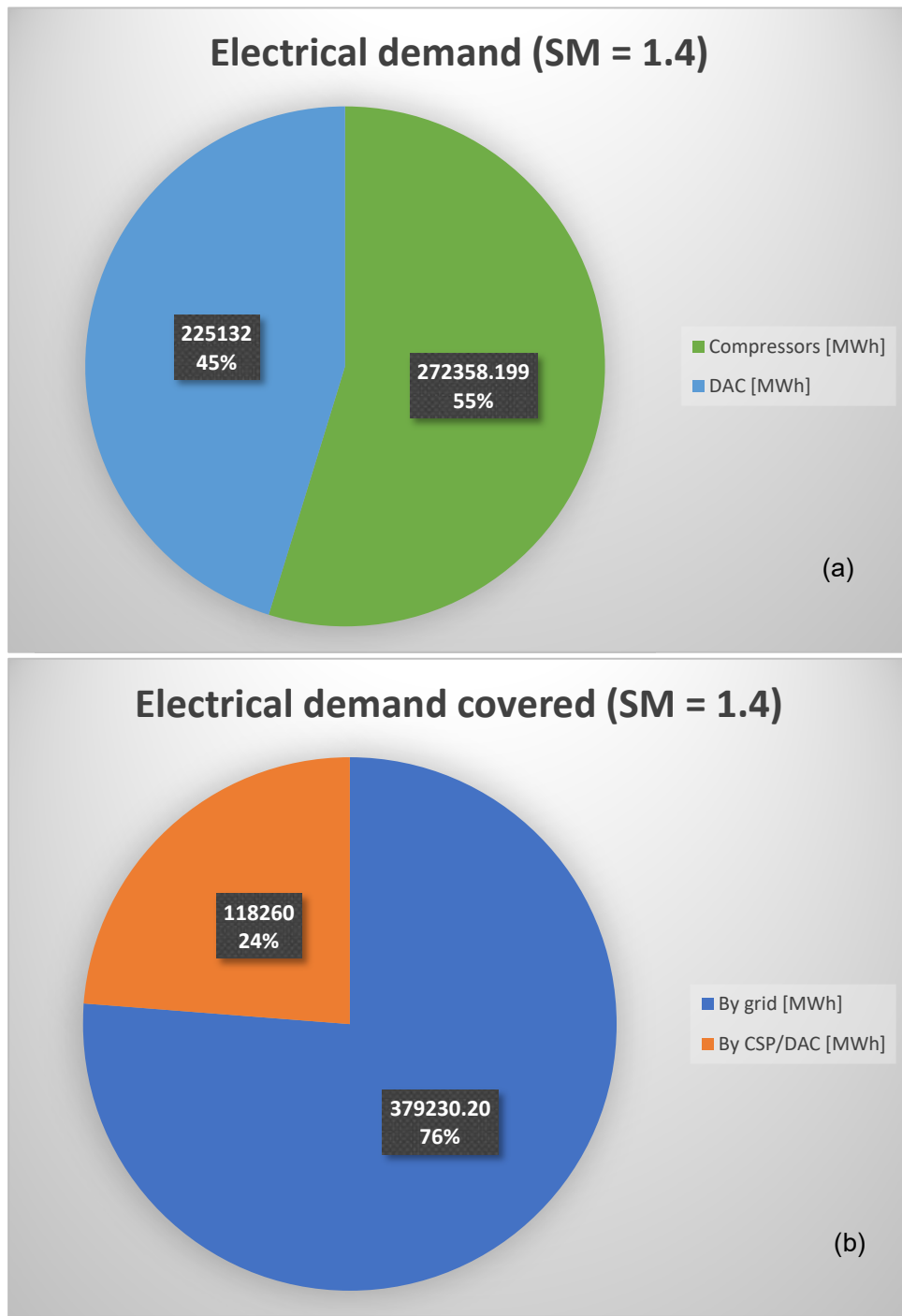


Figure 49. Electrical demand (a) and its coverage by sources (b) for Layout A

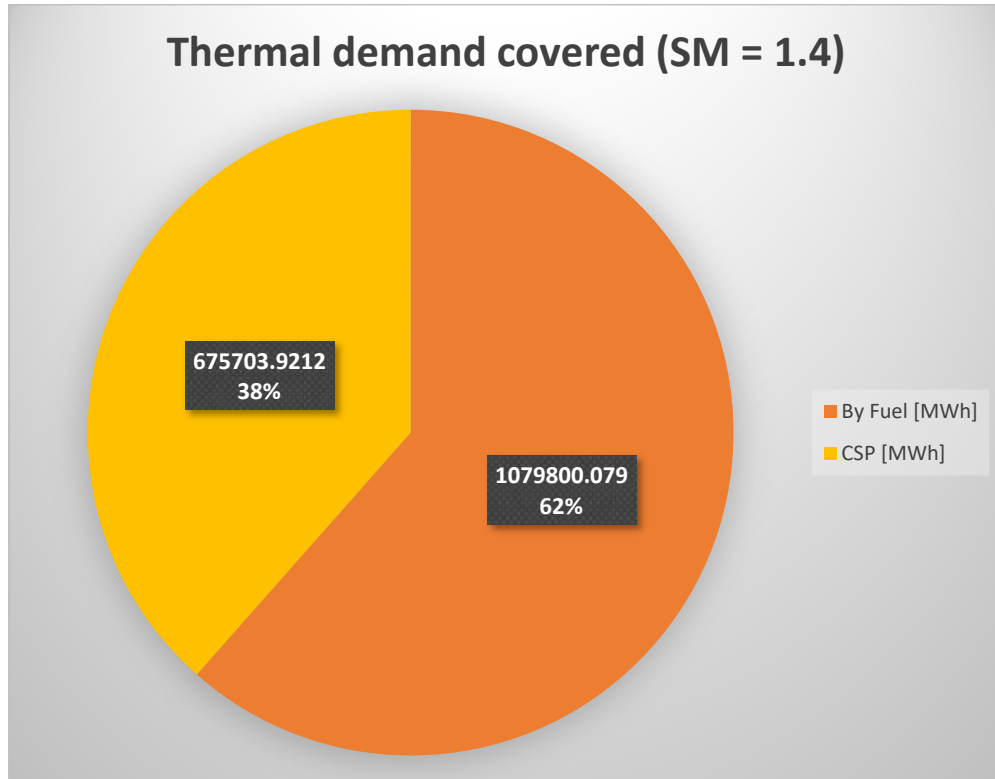


Figure 50. Thermal demand cover by sources

## 7.2 Layout B

LCCA	3	6	9	12	TES/hours
1	333.025602	327.5411	327.4086	327.27361	
1.2	342.732737	327.4356	327.2849	327.13009	
1.4	374.548664	332.2129	329.9723	329.776	
1.6	394.484002	337.4279	333.0902	332.46096	
1.8	450.462248	355.9489	351.9508	349.95756	
2	478.872275	372.2194	366.3071	363.67411	
SM					NG

LCCA	3	6	9	12	TES/hours
1	487.945888	468.2795	467.7057	467.13055	
1.2	491.635945	442.1779	441.6202	441.05708	
1.4	529.740802	410.2217	404.8536	404.30879	
1.6	555.398448	402.275	392.9262	391.52376	
1.8	643.2151	401.5078	393.9649	390.22926	
2	676.841052	411.8934	401.2645	396.58913	
SM					Coal

Table 27. LCCA results for Layout B

SF	3	6	9	12	TES/hours
1	0.47017374	0.481854	0.481854	0.4818537	
1.2	0.50991594	0.542084	0.542085	0.5420854	
1.4	0.57573767	0.658254	0.662549	0.6625488	
1.6	0.60648751	0.712294	0.720707	0.7215542	
1.8	0.65445935	0.808039	0.814947	0.8182555	
2	0.68523612	0.845879	0.855758	0.8598804	
<b>SM</b>					
SC	3	6	9	12	TES/hours
1	0.97576041	1	1	1	
1.2	0.94065614	0.999997	1	1	
1.4	0.86897398	0.993518	1	1	
1.6	0.83910329	0.985492	0.997131	0.9983033	
1.8	0.77612104	0.958251	0.966442	0.9703664	
2	0.75844449	0.93625	0.947184	0.9517471	
<b>SM</b>					

Table 28. Technical KPI results Layout B

As we can see from [Table 27 and 28], in orange it is highlighted the winner LCCA for coal and NG fired DAC systems. Moreover, in [Table 29], can be seen electrical heater DAC system is emitting more than 30 Mt CO<sub>2</sub>, which shows the infeasibility of this scenario, therefore it is not included in economical assessment

LCCA of NG behaves quite strange, the growth in the size of TES affects the LCCA even though, under SM = 1.2, 6-hour TES already is giving maximum SC.

First explanation can be the precision of Excel since CSP system was modeled in Excel. This software as known is 1<sup>st</sup> order precision application, therefore, very small numbers are rounded up.

Second explanation can be understood looking into the CAPEX distribution of the CSP system [Fig. 51]

It turns out, TES is a very cheap component of the CSP system, therefore, even slight increase in solar fraction, affecting the LCCA of the system, whereas oversizing the TES is not affecting the costs that much. Hence, decrement in energy expenditure is higher than increment in TES cost. It can be proved by looking into [Table 29], EE of natural gas is being decreased for 3 mln \$, whereas TES is grown only for 1.6 mln \$.

Emission [Mt CO <sub>2</sub> ]	Coal	Natural gas	Utility elec.	
TES = 6	22.1346123	16.35464621	31.6035236	
TES = 9	22.1230628	16.34956949	31.5813702	
TES = 12	22.1115248	16.34449786	31.5592388	

Expenditure [mln \$]	Coal	Natural gas	Utility elec.	TES cost
TES = 6	1913.21172	2903.285918	4046.79266	2.196052
TES = 9	1912.76433	2901.729771	4043.95594	3.051195
TES = 12	1912.31739	2900.175181	4041.12205	3.861546

Table 29. Emission and Expenditure caused by energy purchase (SM =1.2, TES=6 h)

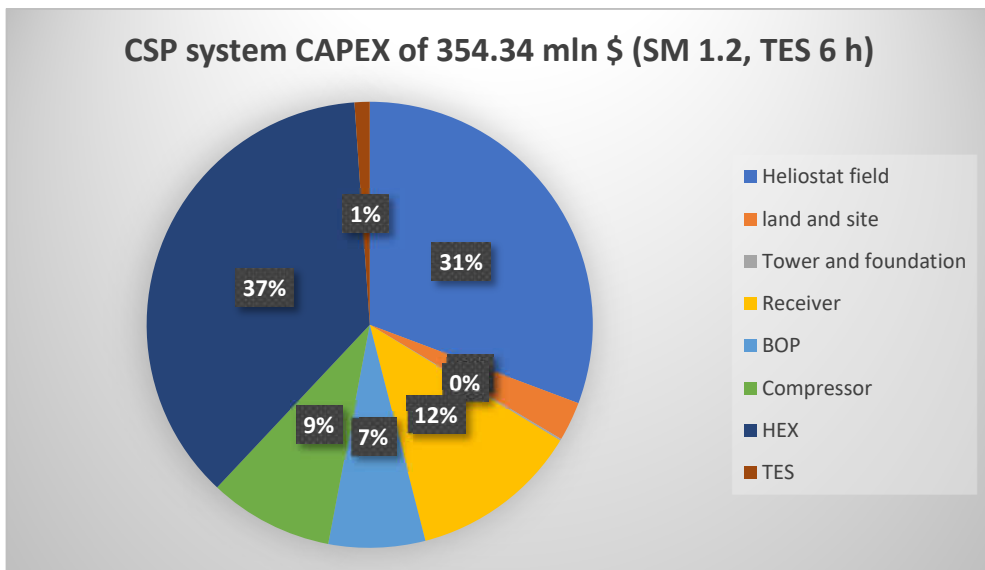


Figure 51. CSP CAPEX distribution

In [Fig. 52], can be observed the performance of the system, compared to the Layout A, the electrical demand of this system is much higher due to the extra compressor work used to charge the TES. Moreover, it can be seen the behavior of TES, compared to the Fig. 45, the heating demand in March 21 is much less than Layout A due to the presence of TES. Moreover, Q<sub>lost</sub> doesn't exist in this model, which validates the [Table 28] results.

Comparing [Fig. 50] and [Fig. 53 c], can be found that the CSP system coverage in Layout B is higher than in Layout A since in this case, TES is implemented, which complies with the expectations.



Figure 52. Performance graph of the Layout B (SM = 1.2, TES = 6 hour)

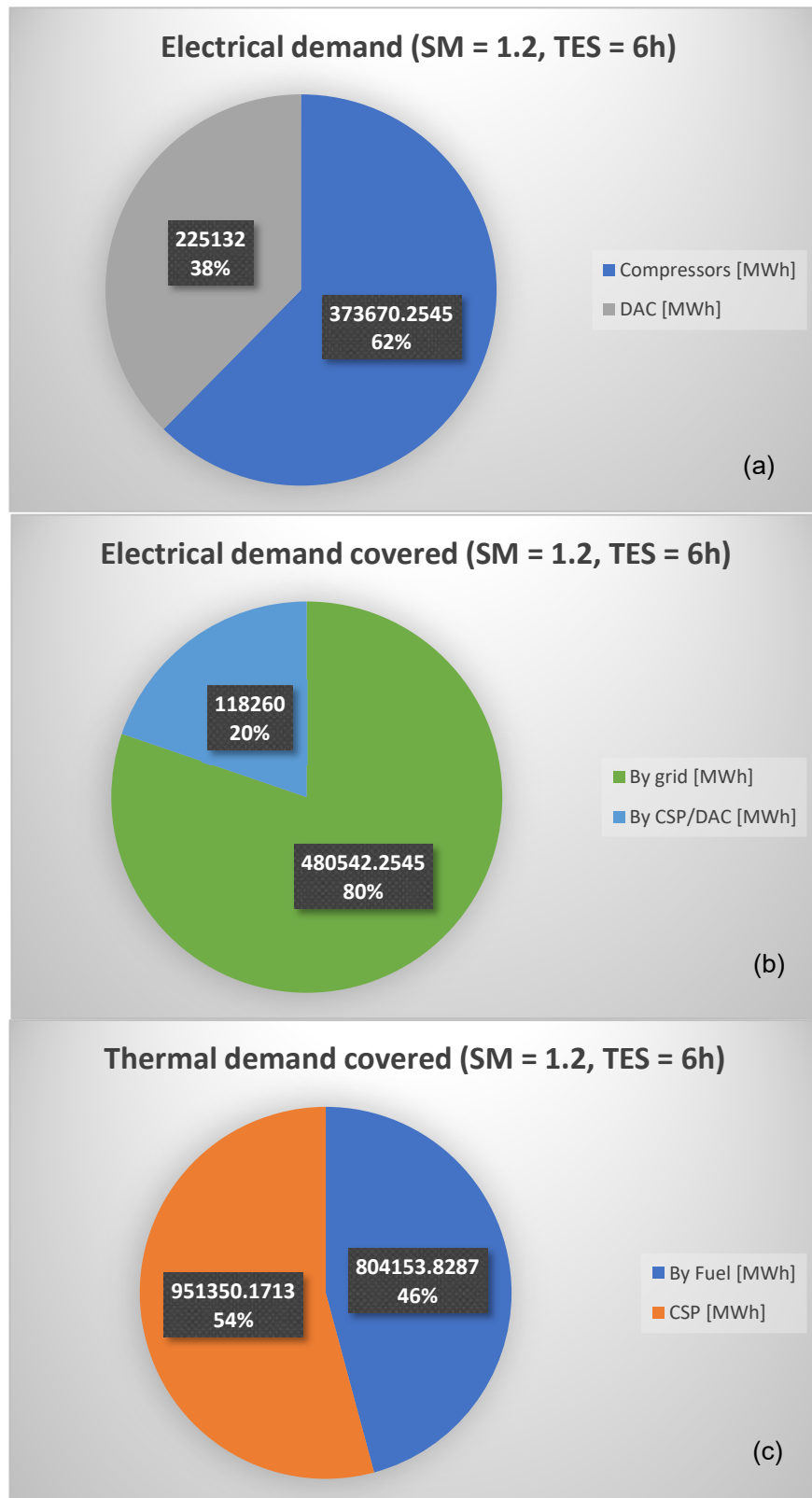


Figure 53. Electrical demand (a), its coverage by sources (b), thermal demand coverage by sources (c) for Layout B

### 7.3 Layout C

SM	SC	SF	Num	Coal			Natural gas				
				LCCA \$/t	LCC \$/t	EE mln \$	LCCA \$/t	LCC \$/t	EE mln \$	NDE mln \$	NCE mln \$
1	0.87	0.42	8	<b>589.472</b>	103.16	1557.5	<b>314.196</b>	160.9046	3289.89	1092.079	445.1718
1.2	0.8	0.43	9	<b>553.624</b>	103.71	1543.2	<b>309.68</b>	160.2687	3240.09	1092.079	475.8898
1.4	0.69	0.46	11	<b>518.51</b>	105.15	1525.2	<b>305.58</b>	160.2237	3177.59	1092.079	537.0379
1.6	0.64	0.46	12	<b>509.456</b>	105.96	1519.2	<b>304.85</b>	160.5381	3156.57	1092.079	567.4927
1.8	0.56	0.47	14	<b>497.451</b>	107.66	1509.4	<b>304.394</b>	161.4259	3122.49	1092.079	628.2081
2	0.53	0.48	15	<b>493.196</b>	108.52	1505.2	<b>304.459</b>	161.9462	3107.83	1092.079	658.4816
2.2	0.48	0.49	17	<b>487.307</b>	110.29	1497.9	<b>305.065</b>	163.112	3082.40	1092.079	718.8857
2.4	0.45	0.49	18	<b>485.762</b>	111.2	1494.9	<b>305.645</b>	163.7687	3071.96	1092.079	749.0241

Table 30. Layout C results

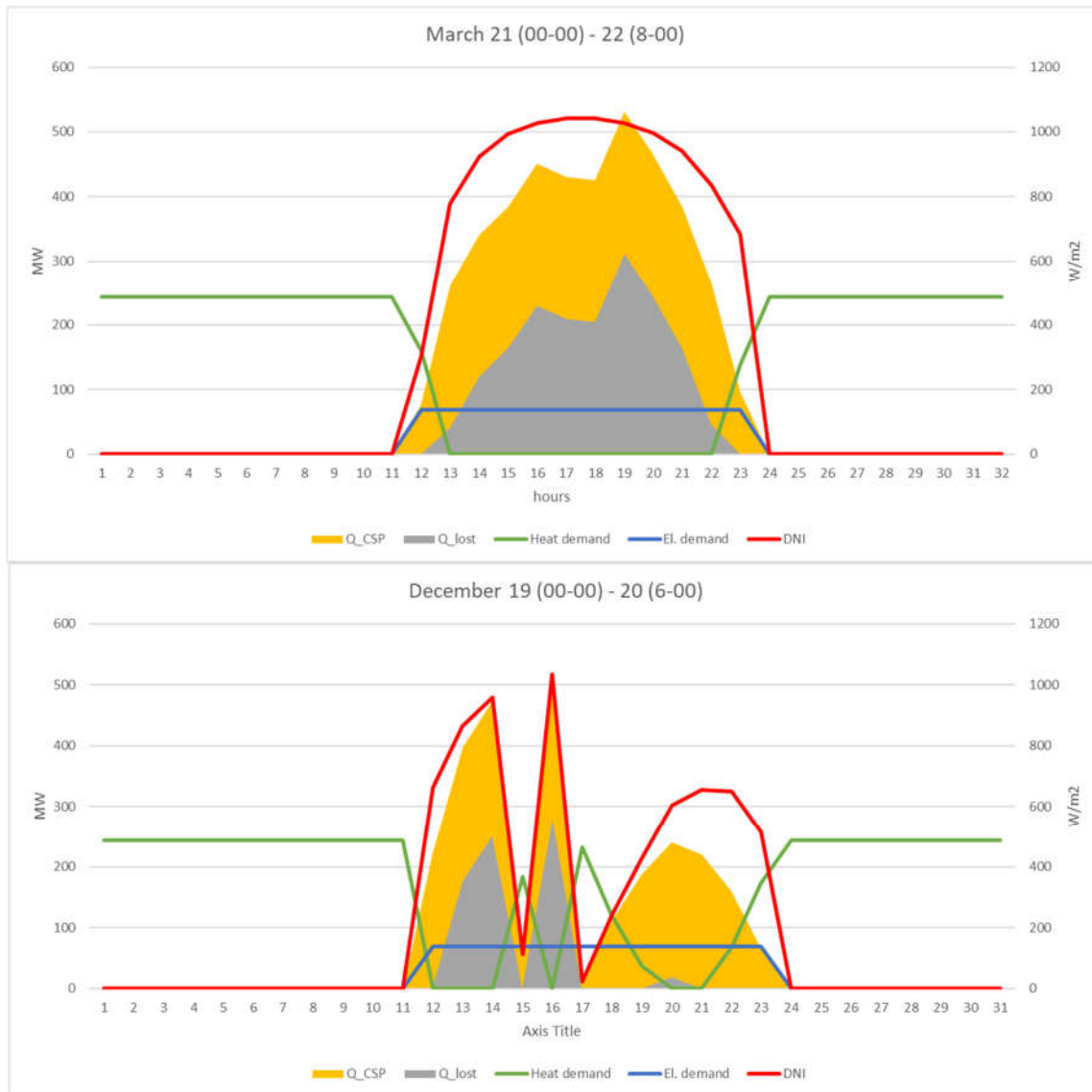


Figure 53. Performance of the Layout C (SM = 1.8)

The behavior of this layout is very similar to Layout A, except the LCCA provided by this layout is improved.

The main difference of the current layout from Layout A can be observed from [Fig. 56]. Electrical demand is remaining the same, but the electric demand coverage has changed very much, in the current layout CSP/DAC system covers for 20% more. That alteration, facilitates the system to produce less emission by purchasing less electricity from grid, which enhances the LCCA of the system.

The [Fig. 53] illustrates the performance of the system, the system operates in the same manner as Layout A, however, due to the economic feasibility, this plant is of a bigger scale. Also, in [Fig. 57], can be seen the new inclusion into CAPEX of CSP which is GT cycle, the power block

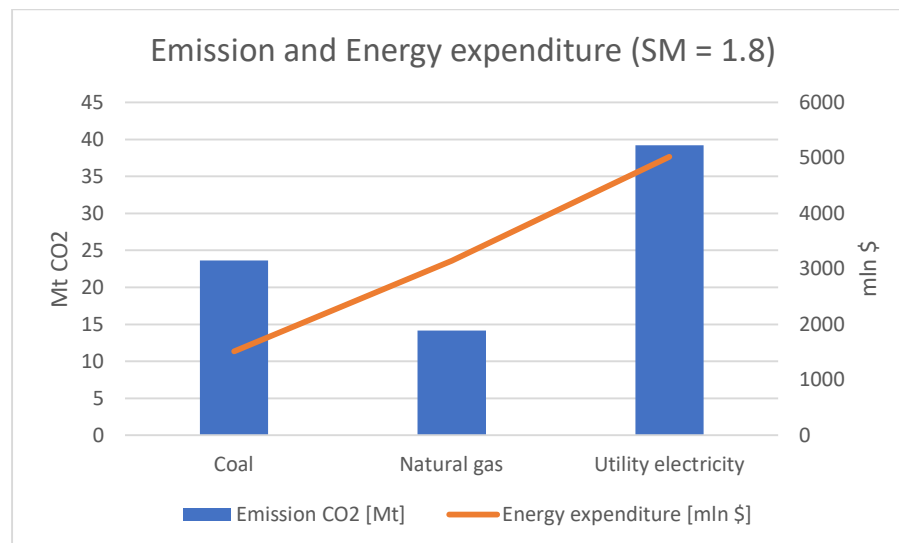


Figure 54. Emission and Energy expenditure of Layout C

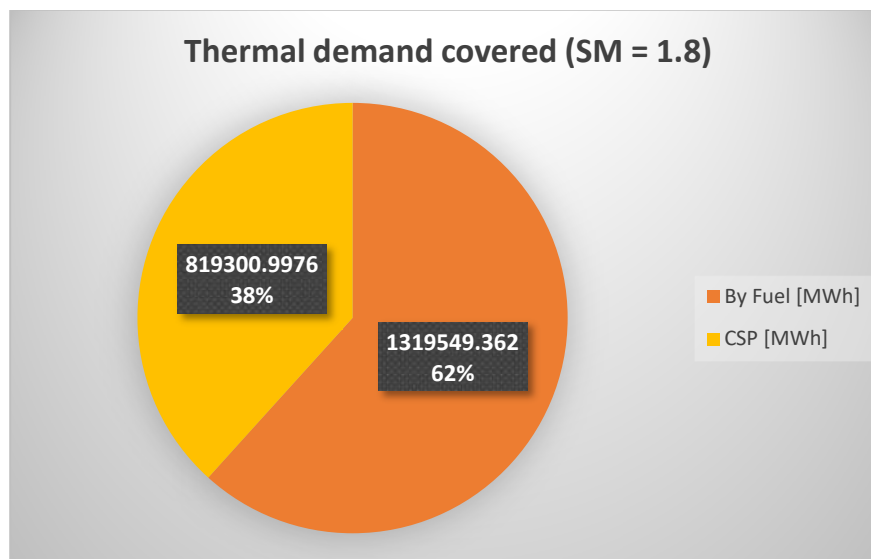


Figure 55. Thermal coverage by sources Layout C

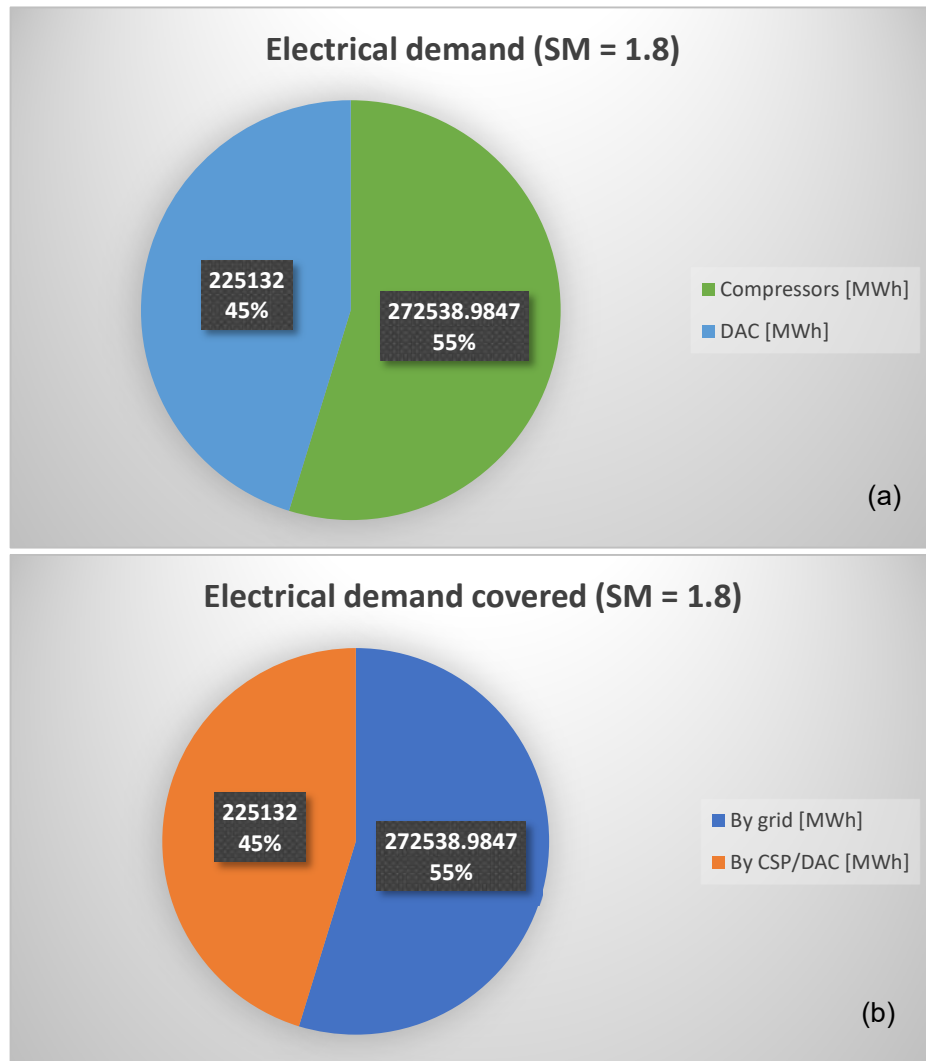


Figure 56. Electrical demand (a) and its coverage by sources (b) for Layout C

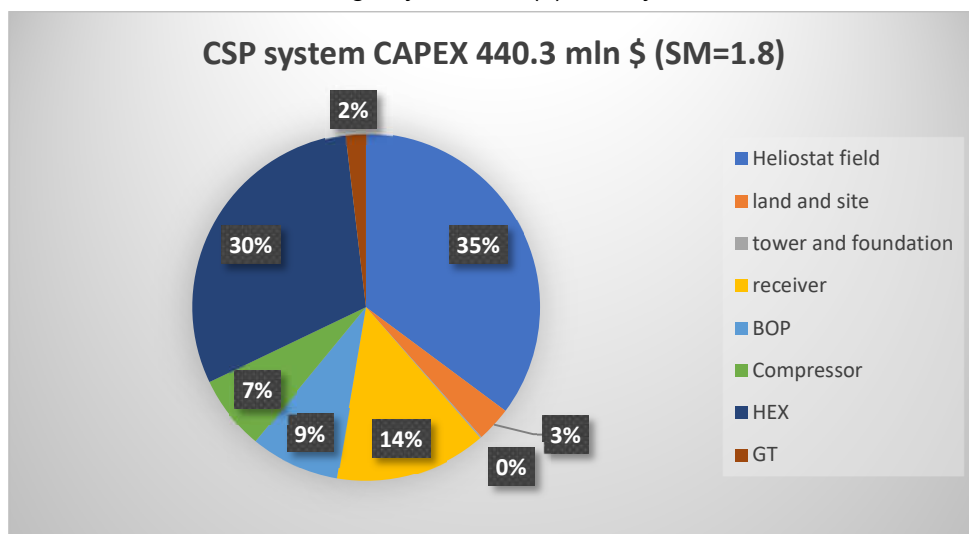


Figure 57. CAPEX distribution of the CSP system for Layout C

## 7.4 Discussion

						Coal		Natural gas					
	TES	SM	SC	SF	Num TW	LCCA \$/t	LCC \$/t	EE mln \$	LCCA \$/t	LCC \$/t	EE mln \$	NDE mln \$	NCE mln \$
Layout A	-	<b>1.4</b>	0.58267	0.386047	11	<b>494.097</b>	111.6562	1736.539	<b>321.798</b>	155.9712	3065.99	1083.561	529.5849
Layout B	6	<b>1.2</b>	0.999997	0.542084	9	<b>422.566</b>	114.7343	1877.34	<b>318.272</b>	147.7368	2867.41	1083.561	481.1279
Layout C	-	<b>1.8</b>	0.562139	0.473535	14	<b>497.451</b>	107.6561	1509.396	<b>304.394</b>	161.4259	3122.49	1092.079	628.2081

Table 30. Results summarize

As can be explored, from the [Table 30], Layout C becomes the most attractive layout. That result is explained by the following. Since the electrical demand is covered more in layout C, less electricity is bought from the grid, therefore less emission is made by the system, which improves the LCCA of the system.

Moreover, compared to the LCC [Table 2], the values gotten from the modeling the system are very similar to the economical values gotten in these publications and pilot plants, which validates that the system is at least technically feasible.

In addition, the gotten LCCA values, compared to the same table, shows that the integration of the CSP system with DAC will give very promising output, and only positively enhances the DAC system, by reducing LCCA 2-3 times.

In general, it can be witnessed, that the main issue of the system is the electrical demand and the emission caused by it. For that reason, it can be concluded that full greenification of the system using PV system in order to fulfill the electrical demand, or using carbon-free electricity from the grid, will enhance the KPI of the system for several times.

Moreover, the results of TES show that the importance of TES is not that high when emission from the used fuel is not high, coal power system responds to the TES layout positively since its inherent emission is very high whereas NG is neutral.

In the end, it may be concluded that the inherent emission from electricity plays an important role when it comes to the LCCA of the system. Therefore, the hybridization with CSP only enhances the system. In fact, increasing the autonomy of the system plays an even more important role on the economical performance of the system

## 8 Conclusion

The techno-economic assessment has shown that such an integration is possible to accomplish.

In the study of DAC technology, there were figure out the challenging parts of DAC system that may be an obstacle in the integration of the CSP and DAC systems. Using proper research works done in that specific area that is explicitly and implicitly related to the problem, the possible solutions were proposed and validated, and the references were put to each of the parameters using the existing projects or companies that work in a similar field.

Next, the economic assessment of different layouts has shown that the hybrid DAC/CSP system is economically feasible and the main issue with CSP/DAC system is the emission caused by the purchased electricity. Therefore, enhancing the SF of the system, and improving its autonomy will improve the system.

In general, the results gotten from the integration have shown that such a system may reduce LCCA 2 times.

Future work suggestions:

1. Hybridize the system with PV to cover the electrical demand
2. Find ways to overcome the issue of quartz windows, to open the possibility of applying new receiver technologies which work under much higher temperatures.



## 9 References

- [1] FASIH, Mahdi, EFIMOVA, Olga and BREYER, Christian. Techno-economic assessment of CO<sub>2</sub> direct air capture plants. *Journal of Cleaner Production*. July 2019. Vol. 224, p. 957–980. DOI 10.1016/j.jclepro.2019.03.086.
- [2] KEITH, David W., HOLMES, Geoffrey, ST. ANGELO, David and HEIDEL, Kenton. A Process for Capturing CO<sub>2</sub> from the Atmosphere. *Joule*. August 2018. Vol. 2, no. 8, p. 1573–1594. DOI 10.1016/j.joule.2018.05.006.
- [3] Carbon Engineering | Direct Air Capture of CO<sub>2</sub> | Home. Carbon Engineering. Online. [Accessed 14 September 2022]. Available from: <https://carbonengineering.com/>
- [4] NATIONAL ACADEMIES OF SCIENCES, ENGINEERING, AND MEDICINE (U.S.) (ed.). Negative emissions technologies and reliable sequestration: a research agenda. Washington, DC : The National Academies Press, 2019. ISBN 978-0-309-48452-7. TD885.5.C3 N36 2019
- [5] HOLMES, Geoffrey and KEITH, David W. An air–liquid contactor for large-scale capture of CO<sub>2</sub> from air. *Philosophical Transactions of the Royal Society A: Mathematical, Physical and Engineering Sciences*. 13 September 2012. Vol. 370, no. 1974, p. 4380–4403. DOI 10.1098/rsta.2012.0137.
- [6] MAZZOTTI, Marco, BACIOCCHI, Renato, DESMOND, Michael J. and SOCOLOW, Robert H. Direct air capture of CO<sub>2</sub> with chemicals: optimization of a two-loop hydroxide carbonate system using a countercurrent air-liquid contactor. *Climatic Change*. May 2013. Vol. 118, no. 1, p. 119–135. DOI 10.1007/s10584-012-0679-y.
- [7] SANTAMARTA, Jose. Modular hybrid concentrated solar power. HELIOSCSP. Online. [Accessed 16 September 2022]. Available from: <https://helioscsp.com/modular-hybrid-concentrated-solar-power/>
- [8] 247Solar Plant. 247Solar, Inc. Online. [Accessed 14 September 2022]. Available from: <https://247solar.com/sustainable-solar-solutions-products/247solar-plant/>
- [9] Archimede | Concentrating Solar Power Projects | NREL. Online. [Accessed 14 September 2022]. Available from: <https://solarpaces.nrel.gov/project/archimede>
- [10] 247Solar Plant. 247Solar, Inc. Online. [Accessed 14 September 2022]. Available from: <https://247solar.com/wp-content/uploads/2022/01/247Solar-Plant-2-Pager-July-21.pdf>
- [11] GOSWAMI, D. Yogi and KREITH, Frank. Energy conversion. . Second edition. Boca Raton : CRC Press, 2017. ISBN 978-1-315-35662-4.

- [12] LOVEGROVE, Keith and STEIN, Wes (eds.). Concentrating solar power technology: principles, developments and applications. Cambridge: Woodhead Publ, 2012. Woodhead publishing series in energy, 21. ISBN 978-0-85709-617-3.
- [13] H. J. Strumpf, D. M. Kotchick, and M. G. Coombs, "Hightemperature ceramic heat exchanger element for a solar thermal receiver," *J. Sol. Energy Eng.*, vol. 104, pp. 305–309, 1982
- [14] I. Hischier, P. Leumann, and A. Steinfeld, "Experimental and numerical analyses of a pressurized air receiver for solar-driven gas turbines," *J. Sol. Energy Eng.*, vol. 134, p. 021003, 2012.
- [15] MERCHÁN, R.P., SANTOS, M.J., MEDINA, A. and CALVO HERNÁNDEZ, A. High temperature central tower plants for concentrated solar power: 2021 overview. *Renewable and Sustainable Energy Reviews*. March 2022. Vol. 155, p. 111828. DOI 10.1016/j.rser.2021.111828.
- [16] AHLBRINK, Nils, ANDERSSON, Joel, DIEHL, Moritz and PITZ-PAAL, Robert. Optimization of the Mass Flow Rate Distribution of an Open Volumetric Air Receiver. *Journal of Solar Energy Engineering*. 1 November 2013. Vol. 135, no. 4, p. 041003. DOI 10.1115/1.4024245.
- [17] DEL RÍO, A., KORZYNIETZ, R., BRIOSO, J.A., GALLAS, M., ORDÓÑEZ, I., QUERO, M. and DÍAZ, C. Soltrec – Pressurized Volumetric Solar Air Receiver Technology. *Energy Procedia*. May 2015. Vol. 69, p. 360–368. DOI 10.1016/j.egypro.2015.03.042.
- [18] C. Kribus, A., Gray, Y., Grijnevich, M., Mittelman, G., Mey, S., Caliot, "The promise and challenge of volumetric absorbers," *Submitt. to Sol.Energy*, vol. 110, pp. 463–481, 2014.
- [19] GIOSTRI, A., BINOTTI, M., STERPOS, C. and LOZZA, G. Small scale solar tower coupled with micro gas turbine. *Renewable Energy*. March 2020. Vol. 147, p. 570–583. DOI 10.1016/j.renene.2019.09.013.
- [20] PABST, Christoph, FECKLER, Gereon, SCHMITZ, Stefan, SMIRNOVA, Olena, CAPUANO, Raffaele, HIRTH, Peter and FEND, Thomas. Experimental performance of an advanced metal volumetric air receiver for Solar Towers. *Renewable Energy*. June 2017. Vol. 106, p. 91–98. DOI [10.1016/j.renene.2017.01.016](https://doi.org/10.1016/j.renene.2017.01.016).
- [21] HAYNES, William M. (ed.). CRC Handbook of Chemistry and Physics. Online. 0. CRC Press, 2014. [Accessed 14 September 2022]. ISBN 978-0-429-17019-5.

- [22] Calcination - Wikipedia. Online. [Accessed 14 September 2022]. Available from: <https://en.wikipedia.org/wiki/Calcination>
- [23] High temperature heat exchangers. Bosal ECI - Energy Conversion Industry. Online. [Accessed 14 September 2022]. Available from: <https://www.eci.bosal.com/high-temperature-heat-exchangers>
- [24] Calcium Carbonate, Calcite (CaCO<sub>3</sub>). Online. [Accessed 15 September 2022]. Available from: [https://www.matweb.com/search/datasheet\\_print.aspx?matguid=bea4bfa9c8bd462093d50da5eebe78ac](https://www.matweb.com/search/datasheet_print.aspx?matguid=bea4bfa9c8bd462093d50da5eebe78ac)
- [25] INFORMATICS, NIST Office of Data and. Welcome to the NIST WebBook. Online. [Accessed 15 September 2022].
- [26] Calcium carbonate - Wikipedia. Online. [Accessed 15 September 2022]. Available from: [https://en.wikipedia.org/wiki/Calcium\\_carbonate](https://en.wikipedia.org/wiki/Calcium_carbonate)
- [27] GAMBHIR, Ajay and TAVONI, Massimo. Direct Air Carbon Capture and Sequestration: How It Works and How It Could Contribute to Climate-Change Mitigation. *One Earth*. December 2019. Vol. 1, no. 4, p. 405–409. DOI [10.1016/j.oneear.2019.11.006](https://doi.org/10.1016/j.oneear.2019.11.006).
- [28] Achieve net zero targets with Climeworks direct air capture. Online. [Accessed 15 September 2022]. Available from: <https://climeworks.com>
- [29] Can Sucking CO<sub>2</sub> Out of the Atmosphere Really Work? *MIT Technology Review*. Online. [Accessed 15 September 2022]. Available from: <https://www.technologyreview.com/2014/10/07/171023/can-sucking-co2-out-of-the-atmosphere-really-work/>
- [30] A Carbon-Sucking Startup Has Been Paralyzed by Its CEO. *Bloomberg.com*. Online. 9 April 2021. [Accessed 15 September 2022]. Available from: <https://www.bloomberg.com/news/features/2021-04-09/inside-america-s-race-to-scale-carbon-capture-technology>
- [31] KEITH, David W., HA-DUONG, Minh and STOLAROFF, Joshua K. Climate Strategy with Co<sub>2</sub> Capture from the Air. *Climatic Change*. January 2006. Vol. 74, no. 1–3, p. 17–45. DOI [10.1007/s10584-005-9026-x](https://doi.org/10.1007/s10584-005-9026-x).
- [32] Socolow, R., Desmond, M., Aines, R., Blackstock, J., Bolland, O., Kaarsberg, T., Lewis, N., Mazzotti, M., Pfeffer, A., Sawyer, K. and Siiriola, J., 2011. Direct air capture of CO<sub>2</sub> with chemicals: a technology assessment for the APS Panel on Public Affairs (No. BOOK). American Physical Society.

- [33] PARKINSON, Giles. How it works: Solar power towers with integrated storage. *RenewEconomy*. Online. 4 July 2013. [Accessed 15 September 2022]. Available from: <https://reneweconomy.com.au/how-it-works-solar-power-towers-with-integrated-storage-78892/>
- [34] HE, Ya-Ling, QIU, Yu, WANG, Kun, YUAN, Fan, WANG, Wen-Qi, LI, Ming-Jia and GUO, Jia-Qi. Perspective of concentrating solar power. *Energy*. May 2020. Vol. 198, p. 117373. DOI [10.1016/j.energy.2020.117373](https://doi.org/10.1016/j.energy.2020.117373).
- [35] POŽIVIL, P., AGA, V., ZAGORSKIY, A. and STEINFELD, A. A Pressurized Air Receiver for Solar-driven Gas Turbines. *Energy Procedia*. 2014. Vol. 49, p. 498–503. DOI [10.1016/j.egypro.2014.03.053](https://doi.org/10.1016/j.egypro.2014.03.053).
- [36] SANTAMARTA, Jose. Modular hybrid concentrated solar power. *HELIOSCSP*. Online. [Accessed 16 September 2022]. Available from: <https://helioscsp.com/modular-hybrid-concentrated-solar-power/>
- [37] SUNDEN, Bengt. High temperature heat exchangers. In : *Compact and Ultra-Compact Heat Exchangers: Science, Engineering and Technology*, Eds. R.K. Shah, M. Ishizuka, T.M. Rudy, and V.V. Wadekar, *Engineering Conferences International*. Online. Hoboken, NJ, USA, September 2005, CHE2005-29. p. QQ6-238. [Accessed 15 September 2022]. Available from: <https://dc.engconfintl.org/cgi/viewcontent.cgi?article=1024&context=heatexchangerfall2005>
- [38] Limestone Cycle - limestone, quicklime and slaked lime | Chemistry | FuseSchool. Online. 10 August 2014. [Accessed 16 September 2022]. Available from: <https://www.youtube.com/watch?v=9LDG9cnGIDo>
- [39] JACOB, Ron. Gas-to-gas heat exchanger for heat utilization in hot CO<sub>2</sub> from an electrically heated calcination process. 115. Online. 2019. [Accessed 16 September 2022]. Available from: <https://openarchive.usn.no/usn-xmlui/handle/11250/2638959>
- [40] Let's make tomorrow different today. *siemens-energy.com Global Website*. Online. [Accessed 5 May 2022]. Available from: <https://www.siemens-energy.com/global/en.html>
- [41] HO, Clifford K. A review of high-temperature particle receivers for concentrating solar power. *Applied Thermal Engineering*. October 2016. Vol. 109, p. 958–969. DOI [10.1016/j.applthermaleng.2016.04.103](https://doi.org/10.1016/j.applthermaleng.2016.04.103).
- [42] ROMERO, M. and GONZÁLEZ-AGUILAR, J. Next generation of liquid metal and other high-performance receiver designs for concentrating solar thermal (CST) central tower systems. In : *Advances in Concentrating Solar Thermal Research and Technology*. Online. Elsevier, 2017. p. 129–154. [Accessed 14 June 2022]. ISBN 978-0-08-100516-3.

- [43] STEINFELD, A., IMHOF, A. and MISCHLER, D. Experimental Investigation of an Atmospheric-Open Cyclone Solar Reactor for Solid-Gas Thermochemical Reactions. *Journal of Solar Energy Engineering*. 1 August 1992. Vol. 114, no. 3, p. 171–174. DOI [10.1115/1.2930001](https://doi.org/10.1115/1.2930001).
- [44] DAVIS, Dominic, MÜLLER, Fabian, SAW, Woei L., STEINFELD, Aldo and NATHAN, Graham J. Solar-driven alumina calcination for CO<sub>2</sub> mitigation and improved product quality. *Green Chemistry*. 2017. Vol. 19, no. 13, p. 2992–3005. DOI [10.1039/C7GC00585G](https://doi.org/10.1039/C7GC00585G).
- [45] Bai F, Zhang Y, Zhang X, Wang F, Wang Y, Wang Z. Thermal performance of a quartz tube solid particle air receiver. In: Proceedings of the SolarPACES 2013 international conference, vol. 49; 2014. p. 284e94.
- [46] J. A. Harris and T. G. Lenz, "Thermal performance of solar concentrator/cavity receiver systems," Sol. Energy, vol. 34, pp. 135– 142, 1985.
- [47] L. B. Railsback, Some Fundamentals of Mineralogy and Geochemistry. 2019
- [48] Thermal energy storage - Wikipedia. Online. [Accessed 15 September 2022]. Available from: [https://en.wikipedia.org/wiki/Thermal\\_energy\\_storage](https://en.wikipedia.org/wiki/Thermal_energy_storage)
- [49] ALVA, Guruprasad, LIN, Yaxue and FANG, Guiyin. An overview of thermal energy storage systems. *Energy*. February 2018. Vol. 144, p. 341–378. DOI [10.1016/j.energy.2017.12.037](https://doi.org/10.1016/j.energy.2017.12.037).
- [50] What Is the Typical Flame Temperature for Different Fuels? *ThoughtCo*. Online. [Accessed 11 September 2022]. Available from: <https://www.thoughtco.com/flame-temperatures-table-607307>
- [51] Spelling JD. Hybrid Solar Gas-Turbine Power Plants A Thermoconomic Analysis. KTH Royal Institute of Technology, 2013.
- [52] Syred, N., et al. "A NOVEL CYCLONE HEAT EXCHANGER." *Energy & Environment*, vol. 3, no. 4, 1992, pp. 387–400. JSTOR, <http://www.jstor.org/stable/43734162>. Accessed 14 Sep. 2022.
- [53] MARTI, Jan, GEISSBÜHLER, Lukas, BECATTINI, Viola, HASELBACHER, Andreas and STEINFELD, Aldo. Constrained multi-objective optimization of thermocline packed-bed thermal-energy storage. *Applied Energy*. April 2018. Vol. 216, p. 694–708. DOI [10.1016/j.apenergy.2017.12.072](https://doi.org/10.1016/j.apenergy.2017.12.072).
- [54] Weiland NT, Lance BW, Pidaparti SR. sCO<sub>2</sub> power cycle component cost correlations from DOE data. ASME Turbo Expo 2019 2019:1–17.
- [55] M.J. Wagner, T. Wendelin, SolarPILOT: a power tower solar field layout and characterization tool, Sol. Energy 171 (2018).
- [56] L. Galanti, A.F. Massardo, Micro gas turbine thermodynamic and economic analysis up to 500 kWe size, Appl. Energy 88 (2011)
- [57] A. Giostri, Preliminary analysis of solarized micro gas turbine application to CSP parabolic dish plants, Energy Procedia 142 (2017).

- [58] MUSI, Richard, GRANGE, Benjamin, SGOURIDIS, Sgouris, GUEDEZ, Rafael, ARMSTRONG, Peter, SLOCUM, Alexander and CALVET, Nicolas. Techno-economic analysis of concentrated solar power plants in terms of levelized cost of electricity. In : *SOLARPACES 2016: International Conference on Concentrating Solar Power and Chemical Energy Systems*. Online. Abu Dhabi, United Arab Emirates, 2017. p. 160018. [Accessed 13 September 2022]. DOI [10.1063/1.4984552](https://doi.org/10.1063/1.4984552).
- [59] Chile natural gas prices, December 2021. *GlobalPetrolPrices.com*. Online. [Accessed 18 September 2022]. Available from: [https://www.globalpetrolprices.com/Chile/natural\\_gas\\_prices/](https://www.globalpetrolprices.com/Chile/natural_gas_prices/)
- [60] Coal Price Today 18.09.2022 = \$112 MT. Online. [Accessed 18 September 2022]. Available from: <https://coal-price.com/>
- [61] RITCHIE, Hannah, ROSER, Max and ROSADO, Pablo. Energy. *Our World in Data*. Online. 28 November 2020. [Accessed 14 September 2022]. Available from: <https://ourworldindata.org/energy-mix>
- [62] Carbon Dioxide Emissions From Electricity - World Nuclear Association. Online. [Accessed 13 September 2022]. Available from: <https://www.world-nuclear.org/information-library/energy-and-the-environment/carbon-dioxide-emissions-from-electricity.aspx>
- [63] Conversion Guidelines- Greenhouse gas emissions - Online. [Accessed 5 September 2022]. Available from: <https://www.eeagrants.gov.pt/media/2776/conversion-guidelines.pdf>
- [64] Chile electricity prices, December 2021. *GlobalPetrolPrices.com*. Online. [Accessed 11 September 2022]. Available from: [https://www.globalpetrolprices.com/Chile/electricity\\_prices/](https://www.globalpetrolprices.com/Chile/electricity_prices/)
- [65] TREVISON, Silvia, JEMMAL, Yousra, GUEDEZ, Rafael and LAUMERT, Björn. Packed bed thermal energy storage: A novel design methodology including quasi-dynamic boundary conditions and techno-economic optimization. *Journal of Energy Storage*. April 2021. Vol. 36, p. 102441. DOI [10.1016/j.est.2021.102441](https://doi.org/10.1016/j.est.2021.102441).

## 10 Appendix

### 10.1 Main HEX code

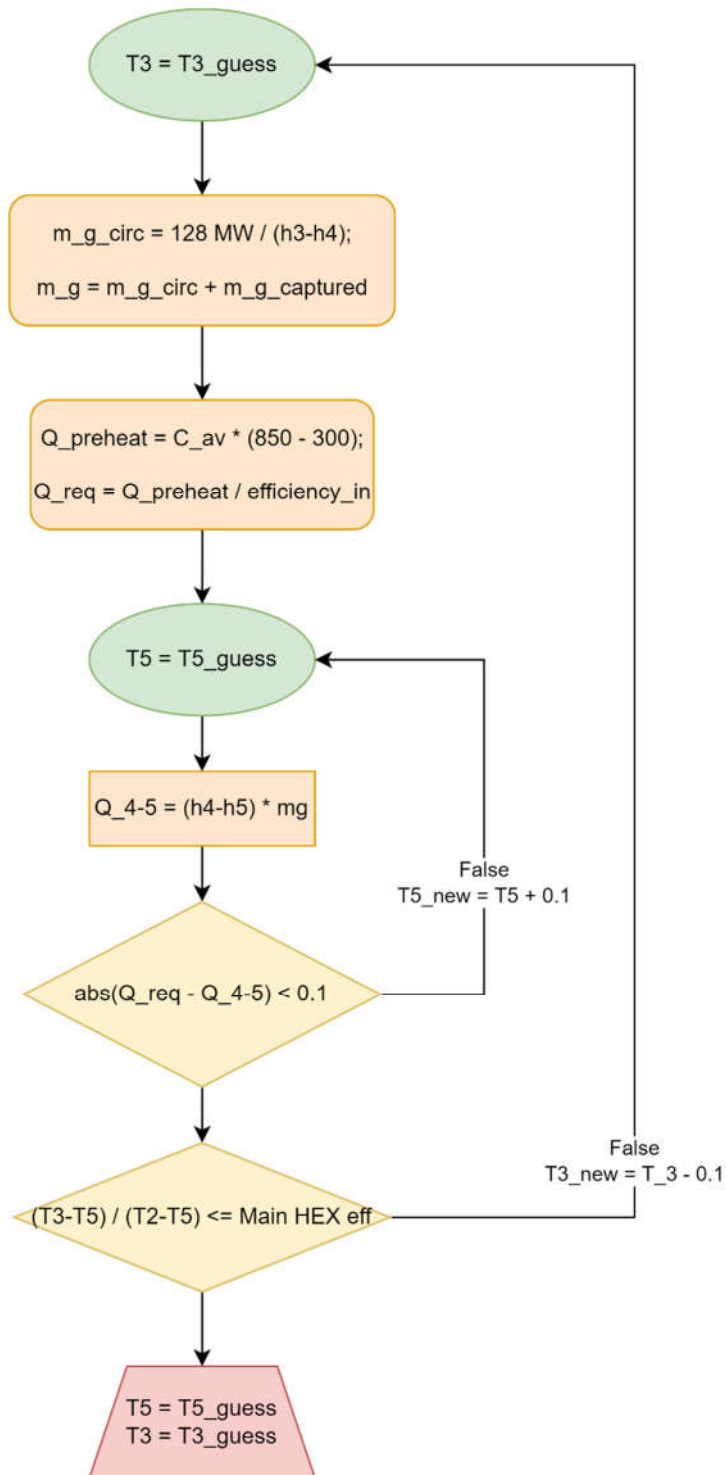


Figure A.1. Workflow of Main HEX script

```

import CoolProp.CoolProp as CP
import numpy as np

T1 = T2 = T3 = T5 = 0
rf = "Air"
T4 = 850
T2 = 1000
Qdac = 128

# content of gas

CO2_fraction = 0.9713
O2_fraction = 0.0136
N2_fraction = 0.0151

# captured

m_cap_CO2 = 46.09883
m_cap_O2 = 0.645469
m_cap_N2 = 0.716661

# pellet props. It should be preheated up to 650 C

Ti = 300
To = 850
eff = 0.7
m_Ca = 83.33
m_K2 = 1.5
cp_Ca = 834.3
cp_K2 = 827.7

heatCapacity_pellet = m_Ca * cp_Ca + m_K2 * cp_K2
Qpreheat = heatCapacity_pellet * (To - Ti)/0.7/1000000 # = 55.6001 MW

print(Qpreheat)

# ----- functions -----

def calc_h_gas(temperature):
    h_CO2 = CO2_fraction * CP.PropsSI("H", "P", 1e5, "T", temperature + 273, "CO2")

```

```

h_O2 = O2_fraction * CP.PropsSI("H", "P", 1e5, "T", temperature + 273, "O2")
h_N2 = N2_fraction * CP.PropsSI("H", "P", 1e5, "T", temperature + 273, "N2")
return h_N2 + h_O2 + h_CO2

def T5_calc(mass):
    i = 1

    T5 = T4 - 10
    deltaTemp = 0.1

    while i > 0:

        h4 = calc_h_gas(T4)
        h5 = calc_h_gas(T5)
        Q4_5 = (h4-h5)*mass/1000000
        if (Q4_5 - Qpreheat)>0 and (Q4_5 - Qpreheat) < 0.1:
            return T5
        else:
            T5 -= deltaTemp

    if i == 3000:
        print("error in mass calculation, loop limit " + str(T5))
        break
    i += 1

# ----- calculation -----
pitch = 18

i = 0
while i > 0:
    T3 = T2 - pitch
    print(T3)
    massGasCirc = Qdac / (calc_h_gas(T3) - calc_h_gas(T4)) * 1000000
    massGas = massGasCirc + m_cap_N2 + m_cap_CO2 + m_cap_O2

    T5 = T5_calc(massGas)
    # print(T5)
    if abs(900 - T3 + 0.1*T5) < 0.5 or (900 - T3 + 0.1*T5) > 0:

```

```

# print(T5)
print("T3 =" + str(T3) + " T5 =" + str(T5) + " pitch =" + str(pitch))
break

if i == 5000:
    print("error, loop max limit")
    break
i += 1
pitch += 0.5

```

## 10.2 PB code

```

import CoolProp.CoolProp as CP
import numpy as np

```

```
T1 = T2 = T3 = T5 = 0
```

```
rf = "Air"
```

```
T4 = 850
```

```
T2 = 1000
```

```
Qdac = 128
```

```
T2_pb = T3_pb = T5_pb = 0
```

```
Ta = 9
```

```
T1_pb = 180
```

```
rf = "Air"
```

```
pressure = 101325
```

```
W_pb = 13 # MW
```

```
effComp = 0.81
```

```
effTurb = 0.84
```

```
effMech = 0.98
```

```
effGen = 0.96
```

```
effInv = 0.96
```

```
beta = 4.1
```

```
# content of captured gas
```

```
CO2_fraction = 0.9713
```

```
O2_fraction = 0.0136
```

```
N2_fraction = 0.0151
```

```
# captured
```

```
m_cap_CO2 = 46.09883
m_cap_O2 = 0.645469
m_cap_N2 = 0.716661
```

```
# pellet props. It should be preheated up to 650 C
```

```
Ti = 300
To = 850
eff = 0.7
m_Ca = 83.33
m_K2 = 1.5
cp_Ca = 834.3
cp_K2 = 827.7
```

```
heatCapacity_pellet = m_Ca * cp_Ca + m_K2 * cp_K2
Qpreheat = heatCapacity_pellet * (To - Ti) / 0.7 / 1000000 # = 55.6001 MW
```

```
# ----- functions -----
```

```
def calc_h_gas(temperature):
    h_CO2 = CO2_fraction * CP.PropsSI("H", "P", 1e5, "T", temperature + 273, "CO2")
    h_O2 = O2_fraction * CP.PropsSI("H", "P", 1e5, "T", temperature + 273, "O2")
    h_N2 = N2_fraction * CP.PropsSI("H", "P", 1e5, "T", temperature + 273, "N2")
    return h_N2 + h_O2 + h_CO2
```

```
def T5_calc(mass):
    i = 1

    T5 = T4 - 10
    deltaTemp = 0.1
```

```
while i > 0:

    h4 = calc_h_gas(T4)
    h5 = calc_h_gas(T5)
    Q4_5 = (h4 - h5) * mass / 1000000
    if (Q4_5 - Qpreheat) > 0 and (Q4_5 - Qpreheat) < 0.1:
```

```

        return T5
    else:
        T5 -= deltaTemp

    if i == 3000:
        print("error in mass calculation, loop limit " + str(T5))
        break
    i += 1

def temp_calc_fromEnthalpy(enthalpy, temperature):
    i = 1
    Tx = temperature
    deltaTemp = 0.1
    # print(Tx)
    while 1 > 0:
        # print(Tx)
        hx = calc_h_gas(Tx)
        if abs(enthalpy - hx) < 1000:
            return Tx
        else:
            Tx -= deltaTemp

    if i == 5000:
        print("error in temperature calculation, loop limit " + str(Tx))
        break
    i += 1

# ----- calculation -----

h_a = CP.PropsSI("H", "P", pressure, "T", Ta + 273, rf)
h_1_pb = CP.PropsSI("H", "P", pressure * beta, "T", T1_pb + 273, rf)

T2_pb = 0
j = 0

pitch = 18

i = 0
while 1 > 0:

```

```

T3 = T2 - pitch
print(T3)
print("i =",i)

massGasCirc = Qdac / (calc_h_gas(T3) - calc_h_gas(T4)) * 1000000
massGas = massGasCirc + m_cap_N2 + m_cap_CO2 + m_cap_O2

T5 = T5_calc(massGas)
h_5 = calc_h_gas(T5)
pitch2 = 5
while 1 > 0:
    print("j= ",j)
    j += 1

    T3_pb = T5 - pitch2
    h_3_pb = CP.PropsSI("H", "P", pressure * beta, "T", T3_pb + 273, rf)
    s_3 = CP.PropsSI("S", "P", pressure * beta, "T", T3_pb + 273, rf)

    h_4is_pb = CP.PropsSI("H", "P", pressure, "S", s_3, rf)
    h_4_pb = h_3_pb - effTurb * (h_3_pb - h_4is_pb)
    T4_pb = CP.PropsSI("T", "P", pressure, "H", h_4_pb, rf) - 273
    m_pb = W_pb * 1000000 / (effGen * effInv * (effMech * (h_3_pb - h_4_pb) - (h_1_pb - h_a)))
    T2_pb = 0.86 * (T4_pb - T1_pb) + T1_pb
    h_2_pb = CP.PropsSI("H", "P", pressure * beta, "T", T2_pb + 273, rf)
    print("T2_pb=", str(T2_pb), "T3_pb=", str(T3_pb),"T4_pb=", str(T4_pb), "m_pb = ", m_pb, "m_circ =",
",massGasCirc)

    h_6 = h_5 - (m_pb / massGasCirc) * (h_3_pb - h_2_pb)
    print("h_6=", str(h_6), "h_5=", str(h_5))
    T6 = temp_calc_fromEnthalpy(h_6, T5)

    if ((T5 - T6) / (T5 - T2_pb)) < 0.86 or abs((T5 - T6) / (T5 - T2_pb) - 0.86) < 0.05:
        print("T6=", str(T6), "hex_5_6 eff =", str((T5 - T6) / (T5 - T2_pb)))
        break
    if j > 5000:
        print("error pechal")
        break

    pitch2 += 0.5

```

```
if abs(900 - T3 + 0.1 * T6) < 0.5 or (900 - T3 + 0.1 * T6) > 0:  
    # print(T5)  
    print("T3 =" + str(T3) + " T6 =" + str(T6) + " T5 =" + str(T5) + " pitch =" + str(pitch))  
    break  
  
if i == 5000:  
    print("error, loop max limit")  
    break  
i += 1  
pitch += 0.5  
print("====")
```